Aus dem Institut für Laboratoriumsmedizin
Institut der Ludwig-Maximilians-Universität München
Vorstand: Prof. Dr. med. D. Teupser

Role of Blood Coagulation and Extracellular Vesicles in Pancreatic Cancer Cell Extravasation

Dissertation
zum Erwerb des Doktorgrades der Humanbiologie
an der Medizinischen Fakultät der
Ludwig-Maximilians-Universität zu München

Xiaopeng Zhang

From
Jinan, Shandong, PR China

2020

Mit Genehmigung der Medizinischen Fakultät

der Universität München

Berichterstatter:

Prof. Dr. Bernd Engelmann

Mitberichterstatter:

Prof. Dr. Michael Spannagl

PD Dr. Michael Haas

Mitbetreuung:

Dekan: Prof. Dr. med. dent. Reinhard Hickel

Tag der mündlichen Prüfung: 28.04.2020

Abbreviations

Ab/α	Antibody
Ang-1	Angiopoietin-1
Ang-2	Angiopoietin-2
BSA	Bovine serum albumin
Ca	Calcium
DNA	Deoxyribonucleic acid
DMSO	Dimethylsulfoxid
EVs	Extracellular vesicles
f12-/- mice	FXII deficient mice
Gas6	Growth-arrest-specific gene-6
HIF1α	Hypoxia-inducible factor 1-α
LSM	Laser scanning microscope
LOs	Large oncosomes
MV	Microvesicles
NC monocytes	Non classical monocytes
NEAA	Non-essential amino acids
NETs	Neutrophil extracellular traps
Padi4	Peptidyl Arginine Deiminase 4
PBS	Phosphate buffer saline
STED	Stimulated emission depletion
SEM	Scanning electron microscope
TAMs	Tumor-associated macrophages
TEM	Transmission electron microscopy
TEG	Thromboelastography
TF	Tissue factor
TFPI	Tissue Factor Pathway Inhibitor
WB	Western Blotting
WT	Wild type

Contents

1. Introduction

1.1 Overview of Pancreatic cancer

To date, owing to the soar of mortality rate, pancreatic cancer has become one of the most lethal cancers. It occupies the third largest proportion of tumor-associated mortality in Western countries.[1] When taking all stages into account, 5-year survival rates have remained at only around 5% during the last decades.[2]

During the year of 2018, approximate 55,440 patients (29,200 men and 26,240 women) were diagnosed with pancreatic cancer while around 44,330 (23,020 men and 21,310 women) died of pancreatic cancer in United States.[3] Several factors can contribute to an increased risk of pancreatic cancer, such as smoking, age, race, obesity, diabetes, exposure to certain chemicals (benzene, petrochemicals, dyes, and pesticides), gender, inherited genetic syndromes, family history, chronic pancreatitis, liver cirrhosis and consumption of alcohol.[3] The signs and symptoms are largely affected by the stage and the location of pancreatic tumors. As a result of steatorrhea and diarrhoea, weight loss and obstructive jaundice usually happen in tumors located in the head of the pancreas while tumors of the body and tail elicit abdominal pain and weight loss. The pain is normally located in the upper abdomen and radiate to the back, presenting as a deep and dull pain. At an early stage of pancreatic cancer, most of the symptoms are unspecific, which hinder the early diagnosis of this fatal disease.[4] So far, the exclusive way to obtain curative level is surgical excision which is only suitable for less than 20 % of affected patients. These patients are at an early stage of the cancer. Locally advanced tumor and metastasis are considered to be the two main

counter-indications for surgical intervention. With the improvement of surgical techniques, most of the patients whose tumor are recognized as locally restricted pancreatic cancer, undergo radical resection of the tumors and have the chance to achieve curative results. Since metastasis is a crucial counter-indication for the surgical procedure for pancreatic cancer, only chemotherapy and radiotherapy can be employed. Consequently, the prognoses for these patients are very poor. That is the reason why considerable research focuses on pancreatic cancer metastasis nowadays. [1, 4]

1.2 KRAS mutation in pancreatic cancer

1.2.1 KRAS and its function

KRAS is one of most frequent oncogenes which acts as an on/off switch in cell signaling. When activated, it regulates cell proliferation. Certain KRAS mutations important for pancreatic cancer interrupt negative regulation of cell proliferation. In this way, cells ceaselessly proliferate and, ultimately, malignancy develops.

The gene product of KRAS was first found to be a p21 GTPase.[5, 6] There is an isoprene group on KRAS's C-terminus, which contributes to tether the protein to the cell membrane. Two proteins named K-Ras4A and K-Ras4B are respectively produced in mammalian cells by exon 4A and exon 4B of the KRAS gene. The structures of the two proteins differ in their C-terminal region. Besides, they tether to cellular membrane including the plasma membrane via different mechanisms.[7]

As an on-and-off switch to control molecular, KRAS cycles between the GTP-bound

active and the GDP-bound inactive states. Guanine nucleotide exchange factors (GEFs) play a key role in the conversion from GDP to GTP, promoting the activation of KRAS; however, GTPase-activating proteins (GAPs) elicit the inactivation of KRAS, inducing hydrolysis of GTP. Activating mutations of KRAS found in human PDAC i.e. pancreatic ductal adenocarcinoma not only whittle down the innate GTPase activation by the protein product of KRAS but also cut off the connection between KRAS and GTPase-activating proteins (GAPs). There are only three point mutation sites of KRAS that drive the development of pancreatic carcinoma. They concern amino acids G12, G13 and Q61. Among them, 98% of all KRAS mutations in PDAC are point mutations at amino acid G12. The mutations trigger sustained cell proliferation, reprogramming of cell metabolism, resistance to apoptosis, reshaping of the tumor microenvironment, immune escape, cell migration and metastasis.[8]

1.2.2 Effector pathways of oncogenic KRAS

The mechanism of KRAS signaling is rather intricate and changes flexibly every second in our body. What matters most here is the recruitment of downstream signaling factors, such as canonical Raf/Mek/Erk, phosphatidylinositol 3-kinase (PI3K)/3-phosphoinositide-dependent protein kinase-1 (Pdk1)/Akt, RalGDS/p38MAPK, Rac and Rho, Rassf1, NF1, p120GAP and PLC-e. It is believed that oncogenic signals of KRAS in PDAC transmit by three main pathways: Raf/ Mek/Erk, PI3K/Pdk1/Akt and the Ral guanine nucleotide exchange factor pathway[9-12] (Figure 1).

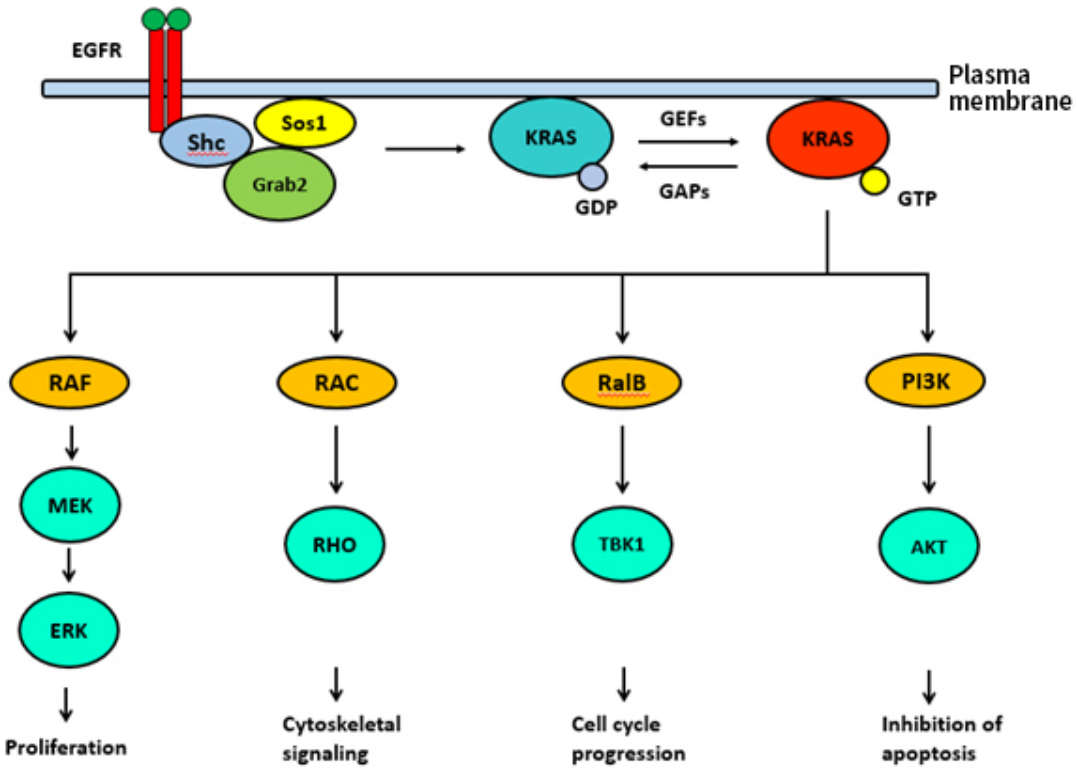

Figure 1 Important downstream effectors of the KRAS signaling pathway

1.2.3 Cross-signaling and signaling annuli

It has lately been recognized that autocrine and paracrine signaling circuits play a facilitating role in the amplification of tumorigenic KRAS signaling among different tumors.[13-15]

Experiments in vivo with PDAC murine models illustrated that when EGFR is activated by a KRAS-induced autocrine-positive feedback mechanism, formation of acinar-to-ductal metaplasia (ADM) and promotion of early pancreatic intraepithelial neoplasia (PanIN) lesions will be induced, which ultimately lead to the development of Pancreatic ductal adenocarcinoma (PDAC).[13, 14] However, the detailed mechanism during the process has not been completely elucidated. We currently believe that the

type of regenerative feedback mechanism enhances KRAS signaling and when a certain threshold level is reached causing sustained proliferation of pancreatic acinar cells, carcinoma develops.[13, 15] Apart from KRAS mutation, deletion of p53 also results in the generation of PDAC even with only change in EGFR signaling.[15] During the development of PDAC, severed detailed steps such as for example how loss of p53 function decouples KrasG12D from EGFR input are not completely known. Similarly, more efforts are needed to uncover whether EGFR signaling makes contributions to the formation of PanIN progression and PDAC maintenance and how these three elements interplay with each other. As is shown from clinical trials, there is a subpopulation (＜10%) of PDAC patients who benefit from treatment with the EGFR inhibitor Erlotinib, which raises the question whether a small amount of PDAC patients remain addicted to KRAS signaling amplification via EGFR[16,17].

1.3 Tumor metastasis

Cancer metastasis is a complex process that includes different steps such as intravasation and extravasation. The majority of tumor cells spread through the body via the bloodstream. Plenty of evidence suggests that a small percentage of tumor cells survive ultimately once entering into circulatory system and extravasate to localize at other organs, also known as distant metastases. Studies in experimental murine animal models and mankind tumors have suggested that a plethora of cells depart every day from the original site and pass into the bloodstream, but only few of them support development of metastases at distant sites.[17, 18] This is consistent with

the studies that have monitored the survival of tumor cells after intravenous injection in syngeneic mice, which showed that most cells die within 1-2 days,[19] while less than 0.1% of the injected cells eventually form metastases.

Cancer cells cannot easily survive in the circulatory system, which is mainly owing to the attack by the immune system. The anti-tumor effect executed by the immune system enormously attenuates the progression of carcinoma.[20] Once tumor cells leave the original tumor and get into the blood system they will interact with immune cells comprising natural killer cells and cytotoxic $CD8^+$ T cells, which play a significant role in the elimination of tumor cells. However, tumor cells protect themselves from immunological stress via various strategies. Some escape mechanisms are performed by the tumor cells themselves, others require interaction with cells such as myeloid cells and platelets. Ultimately, tumor cells escape from the hostile intravascular environment by transmigrating through the endothelial barrier.[21] Various mechanisms mediating the different stages of cancer cell extravasation have been identified, comprising direct communication of cancer cells with endothelial cells, and indirect processes involving blood cells such as platelets and leukocytes.

After tumor cells extravasation, the cells eventually form a pre-metastatic niche. Indeed, the early metastatic niche has already been formed during the first hours after tumor cell arrest in the microvasculature according to latest research. Then, these niches can either be swept by immune cells or develop into mature metastases after several days.[22, 23]

1.4 Blood coagulation

1.4.1 Overview of the blood coagulation cascade

In general, the coagulation, anticoagulation and fibrinolysis systems work together to maintain homeostasis when blood vessel injury occurs. The coagulation cascade, which apart from injury can also be triggered by infections and other conditions, induce the formation of fibrin as a final product. In parallel, the anticoagulation system is activated to limit the extension of the clot. Thereafter, fibrinolysis system comes into work to resolve the fibrin-rich thrombi. Essentially, the coagulation cascade activation consists of a complicated set of biochemical mechanisms triggering zymogens to become active and to amplify these interactions, which in the end result in the switching from soluble fibrinogen to insoluble fibrin. The coagulation cascade can be activated by two classical pathways: one is the contact pathway and the other is the tissue factor (TF) dependent pathway (Figure 2).

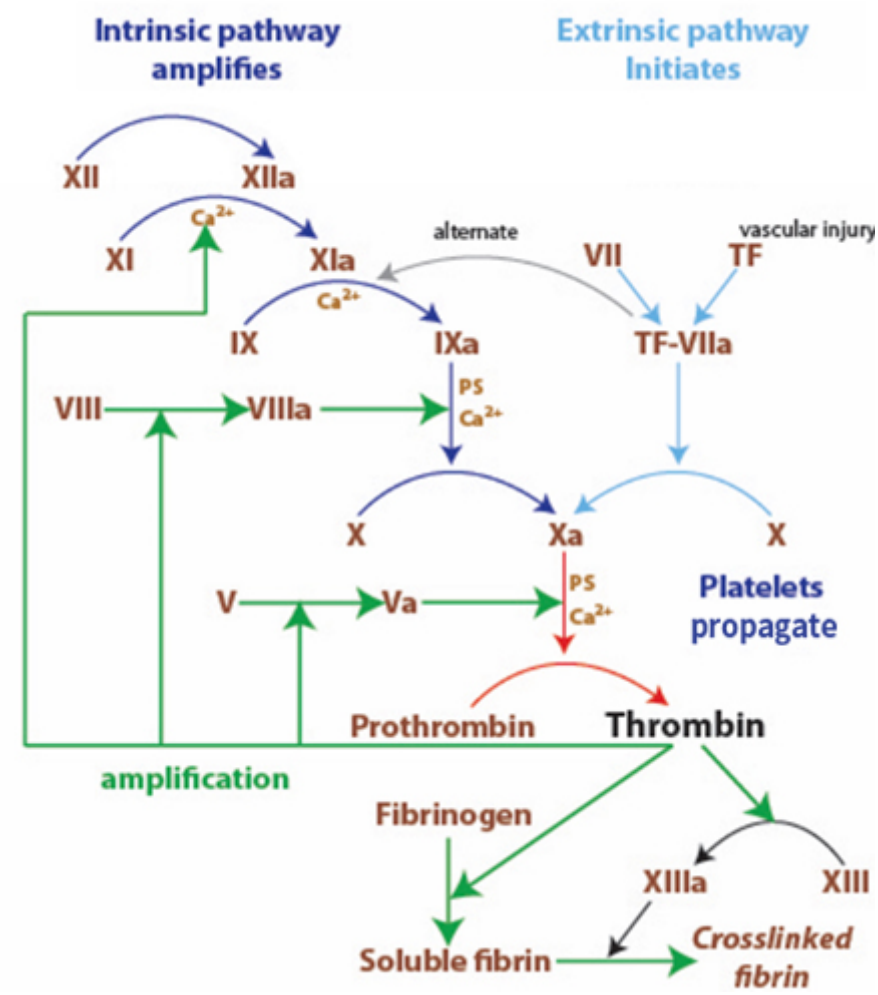

Figure 2 Blood coagulation cascade. See Ref [24]

The contact of blood with negative charges on artificial materials can convert zymogen Hageman factor (Factor XII) to the active enzyme FXIIa, which successively activates FXI to FXIa that in turn activates FIX to FIXa. The latter proteinase can be part of the tenase complex with FVIIIa to trigger downstream formation of FXa. In general, the TF-dependent pathway is the more crucial pathway in blood coagulation under biological and physiological conditions. TF is widely expressed in different types of subendothelial cells, and once the protein gets in contact with blood it will immediately form a complex together with FVII/FVIIa. This

TF-VIIa complex can either trigger the conversion of FIX to FIXa, which enhances the intrinsic pathway, or directly activate factor X. FXa, FVa, prothrombin and Ca^{2+} ions form the prothrombinase complex to convert prothrombin into thrombin, which in turn converts fibrinogen to fibrin. The clots finally formed not only contain fibrin polymers but also platelets, RBCs and/or WBCs. There are three important positive feedbacks in the coagulation cascade, which aim to amplify and accelerate the formation of thrombus in response to injury. One has been referred above, the other two are that thrombin can activate FVIII and FXI into FVIIIa and FXIa respectively, which are considered as one of the most important way to trigger the intrinsic pathway under physiological conditions.[24, 25]

1.4.2 Role of FXII in blood coagulation

The contact pathway of blood coagulation is triggered by FXII, together with kininogen (HK) and plasma kallikrein (PK). When getting in contact with surfaces rich in negative charges, zymogen FXII changes its conformation, resulting in a few FXIIa (molecules). Then, FXIIa activates PK, which in turn increase activation of FXII. Similar to other contact system proteins, such as PK and HK, deficiency in FXII severely prolongs the activated partial thromboplastin time (aPTT), a diagnostic coagulation assay that relies on contact system activation. However, patients with severe deficiencies in FXII, PPK or HK do not suffer from spontaneous or injury-related excessive bleeding, in contrast to deficiency in TF, VIII and IX, which means that activation of FXII is dispensable for the process of haemostasis. However,

new insights in FXII have emerged in the last decade due to the observation that *f12-/-* mice appear to be protected from arterial thrombosis[26, 27]. Several triggers contribute to FXII activation during thrombosis, in particular extracellular RNA, and or exposed collagen in the arterial wall [28, 29]. Taken together, several studies suggest that FXIIa inhibitors may reduce the extent of arterial thrombosis in vivo.

The contact system has drawn strong scientific attention as a result of its contribution to pathological thrombosis formation. However, this system has also been involved in inflammatory reactions. Taking sepsis patients as an example, inhibition of the contact system attenuates complement activation and reduces neutrophil degranulation. Consequently, overall survival rates increase.[30] Nevertheless, the role of FXII in tumor extravasation and metastasis is still ambiguous and needs to be investigated.

1.4.3 Cancer and thrombosis

The occurrence of cancer is accompanied by an increase of the incidence of venous thromboembolism (VTE) (4% to 20%) and arterial thrombosis (2% to 5%);[31-33] the rates of VTE are dependent on the cancer type.[32, 34, 35] Based on a risk assessment of VTE, the type of cancer can be roughly split into 3 classes: the first class is high risk, which includes pancreatic cancer, ovarian cancer, brain cancer, stomach cancer, gynecologic cancer, and hematologic cancer; the second is intermediate risk, consisting of colon cancer and lung cancer; the third is low risk, comprising breast cancer and prostate cancer. Many previous studies have attempted to elucidate why tumor can activate blood coagulation and thus cause VTE. One obvious reason is that

tumor cells themselves can directly induce blood coagulation and fibrin formation. It is less clear whether also the host triggers coagulation in response to tumor cells.

As an example, human pancreatic cancer express larger amounts of TF than the normal tissues and the expression of TF is relevant to the histologic grade of tumors.[36] One study showed that there is an association between intra-tumoral TF expression and VTE.[37] In addition, human pancreatic cell lines also express high levels of TF and release TF^{+} extracellular vesicles (EV).[38] MVs (also known as microparticles) are released from pancreatic cancer cells which are activated or apoptotic as small membrane vesicles[39]. They are procoagulant by providing a surface for the assembly of different coagulation factor complexes.[40] When negatively charged phospholipids such as phosphatidylserine (PSer) are exposed on the vesicle membrane, the procoagulant activity of MV is enhanced. Dvorak et al first proposed a connection between tumor-derived MV and thrombosis.[41] They showed that deciduous vesicles have procoagulant activity, facilitating fibrin deposition. Late studies showed that enhanced procoagulant activity of the MV derived from malignancy is TF-dependent[42, 43].

Meanwhile, it is believed that leukocytosis may be associated with increased VTE in tumor patients as well.[44, 45] For example, neutrophils may promote the formation of thrombosis by generating neutrophil extracellular traps (NETs),[46] while monocytes synthesize TF themselves.[47] Thrombocytosis is a common phenomenon for tumor patients, especially those who are diagnosed with ovarian, breast, lung, and gastrointestinal cancer. Patients with high platelet counts have a higher rate of

developing VTE in the absence of cancer, meaning that the level of peripheral blood platelet counts is directly proportional to the incidence of VTE.[48] Interestingly, a similar phenomenon may be relevant in tumor patients, namely cancer patients with high platelet counts had a higher rate of developing VTE.[49, 50] However, the underlying mechanisms for leukocytosis and thrombocytosis in cancer patients are still unclear today.

1.5 Monocytes, inflammation and Cancer

Monocytes are a type of circulating leukocyte that can differentiate into several types of the immune cells including macrophages and dendritic cells, which together form the "mononuclear phagocyte system" (MPS).[51] Monocytes are generated in the bone marrow and are continuously released into the peripheral circulation where they play a crucial role in tissue homeostasis and immunity.[52] During the past 4 decades, our knowledge about the characteristic of monocytes has evolved from considering them as a homogenous group to their appreciation as a heterogeneous population, which has diverse functions in the immune response. Nowadays, three subgroups of monocytes are known based on the quantity of their surface markers:1) classical monocytes or inflammatory monocytes (CD14+CD16- in human, $Ly6C^{high}CD43^{low}CX3CR1^{low}$ in mice); 2) non-classical monocytes or patrolling monocytes ($CD14^{low}CD16+$ in human, $Ly6C^{low}CD43^{high}CX3CR1^{high}$ in mice); 3) intermediate monocytes (CD14+CD16+ in human, $Ly6C^{int}CD43^{high}CX3CR1^{high}$ in mice). The percentage of classical and non-classical monocytes are species-dependent,

for example classical monocytes dominate in humans.[53] Circulating monocytes are recognized to originate from the bone marrow after birth, sharing common myeloid progenitors (CMPs) with red blood cells, platelet, and granulocytes. Monocytes have long been considered to be the main source of tissue resident macrophages. However tissue-specific macrophages can also originate from yolk sac during embryogenesis and migrate to the fetal liver to become fetal hepatomacrophages, which can then disseminate to various organs on the condition that the fetal circulation exists.[54] After residing in the tissue, they maintain themselves via self-renewal, which is the main resource of tissue resident macrophages.[55]

Classical monocytes, which are rapidly recruited after infection or inflammation, only remain for about one day in the peripheral blood. They can either migrate to the tissue to repopulate the tissue specific monocytes or lose the Ly6C marker to get converted into non-classical (patrolling) monocytes. Non-classical monocytes have a longer lifespan than classical monocytes, which are approximately 2 days in mice and 7 days in humans. The most important function of non-classical monocytes is to patrol and survey the endothelium as a local innate surveillance under physiological conditions[56-58].

In cancer, monocytes can accompany each stage of the disease, from early growth to the establishment of metastasis[59, 60]. Inflammatory monocytes are in particular precursors of tumor-associated macrophages (TAMs). The appearance of TAMs correlates with a poor prognosis in the majority of clinical studies and animal models[61, 62]. Non-classical monocytes, on the contrary, which are recruited and

localized in microvessels after injection of tumor cells, attenuate tumor metastasis such as via recruitment of NK cells[63, 64].

1.6 Neutrophils and neutrophil extracellular traps (NETs)

Neutrophils make up the largest proportion of innate immune cells in the human immune system. They are equipped with broadly effective antimicrobials that are stored predominately in specialized granules. Beside this, the neutrophil arsenal can also cause injury to host tissues. Deployment of these cells sets in motion three major antimicrobial strategies: phagocytosis, degranulation and the release of NETs. The releasing process of NETs is called NETosis (Figure 3), which is clearly different from necrosis or apoptosis and was first discovered by Brinkmann et al. [46] NETs are extracellular strands of decondensed (unwound) DNA decorated with histones and neutrophil granule proteins.[46, 65]

DNA is wrapped around histones to form nucleosomes and further organized into chromatin. Heterochromatin de-condensation is mediated by peptidyl arginine deiminase 4 (PAD4), which catalyzes the conversion of histone arginines to citrullines, reducing the strong positive charge of histones and consequently reducing histone-DNA binding. This weakened interaction subsequently unwraps the nucleosomes, a prerequisite for NETs formation. In case of PAD4, neutrophil elastase (NE) is also regarded as a crucial factor that contributes to the formation of NETs, since it can cleave histones during this process.[66, 67]

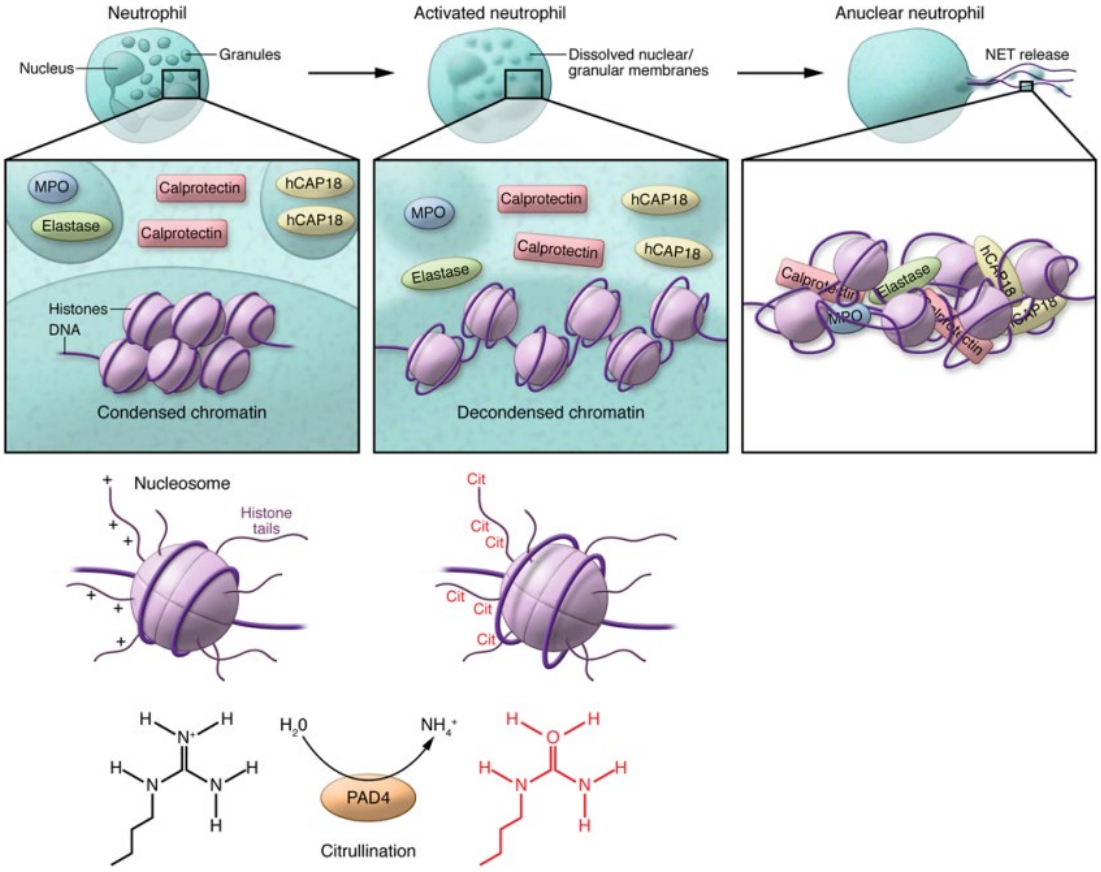

Figure 3 Process of NETs formation. See Ref[68]

There is a large body of evidence showing that the generation of NETs is essential to the incidence of carcinoma. Some murine models with cancer injections have suggested that when microorganisms such as bacteria enter the blood stream or tissue injury by surgery is sensed, NETs will be produced and released in the circulation system, which in turn promotes the formation of distant metastasis. NETs can catch tumor cells.[69, 70] NETs within the blood vessel were shown to increase the vessel permeability, facilitating for tumor cells to diffuse out of the blood stream. What's more, NETs facilitate the process of epithelial-to-mesenchymal transition through degeneration of vascular endothelial cadherin and the promotion of the β-catenin signalling pathway.[71] In contrast, Millrud *et al.* suggested that the amount of

recruitment of neutrophils that has a strong ability to secret NETs, was accompanied by better survival in patients with head and neck squamous cell carcinoma,[72] which suggests, to some extent that, NETs had killed the tumor cells. Based on abundant studies which focus on the function of NETs in tumor formation, it is widely accepted that NETs are crucial in the process of development of primary tumors, tumor cell extravasation and distant metastasis; whereas, whether the function of NETs is pro- or anti- metastatic is still not clear and needs to be further investigated.

1.7 Extracellular vesicles (EVs)

1.7.1 Overview of extracellular vesicles

EVs are small globular particles encircled by a lipid bilayer with different diameters (from 30 nm to a few μm), which can be secreted by any type of cell and can be detected in all body fluids. EVs can perform multiple biological functions and can affect the microenvironment by the horizontal transfer of bioactive molecules such as proteins, lipids, DNA, and RNA.[73, 74] The description of EVs began in the late 1960s and researchers found that EVs could affect coagulation or to contain calcification-inducing factors in plasma or bones.[75, 76] In the 1970s and 1980s, terms like microparticles,[77] microvesicles,[78, 79] 'membrane fragments'[80] and 'membrane vesicles' [81, 82] were used to depict vesicles produced by cultured tumoral and non-tumoral cell lines. At that time, EVs were assumed to be released by outward budding of the cells' plasma membrane. In the early 1980s, a more complex EVs secretion pathway was described, in which vesicles initially formed intracellularly

within so-called multivesicular endosomes (MVE) or multivesicular bodies (MVBs) from which they were subsequently secreted. After then, the word exosomes was used to describe EVs released from MVE.[83] During the end of 1990s, two studies on antigen-presenting cells appeared, revealing that the existence of surface molecules on exosomes may play a part in the signalling pathway in acceptor cells; therefore, they not merely function as 'dust bins', but are messengers in pathway signaling as well; surprisingly, before that, MVs and other shed membrane vesicles have been studied for their functions in cell-cell communications for quite a long time.[84, 85]

1.7.2 Role of EVs in tumor growth and metastasis

Tumor cells can release several types of EVs, which differ in terms of size, biogenesis and molecular compositions. Specifically, these are exosomes, which are nano-sized EVs (30-100 nm) that are derived from MVBs and released by fusion with the plasma membrane. MVs are larger EVs than exosomes and are derived from the surface of cells. They originate from the plasma membrane. Apoptotic bodies are particles of a relatively large size (1-4 μm), and are released by apoptotic cells. Finally, large oncosomes (LOs), which are representative of an extra type of EVs originated from tumor cells, possess an atypical larger size compared to the particles previously mentioned and are rich in tumor cell-derived nucleic acids. [83, 86-88]

The formation of LOs is especially easily detected in highly migratory, aggressive tumor cells with an amoeboid phenotype.[88, 89] They are products of non-apoptotic cell membrane blebs used by amoeboid cells as promoters of migration.[90] Measurements

of the LOs size have uncovered that though the LOs diameter vary from 1 to 10 μm, the average diameters is 3–4 μm. LOs can only be produced by tumor cells, and the very little expression level in non-tumor cells can be neglected. LOs detachment can be detected commonly in distinct kinds of tumors, including prostate, breast, bladder, and lung cancer. To date, LOs have been successfully detected in the blood stream of mice and patients with metastatic prostate cancer, indicating that LOs may be a potential candidate for clinical biomarkers of tumor diagnosis.[89, 91]

Recent studies suggest that interactions between EVs and cells in the tumor microenvironment are significant for tumor progression and metastasis. Cancer associated fibroblasts (CAFs) are one of the most frequent cell type in the tumor microenvironment. Upon exposure to cancer cells, CAFs change their phenotypes.[92] In turn, when CAFs get in touch with tumor cells in cell culture media, they will become increasingly aggressive, which might depend on CAF-induced stemness and metabolic reprogramming.[93] Tumor cells and fibroblasts can both produce a variety of EVs, which take part in the reciprocal interaction with the two cells, and this plays a significant part in tumor progression.

It is currently assumed that exosomes produced by tumor tissues can regulate the structure of stroma to support the progression of tumors by providing nutrition support from the blood stream and by promoting proliferation of transformed cells.[94] Furthermore, some tumor exosomes can induce fibroblasts to differentiate into CAFs, which strengthen the aggressiveness of tumor cells. More and more focus has been placed on the role of cancer-derived microvesicles on the tumor microenvironment.

Tumor microvesicles have been regarded as enhancers of the proteolytic cascade allowing cancer cells to degrade the extracellular matrix and invade the surrounding environment.[95] Antonyak and colleagues demonstrated that microvesicles, generated from various human cancer cells (like breast carcinoma and glioma cells) can alter the characteristic of normal fibroblasts and prolong their survival which is similar to the transformed cells.[96]

The interactions between tumor cells and immune cells are also important for the emergence of the tumor microenvironment. Immune cells can capture EVs originating from tumor tissues, resulting in either immune escape or immune suppression. Which subsets of EVs regulate the immune system, and the detailed functional mechanisms at the molecular level underlying the transfer and immune cell modulation by receptors, proteins, RNA, and DNA carried in EVs, are still largely unclear. Nevertheless, the education of immune cells by cancer-generated EVs, might be target for the preparation of cancer vaccines and for investigations of novel cancer therapies. Monocytes are an acceptor cell for cancer-generated EVs in the tumor microenvironment. Baj-Krzywirzeka and colleagues[97] have identified a series of cell surface markers and mRNA transcripts in EVs from pancreatic adenocarcinoma (HPC-4), colorectal carcinoma (DeTa) and lung carcinoma (A549) cells and they have found that IL8, VEGF, HGF, and CD44 mRNA were expressed at high levels in EVs, suggesting a profound functional significance for these signaling mediators in monocyte re-education. Moreover, the communication of EV cell surface proteins with monocytes alters the production level of CCR6 and CD44 and activates Akt,

causing more chemotaxis and longer cell survival. This may lead to the migration of monocytes into the tumor tissue, where monocytes can differentiate into tumor-associated macrophages (TAMs) and support tumor formation, amplify local tumor progression, and facilitate distant metastasis.[98] The invasion and persistent colonization of tumor MVs in liver tissue can be regulate by CD36, a lipid receptor, which has already shown to mediate the engulfment of cancer MVs by myeloid cells.[99]

Angiogenesis is an important step in cancer progression. Construction of the tumor vascular network is rather important for sustained signaling of cell proliferation because tumor cells absorb oxygen and nutrients and eliminate useless metabolite via the blood channel. When distant metastasis is undergoing, the support of vasculature seems more indispensable for the tumor cells because it helps tumor cells get into the blood vessels and eventually settle down in another organ. Noticeably, exosomes produced by tumor tissues comprise key pro-angiogenic factors closely related to endothelial cell migration and the newly-born blood vessel formation, such as Vascular Endothelial Growth Factor (VEGF), which is overexpressed in the majority of tumors.[100] Recent studies have demonstrated that tumor exosomes contribute to angiogenesis by transferring also mRNAs[101].

1.8 Mediators of tumor cells extravasation

1.8.1 Ang/Tie signaling pathway

Angiopoietins, ligands of the Tie-2 receptor, which is a tyrosine kinase receptor

composed of immunoglobulin and epidermal growth factor homology domains, control blood vessel development and stability.[102] So far, four different angiopoietins have been discovered: Ang-1, Ang-2, Ang-3 and Ang-4. As shown in figure 4, the angiopoietins generally consist of an N-terminal super clustering domain (SCD), a central coiled-coil domain (CCD) for ligand homo-oligomerization, a linker region, and a C-terminal fibrinogen-related domain (FReD) for binding to the Tie-2 receptor. Ang-1 and Ang-2 can form dimers, trimers and tetramers. Moreover, Ang-1 can assemble into higher order multimers via its SCD. Tie-2 can be only activated by tetrameric or higher multimeric forms of Ang-1. Oligomeric Ang-2 can be a weak agonist of Tie-2.[103, 104]

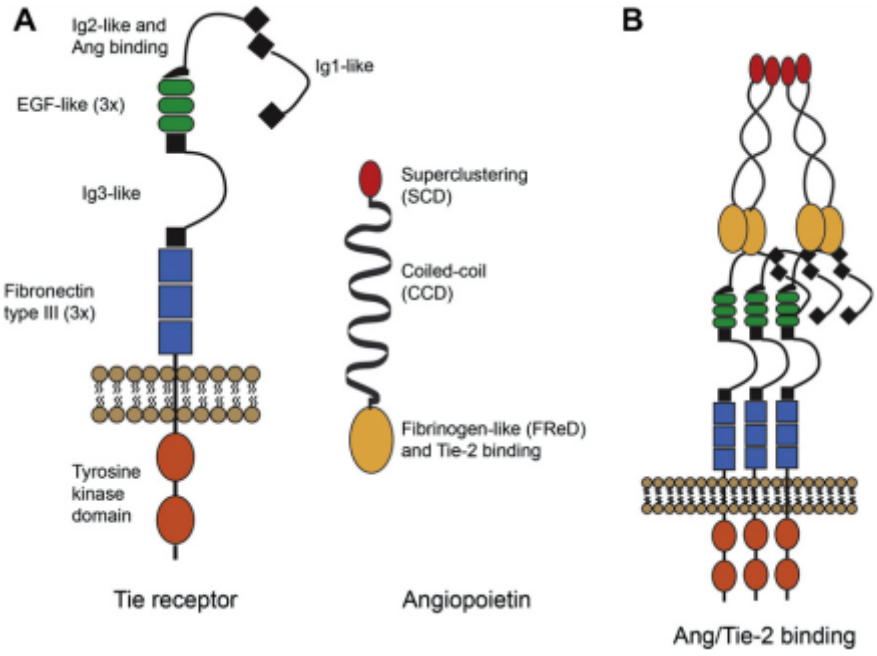

Figure 4 Structure of Tie-2 receptor, Angiopoietin and Ang/Tie-2 binding. Ref [105].

The Ang/Tie-2 signaling is essential for blood vessel remodeling and for the recruitment of vessel wall cells and blood vessel maturation during embryonic development and adult vessel homeostasis.[106] Ang-1 is predominantly expressed in

perivascular cells such as pericytes, vascular smooth muscle cells, fibroblasts and tumor cells.[107, 108] After binding of Ang-1 to Tie-2 receptor, Tie-2 receptor is activated, which can further stimulate numerous downstream intracellular signaling pathways. Consequently, it will promote the survival of endothelium cells (ECs), the maintenance of an endothelium barrier and a quiescent vasculature.[109, 110] Ang-2 is mainly produced by ECs and its expression is manipulated by various growth factors at the mRNA expression level.[111, 112] Ang-2 is usually preserved in endothelial Weibel-Palade bodies and can be quickly secreted in response to phorbol esters, thrombin, and histamine. Ang-2 seems to work mainly as an antagonist for Ang-1 by replacing the more active ligand Ang-1 from the Tie-2 receptor.[113] Ang-2 can destabilize the endothelium in an autocrine manner and this effect can be counteracted by Ang-1. Therefore, the ratio of Ang-1 to Ang-2 is critical in balancing Tie-2 receptor mediated signaling and regulating vascular homeostasis.[114]

1.8.2 Ang/Tie-2 signaling and tumor progression

It is still controversial whether Ang-1 and Ang-2 can contribute to tumor growth or tumor-induced angiogenesis. The expression of Ang-1 is upregulated in different types of cancers, while a clear correlation with tumor malignancy has never been shown. Moreover, overexpression of Ang-1 in different tumor cells and in tumor models can have different effects. In some cases, the growth rates have been dramatically increased. In contrast, they are reduced in other cases.

It is generally accepted that Ang-2 expression is elevated in many human cancers and

high serum expressions of Ang-2 correlate with increased blood vessel density in tumors, tumor metastasis and a poor survival rate. A number of studies carried out in several pre-clinical murine animal models have shown that blocking Ang-2 inhibits tumor growth and tumor blood vessel sprouting.[115] Additionally, blocking Ang-2 ameliorates tumor lymphangiogenesis and improves the "normal" vessel phenotype by increasing pericyte coverage and the levels of adhesion molecules in EC-EC junctions. Blocking Ang-2 also reduces tumor metastasis by inhibiting early metastatic growth and by improving blood capillary EC junctions, thereby inhibiting tumor cell extravasation into the lungs.[116, 117]

2. Objectives of the thesis

As previously referred to, patients with tumors are more likely to develop thrombotic diseases.[31, 35] Thus, anticoagulant therapies are usually employed to prevent these complications. It is still unclear, what kind of role blood coagulation plays in tumor extravasation and metastasis. The following questions will be addressed in this thesis.

1. What are the mechanisms of tumor-induced blood coagulation and which role do they play in tumor cell extravasation and metastasis?
2. How does host-induced blood coagulation in response to circulating tumor cells affect tumor cell movements and what are the underlying mechanisms?
3. What are the effects of EVs, in particular of LOs, on the prometastatic effects of tumor cells?

3. Materials and methods

3.1 Materials

3.1.1 Equipment

Items	Company, Type
Balance MC1 LC 620 S	Sartorius (Göttingen, D)
Cell culture incubator	Binder, Serie C
Cell culture microscope	Zeiss, Axiovert 100
Count chamber Neubauer Improved	Brand (Wertheim, D)
Culture Hood	ThermoScientific™ MSC-Advantage™
Pipet boy	Integra-Bioscience (Biebertal, D)
Serological pipette (5ml, 10ml, 25ml)	Omnilabs
Micropipettes (10µl, 20µl, 100µl, 200µl, 1000µl)	Eppendorf (Hamburg, D)
Centrifuge (Mikro 22R, Rotina 35R, Universal 32)	Hettich
Ultracentrifuge	Beckman, Optima™, LE-80K
Thermomixer R	Eppendorf
Electrophoresis unit	Invitrogen, XCell *SureLock*® Mini-Cell und das XCell II™ Blot-Modul
Electrophoresis power supply	BIO-RAD, POWER PAC 300
Film development machine for Western Blot	CURIX60, AGFA

Multi-Mode Detection Platform	SpectraMax, Molecular Devices
Cryotome Machine	Leica CM3050
LSM 510 Meta	Zeiss (Jena, D)
Lamin Air flow HLB 2472	Thermo Scientific (Braunschweig, D)
Thermocycler	Applied Biosystems™
Nano Drop	Thermofisher
Real-Time PCR Detection System	BIO-RAD
pH meter	HANNA instruments HI 221
Thrombelastograph	RoTEG Dynabyte
Items	Company, Type
Vortexer	Sartorius (Göttingen D)
Water bath Julabo U3	Julabo Labortechnik (Allentown, USA)

3.1.2 Kits

Item	Company	Catalog number
Antibody Labelíng Kit Alexa488	Life/Thermo	A-20181
Antibody Labeling Kit, Alexa555	Life/Thermo	A-20187
Plasmid Maxi Kit (10)	Qiagen	12362
High-Capacity RNA-to-cDNA™ Kit	Thermofisher	4387406

3.1.3 Primary antibodies

Antibody	Reactivity	Concentration	Host	Company	Catalog number
CD4	mouse	1:100	rat	Biolegend	100442
CD8a	mouse	1:100	rat	Biolegend	100702
CCR3	mouse	1:250	rabbit	Cell Singaling	9664
CD45	mouse	1:50	rat	AbD Serotec	MCA1031GA
MPO	mouse	1:100	rabbit	abcam	ab9535
Anti-Histone H3	mouse	1:100	rabbit	abcam	Ab18521
Angiopoietin I	mouse	1:400	rabbit	abcam	ab8451
Angiopoietin II	mouse	1:400	rabit	abcam	ab8452
ß-actin	mouse	1:3000	rabit	abcam	ab179467
PADI4	mouse	1:1000	rabbit	Sigma-Aldrich	SAB2101710
SLC9A2	mouse	1:1000	rabbit	Invitrogen	TK2678666
mNKp46	mouse	1:500	goat	Biolegend	AF2225
FXII	mouse	1:250	rabbit	Invitrogen	PA5-76120
TF (1H1)	mouse	1:50	rabbit	Gentech-Roche (Rotkreuz, CH)	18350-01
CX3CR1	mouse	1:100	rabbit	Novus Biologicals	bs-1728R
CX3CR1-FITC	mouse	1:100	-	Biolegend	149020
F4/80	mouse	1:200	rat	Biolegend	123102
Fibrin	mouse	1:100	mouse	WAK	NYBT2G1
Ly6C	mouse	1:400	rat	Thermofischer	1804

Ly6G	mouse	1:50	rat	BD Biosciences	551459
Mouse IgG	mouse	2µg/ml	mouse	Vector	BA9200
Rabbit IgG	rabbit	2µg/ml	rabbit	Vector	I-1000
Rat IgG	mouse	2µg/ml	rat	Vector	I-4000
GAS6	mouse	1:50	rabbit	Santa Cruz	sc-376087
Stabilin II	mouse	1:100	mouse	Invivo Biotech	AK2810/01

3.1.4 Secondary antibodies

Antibody	Reactivity	Concentration	Host	Company	Catalog number
Alexa488	mouse	1:1000	donkey	Life Technologies	1915874
Alexa488	rat	1:1000	goat	Life Technologies	1814724
Alexa488	rabbit	1:1000	goat	Life Technologies	1937195
Alexa448	goat	1:1000	donkey	Life Technologies	A32841
Alexa546	mouse	1:1000	goat	Life Technologies	1809360
Alexa546	rat	1:1000	goat	Life Technologies	1848462
Alexa546	rabbit	1:1000	goat	Life Technologies	1904467
Alexa594	mouse	1:1000	goat	Life Technologies	1579585
Alexa594	rat	1:1000	goat	Life Technologies	A11007
Alexa594	rabbit	1:1000	goat	Life Technologies	1981132
IgG-HRP	rabbit	1:5000	chicken	Santa Cruz	Sc-2955

3.1.5 Buffers

Blocking buffer

1x PBS

0.1 % Tween 20

2% / 5 % / 10% BSA (as per protocol)

$CaCl_2$ (Faktor Xa Formation; 50ml)

225 mg CaCl2 .2H2O

ddH2O

Ca/Hepes (TEG)

10 mM Hepes

100 mM CaCl2,

ddH2O, pH 7,4

$ZnCl_2$ (Factor XIIa Formation)

10 mM $ZnCl_2$

ddH_2O

PBS (Phosphate Buffered Saline) (1L)

8 g NaCl

0.2 g KH2PO4

1.42 g Na2HPO4.2H2O

0.2 g KCl

Permabilisation/ Blocking-Buffer

0.5 % BSA

0.1 % Triton _

Sterile filtered

TNC (Tri-Nitrium Citrate for blood drawing)

3.68 g TNC

100 ml ddH_2O

Sterile filtered

SDS-PAGE running buffer (1L)

50ml NUPAGE SDS MOPS 20X

950ml ddH_2O

Resuspension buffer (1L)

138 mM NaCl

2.7 mM KCl

12 mM NaHCO3

0.4 mM NaH2PO4

1 mM MgCl2.6H2O

5 mM D-Glucose

5 mM Hepes

pH 7.35

Tryphan Blue in PBS (cell counting and LOs counting)

0.4% Tryphan blue

1 mM Ca^{2+}

ddH_20

SDS-PAGE transfer buffer (250ml)

12.5 ml NUPAGE Transferbuffer 20X

250 µl NUPAGE Antioxidant

50 ml Methanol

ddH_2O

Blocking buffer for WB membrane (1L)

100 ml 10X TBS

1 ml Tween 20

50 g non-fat dry milk (BSA)

900 ml distilled water

Filter with 0.2 mm Whatmann filter paper

Washing buffer for WB membrane (1L)

100ml 10X TBS

3 ml Tween 20

3.1.6 Cell lines

Cell Line ID	Sample location	Host	Genomic Kras status
5320	Primary pancreatic tumor	mouse	CN-LOH
16990	Primary pancreatic tumor	mouse	het
S134	Primary pancreatic tumor	mouse	amp-focal
53631	Primary pancreatic tumor	mouse	amp-arm
8028	Primary pancreatic tumor	mouse	CN-LOH
8182	Primary pancreatic tumor	mouse	het
8305	Primary pancreatic tumor	mouse	amp-arm
8570	Primary pancreatic tumor	mouse	CN-LOH
8661	Primary pancreatic tumor	mouse	amp-arm
9091	Primary pancreatic tumor	mouse	CN-LOH
9203	Primary pancreatic tumor	mouse	het

3.1.7 Mouse models

C57BL/6 M/F 21-25 G ca. 8+ weeks	Charles River
C57BL/6J-F12^{tm1}, M/F 21-25 G ca. 8+ weeks	Institute of Experimental Biomedicine Chair I, University of Würzburg, Germany
C57BL/6Nur77$^{-/-}$, M/F 21-25 G ca. 8+ weeks	Department of Physiology, University of Santiago de Compostela, Spain

3.1.8 Reagents and chemicals

Item	Company	Catalog number
Aceton 99,5% PA	Carl Roth	9372.2
Acrylamide bis-Acryl	Sigma-Aldrich	A3699
Beriplex	CSL Behring	Apotheke
Cell culture Flasks: 175cm^2 straight neck	BD Pharmingen	353112
Cell culture Flasks: 25cm^2 straight neck	BD Pharmingen	353107
Chromogene Substrate S-2222	Haemochrom Diagnostic	41201
CTI (Corn Trypsin Inhibitor)	Calbiochem	650345
DAKO Pen für Immunocytochemie	Dako Cytomation	S200230
Desirudin (S.cerevisiae) AFl 15mg	Inresa	REVASC
DMEM 1g/l Glucose	Life/Thermo	31885-023

DMEM 4.5g/l Glucose	Life/Thermo	41965-039
DMSO Hybri-Max	Sigma-Aldrich	D2650
Duramycin-LC-Biotin	Mol. Targeting Techn.	D-1003
Essigsäure / Acetic acid	Carl Roth	3738.1
Ethanol Vergällt 99,8%	Carl Roth	K928.3
FBS	Thermofisher	10270106
Freezing Medium	Ibidi	80023
Gelantin 2% Solution	Sigma-Aldrich	G1393-20ML
HCl REINST 37%	Carl Roth	9277.1
Kaliumhydroxid Potassiumhydroxid	Carl Roth	3904.1
Lipofectamine 3000 Reagent	Life/Thermo	L3000008
Mayer´s Hematoxylin	Science Service GmbH	26381-02
MEM alpha Medium	Life/Thermo	22571-020
Methanol reinst >99,5%	Carl Roth	CP43.4
Multiwell: 12-well	BD Pharmingen	353225
Multiwell: 24-well	BD Pharmingen	353226
Multiwell: 6-well	Omnilab	353046
Multiwell: 96-well	BD Pharmingen	353072
NaCl 1KG	Carl Roth	P029.2
NaOH Plätzchen	Roth	041300
Objektträger SuperFrost	Omnilab	J1800AMNZ

OPTI-MEM(1X) + L-GL.	Life/Thermo	31985-047
PBS	Sigma-Aldrich	D8537
Penicillin/Streptolysin (100X)	Invitrogen	15140-122
Pipette serol, Wattestopf.einzeln 10ml	Omnilab	4488 5380582
Pipette serol, Wattestopf.einzeln 5ml	Omnilab	4487 606180
Poly-L-Lysine Solution	Sigma-Aldrich	P8920-100ML
Protease Inhibitor Set 10 Stk	Roche	11206893001
Protein Assay Reagent A	BioRad	500-0113
Protein Assay Reagent B	BioRad	500-0114
Puromycin DIHCI	VWR	540411-25MG
Eppi-Cup Safe-Lock farbl. 1,5ml	Eppendorf	0030120086
Eppi-Cup Safe-Lock farbl. 2ml	Eppendorf	0030120094
Roteg-Küvetten (Cup and Pin pro) 2	Rotem	200011
Sodium Carbonate Anhydrite	Sigma-Aldrich	S7795-500G
SYTO 62	Life/Thermo	S11344
Thromborel S 400T	Siemens Healthscare	OUHP29
Tissue Tek T-TEK	Hartenstein	TTEK
Trypan Blue	Carl Roth	CN76.1
Trypsin-EDTA Solution (10X)	Sigma-Aldrich	59418C
Tween20 (Polyoxethylene)	Sigma-Aldrich	P1379-100ML
Vectashield Hard Set with DAPI	Linaris	H-1500

Vectashield with DAPI	Enzo/Life/Thermo	VC-H-1200-L010
Water Tissue culture tested	Sigma-Aldrich	W3500-500ML
$ZnCl_2$	Sigma-Aldrich	208086-5G
Human FXII	HTI	GG-1218
Chromogene Substrate S-2302	Haemochrom Diagnostic	41205
R428	Selleckchem	S2841
FXII deficient plasma	CellSystems	561404
FVII deficient plasma	Siemens Healthscare	504740
NucleoZOL	MACHEREY-NAGEL	740404.200
RNase-free water	Invitrogen	AM9935
2-Propanol	Sigma-Aldrich	278475
PowerUp™ SYBR™ Green Master Mix (2X)	Applied bio systems	A25741
Actb Mouse qPCR Primer Pair	ORIGENE	NM_007393
Gapdh Mouse qPCR Primer Pair	ORIGENE	NM_008084
Padi4 Mouse qPCR Primer Pair	ORIGENE	NM_011061
Slc9a2 Mouse qPCR Primer Pair	ORIGENE	NM_001033289
pLKO.1-puro Padi4 shRNA Plasmid DNA	Sigma-Aldrich	04241817MN
pLKO.1-puro Non-Target shRNA Control Plasmid RNA	Sigma-Aldrich	SHC016-1EA

Silencer™ Pre-designed SLC9A2 siRNA	Thermofisher	284094
Silencer™ Negative Control siRNA	Thermofisher	AM4635
NuPAGE™ 4-12% Bis-Tris Protein Gels	Invitrogen	NP0335BOX
RIPA Lysis and Extraction Buffer	Thermofisher	89901
Protease Inhibitor	Thermofisher	36978
NuPAGE™ Antioxidant	Invitrogen	NP0005
NuPAGE™ MOPS SDS Running Buffer	Invitrogen	NP0001
NuPAGE™ Transfer Buffer	Invitrogen	NP00061
SuperBlock™ (TBS) Blocking Buffer	Thermofisher	37535
Pierce™ ECL Western Blotting Substrate	Thermofisher	32106
ECL™ Prime Western Blotting System	Sigma-Aldrich	GERPN2232

3.1.9. Primer for Qpcr

gene		Sequence (5’-3’)
Mus GAPDH	F	GATCATCAGCAATGCCTCCT
	R	TGTGGTCATGAGTCCTTCCA
Mus β-Actin	F	ACCAACTGGGACGACATGGAG
	R	TAGCACAGCCTGGATAGCAAC
Mus Gapdh	F	CATCACTGCCACCCAGAAGACTG
	R	ATGCCAGTGAGCTTCCCGTTCAG
Mus Actb	F	CATTGCTGACAGGATGCAGAAGG
	R	TGCTGGAAGGTGGACAGTGAGG
Mus Slc9a2	F	GTGTCCACTGTTGGGAAGAACC
	R	ACTGGTCCTTGAAGGTTAGCGG
Mus Padi4	F	ACGCTGCCTGTGGTCTTTGACT
	R	ACCTCCAGGTTCCCAAAGGCAT

3.2 Methods

3.2.1. Animal experimentation protocol

Mice were in general purchased from Charles River Laboratory and housed under specific pathogen free conditions at the animal facility of Walter Brendel Centrum. The mice used for all experiments were aged from 9 weeks to 14 weeks. Mice were sacrificed by strangulating the neck and subsequently the organs were collected. All experiments involving mice were conducted with approval by the local Animal Experimentation Committee (Regierung of Oberbayern, Munich). All experiments were performed in accordance with the ARRIVE guidelines and regulations.

3.2.2. Injection protocols

The animal experiments were performed as described in Figure 5. In brief, 2×10^6 of cancer cells were suspended in 350 µl of PBS and subsequently used for i. v. injection. For metastasis experiments, 500 µl solution of Matrixgel (Matrixgel : PBS=1:1) containing 2×10^5 cells were injected into the spleen capsule as described in Figure 6. Mice were sacrificed at the indicated time points, and the organs were collected for further analysis.

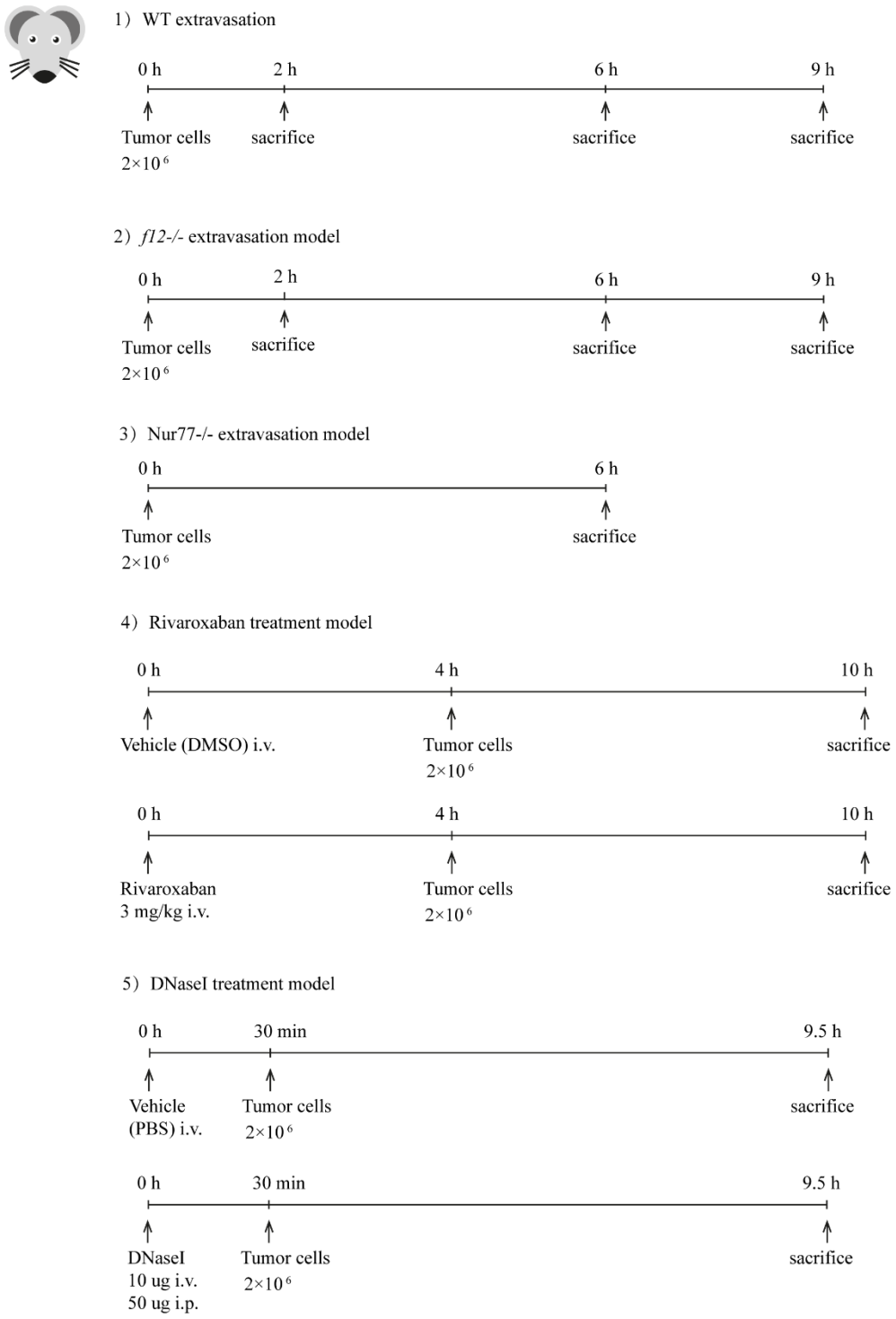

Figure 5 Time schedule of animal experiments with different mouse models

Figure 6 Time schedule of metastasis experiment. Picture shows the spleen capsule injection

3.2.3 Preparation and storage of organs

Organs were isolated from mice and washed with PBS twice at room temperature to remove traces of blood and other contaminants. Fixation of the organs was performed in 4% formalin solution for 2 h, and subsequently transferred to 30% sucrose solution for incubation overnight. All organs were stored at -80˚C before use.

3.2.4 Cryosections

Cryosections were obtained using a cryostat to freeze the tissue and to cut the frozen tissue for microscopic analyses. During the procedure, the rapid freezing of the tissue sample converts the water into ice that acts as embedding medium to cut the tissue [118]. The tissues were stored at -80˚C one day before being sectioned. The procedure of cryosections was performed strictly according to the instructions and resulted in sections ranging from 5-19 μm. The slides were stored at -20˚C.

3.2.5 Paraffin embedded sections

The tissues were collected in plastic embedding cassettes and fixed in 4% formalin overnight, after which the cassettes were washed with distilled water. Then, the samples cassettes were incubated in a container with 70% ethanol for 1 day. Dehydration, clearing, and wax infiltration were done by an automated tissue processor. Finally, the tissues were manually embedded in paraffin. The paraffin embedded tissues were cut into 4 μm thick sections by a microtome.

3.2.6 Cell culture

The basic principle of the technique is to maintain cells isolated from various tissues of animals in an artificial (in vitro) environment that is suitable for cell viability and growth [119]. The culturing conditions differ with every cell line. KCP cell lines were isolated from the pancreas of genetically modified mice that produce spontaneous metastasis, and were maintained in a high glucose/Dulbecco`s modified Eagles medium (DMEM, 4.5g/l) containing 2.5% NEAA and 10% fetal bovine serum (FBS). The primary pancreatic tumor-derived cell lines used were: 5320, 16990, S134, 53631, 8028, 8182, 8305, 8570, 8661, 9091 and 9203 (kindly provided by Prof. Dr. Roland Rad (Technical University, Munich)), and were cultured in DMEM medium containing 10% FBS. The cells were grown in cell culture flasks of various sizes containing appropriate amounts of culture medium as stated in the catalogue. All cells were cultivated in presence of 100 units/ml penicillin and 0.1 mg/ml streptomycin at 20% O2, 5% CO2 and 37°C.

3.2.7 Splitting of cells

The Trypsin-EDTA solution and media were pre-warmed in a 37°C waterbath. The culture medium was removed from the flask. Enough sterile PBS (5 ml for 25 cm^2 flask, 10 ml for 75 cm^2 flask) was added into the flask to wash the cells and to remove any residual FBS in the culture media. The flask was tipped gently for a few times to rinse the cells and carefully remove the PBS. Appropriate amounts of trypsin-EDTA solution were added to cover the cells at the bottom of the flask, and incubated at 37°C for 2-7 min until the cells were detached completely. Different cell lines required different trypsinization times. To avoid over-trypsinization that can severely damage the cells, it was essential to check the cells' shape every few minutes. As soon as the cells were detached, full medium containing FBS was added to the flask to inactivate the trypsin. The trypsinised cells were collected in falcons and subjected to centrifugation at 1,500 rpm for 5 min. After removal of the suspensions, the cell pellet was re-suspended in PBS and pipetted into new flasks with full medium at the required split ratio (approx. 1:10). Cell counting was performed using Neubauer's chamber before the experiments and the appropriate number of cells were seeded in respective plates. Media were changed every two days. To change the medium, the media were carefully removed from the flask into a waste pot, the medium was replaced with fresh pre-warmed culture medium. The compositions of the different media are described in 3.2.6.

3.2.8 Preparation of cell stocks

Cells were collected in falcons and washed twice with ice-cold PBS. After centrifugation at 1,500 rpm for 5 min, the supernatant was removed by gently pipetting. The cell pellet was re-suspended in Cryoprotectant Medium (Ibidi Freezing Medium) to achieve a concentration of at least 2 x 10^6 cells per ml, after which the suspension was transferred into cryogenic tubes and stored in liquid nitrogen.

For cell recovery, cryo-preserved cells were rapidly thawed in water bath at 37°C, resuspended in 10 ml pre-warmed full medium and pelleted by centrifugation at 1,500 rpm for 5 min. After that, the cells were re-suspended in 5 ml of full medium and transferred into cell culture flask for further cultivation. The compositions of the different media are described in 3.2.6.

3.2.9 Isolation of plasmid

The plasmid was isolated by using the Promega kit that can be used to extract any plasmid from *E. coli* hosts. The kit works well when the size of plasmid is up to 20,000 bp. After isolation and purification, the plasmid was used for automated fluorescent DNA sequencing without further manipulation.

The LB medium in which the bacteria were grown was transferred to a 1.5 ml microcentrifuge tube. 100 µl of Cell Lysis Buffer was added and mixed by inverting six times. The color change of the solution from opaque to clear blue indicated complete lysis of the bacteria. The next step proceeded within 2 min. 350 µl of ice-cold Neutralization Solution was added and mixed thoroughly by inverting the

tube. The color of the solution changed to yellow when the neutralization was complete, and a yellow precipitate was formed. After the complete neutralization, the tube was centrifuged at a speed of 13,000g for 3 min. Subsequently, the supernatant resulting from the centrifugation was transferred to a PureYield minicolumn provided by the kit. The minicolumn was placed into a PureYield Collection Tube (provided in the kit), and centrifuged at maximum speed in a microcentrifuge for 30 sec. The flow through was discarded and the minicolumn was placed into the same PureYield Collection Tube. 200 µl of Endotoxin Removal Wash was added to the minicolumn, and centrifuged at maximum speed for 30 sec. The centrifugation was repeated again after addition of Column Wash Solution. Next, the minicolumn was transferred to a clean 1.5ml microcentrifuge tube, after which 30 µl of Elution Buffer was added directly to the minicolumn matrix and incubated for 1 min at room temperature. Finally, the plasmid was eluted by centrifugation for 20 sec. The isolated plasmid was stored in freezer until use.

3.2.10 Transient transfection

Lipofectamine 3000 was used for transfection of siRNA Slc9a2 (284094, Thermo Fisher Scientific) and control siRNA (AM4611, Thermo Fisher Scientific) according to the manufacturer's instructions. Cells were counted in Neubauer's chambers and appropriate numbers of cells were seeded in 6-well plates to attain a confluence of 70% - 80% before the start of transfection. All reagents were warmed up to room temperature before the start. 5 µl of Lipofectamine 3000 was diluted in 125 µl of Opti MEM reduced serum medium (solution A). The master mix of siRNA was prepared

by diluting siRNA in 125 µl of Opti MEM reduced serum medium, followed by adding 5 µl of P3000 reagent (solution B). The diluted Lipofectamine 3000 reagent (solution A) and the master mix of siRNA (solution B) were mixed at a ratio of 1:1. After 15 min incubation at room temperature, the mixture was drop-wise added to the cells in 6-well plate containing 2 ml DMEM medium with 10% fetal bovine serum and 1% antibiotics. Cells were harvested and subjected to western blot 48 h-72 h after transfection.

3.2.11 Stable transfection

Stable transfection for shRNA was performed in principle as described above for transient transfection. Briefly, after 48 h transfection the appropriate antibiotic (Puromycin) was used to select the transfected cells. In order to eliminate the non-transfected cells, the selection was initiated with 3 µg/ml of antibiotic, followed by increasing concentrations (3-20 µg/ml) until no more dead cell were observed. The selected cell pool was maintained in full medium containing 10 µg/ml antibiotic.

3.2.12 Puromycin selection

Cells expressing the puromycin-N-acetyl-transferase (*pac*) gene were selected by puromycin. The recommended working concentration range for puromycin was 0.5-10 µg/ml. Since the appropriate concentration of puromycin varies according to the cell type, cell survival curve was obtained to determine the optimal working concentration before the selection of pac-positive cells.

After transfection the cells were seeded in 0.5 ml full growth medium per well in a 24-well tissue culture plate. The cell density of the adherent cells was 20,000/ml, while the density for suspension cells was 40,000 cells/ml. Cells were cultured overnight to attain 70% confluency before adding increased amounts of puromycin. As for example, 0, 0.5, 1.0, 2.0, 3.0, 4.0, 5.0, 6.0, 7.0, 8.0, 9.0, and 10.0 μg/ml of puromycin was added to duplicate wells of cells in complete growth medium (Figure 7). For the no-antibiotic control, the same amount of distilled water was used. The culture medium containing puromycin was replaced every 2-3 days for up to 7 days. The signs of visual toxicity were examined every day, and three puromycin doses were determined: Low dose, optimal dose, and high dose. low dose, which means the puromycin concentration at which minimal visual toxicity is apparent after a week; optimal dose means the lowest puromycin concentration at which all cells were dead after a week; high dose means the puromycin concentration at which visual toxicity is evident within the first 2-3 days.

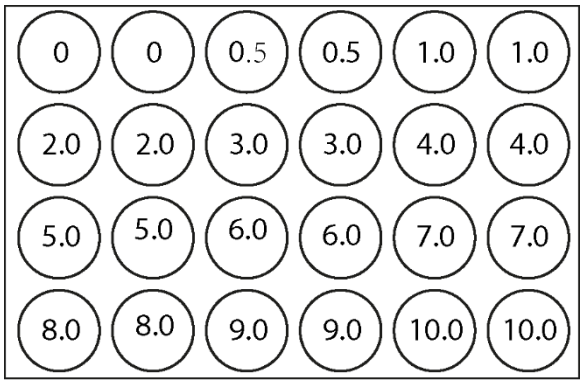

Figure 7 Antibiotic selection to obtain stable transfected cell line. Numbers refer to the concentration of antibiotics

3.2.13 Protein isolation

Protein for western blot was isolated as described previously [120]. In order to harvest

cells under nondenaturing conditions, cells were washed twice with ice-cold PBS. RIPA (Thermo Fisher Scientific, MA, USA) lysis buffer and a plastic cell scraper were used to harvest cells. After sonication, the lysates were centrifuged at 16,060 g for 20 min at 4°C in order to separate the protein from cell debris. Subsequently the supernatant containing protein lysate was transferred into a new tube.

3.2.14 Protein estimation

The concentration of soluble protein was estimated using the Bradford assay that is based on the reactions of protein with an alkaline copper tartrate and the folin.[121] The Bradford reagent (DC™ Protein Assay Kit I, Bio-Rad) was diluted in distilled water as per manufacturer's instructions. A standard protein solution of 2 mg/ml BSA was used to prepare serial dilutions ranging from 2 mg/ml to 0.03906 mg/ml of BSA (Figure 8). 500 µl PBS was used to re-suspend the samples. All samples and standards were analysed in triplicate and a negative control was included. 5 µl of the standards and samples were pipetted in triplicates onto 96-well plate. 25 µl of the alkaline copper-alkali-tartrate solution A, which forms a complex with the proteins in the suspension, was pipetted to each well before addition of 200 µl of folin solution B. After 15 min, the absorbance was read at 750 nm in a plate reader.

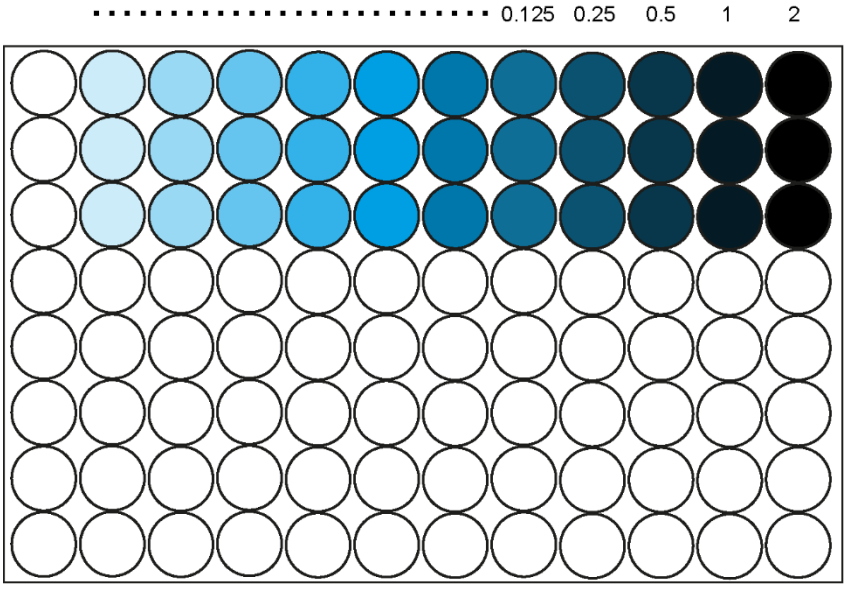

Figure 8 Serial dilutions of BSA. Numbers refer to the concentration of BSA

3.2.15 SDS-PAGE and Western blot

7.5% to 15% polyacrylamide protein gels were prepared depending on the size of the analyzed proteins and overlaid with 4% stacking gel. Subsequently, the cell lysate was mixed with loading buffer, and denatured at 95°C for 5 min. 20 µg of protein per sample was subjected to 7.5% to 15% SDS-acrylamide gels according to protein sizes. A commercial pre-stained protein ladder was used as size control.

Separation of the proteins by electrophoresis was performed at 80-120 V in an electrophoresis unit (Invitrogen) with NuPAGE™ MOPS SDS as running buffer. The separated proteins were transferred onto Immobilon PVDF membranes (Invitrogen) with NuPAGE™ Transfer buffer using the Invitrogen blotting system and a BIO-RAD power supply constantly held at 125 mA and a maximum voltage of 10 V.

In order to block unspecific protein binding, membranes were incubated for 1 h in 5% skim milk/TBS-Tween20 (TBS-T). Then, the membranes were incubated with the

primary antibodies (diluted in TBS-T) at 4°C overnight. After washing three times in TBS-T, the membranes were incubated with horseradish-peroxidase (HRP)-conjugated secondary antibodies for 1 h at room temperature. Then, 3 washing steps were conducted as described above. Enhanced Chemiluminescence (ECL, Thermofisher or Sigma) signals were recorded with film development machine for Western Blot (CURIX60, AGFA). The antibodies used here are listed in 3.1.3.

3.2.16 Isolation of EVs

EVs encompass vesicles that vary from 30 nm to 10 μm. Generally, the vesicles from non-apoptotic tumor cells are called large oncosomes (LOs) if the sizes of them are > 1 μm, which can be detected directly by light microscopy. Tumor cells were cultured in vesicle-free medium till confluence and then the media were changed. After 3 d of changing media, the media were pooled and subjected to an initial centrifugation at 350 g for 5 min (without brake). This was to remove the cells and their large debris. The supernatants were combined and centrifuged at 2,000g for 20 min (without brake). The pellets, which were suspended in PBS, while the supernatants were centrifuged at 100,000g for 2 h in an ultra centrifuge. The pellets were suspended in PBS and the EVs stored at -20℃.

3.2.17 Isolation and count of LOs

Tumor cells were cultured in vesicle-free medium till confluence and then the media were changed. After 3 d of changing media, the media were pooled and subjected to

an initial centrifugation at 350 g for 5 min (without brake). This was to remove the cells and their large debris. Then, the amounts of LOs could count by light microscopy.

3.2.18 Nanoparticle tracking analyses

Before the start of the analyses, the ZetaView PMX 110 instrument was calibrated by polystyrol beads of a known concentration and diameter (100 nm). Post-acquisition parameters were set to a minimum brightness of 5, a resolution of 100 pixels and the frame rate was 30 frames/s. The isolated EVs were resuspended in PBS and 1 ml of the resuspension was injected into the machine with a syringe. Different dilutions were made in each sample to make sure that in each visual field the amount of EVs ranged from 100 to 200 particles, which is the ranges where the optimal accuracy of the measurement is achieved. The samples were measured at 11 different positions during 3 cycles of reading. The amount of EVs was calculated by the machine and exported as pdf file.

3.2.19 FXa formation assay

The formation of FXa is measured by a chromogenic assay to evaluate the procoagulant activity of the extrinsic pathway of the blood coagulation cascade. We prepared serial dilutions of the standard Thromborel-S in a 96-well plate. In each well of this 96-well plate 50 µl of $CaCl_2$ (30mM) and 50 µl of standard or samples, which included 10,000 tumor cells dissolved in PBS, were added. A master mix of

chromogenic substance S-2222, Beriplex and the respective amount of resuspension buffer was prepared such that 100 µl of this mix was added to each well. S-2222 is cleaved by factor Xa which results in a color change that is detected at 405 nm. With the help of a plate reader (softMAXpro), the absorption was measured at 405 nm. Each 6 min, the absorption values were measured and the whole procedure lasted 6 cycles. The final value was calculated by the plate reader and expressed as milliunits (mU)/ml.

3.2.20 FXIIa formation assay

The formation of FXIIa is measured by a chromogenic assay to determine the procoagulant activity of the contact pathway of the blood coagulation cascade. 85 µl samples, which included 10,000 tumor cells dissolved in Hepes buffer, were incubated with 85 µl master mix, consisting of 100 nM FXII and 100 µM $ZnCl_2$, for 20 min at room temperature. In a 96-well plate, 10 µl of the chromogenic substrate S-2302 were added to each well and then 50 µl of the above mentioned samples were added. When S-2302 is cleaved by factor XIIa, this results in a color change that can be detected by ELISA detector at 405 nm. The plate reader (softMAXpro) measured the absorption of the samples for 120 min.

3.2.21 TEG

Thromboelastography (TEG) is a non-invasive method that quantitatively measures the global viscoelastic properties of whole blood clot formation [122]. The principle of

the TEG in vitro test is to detect and quantify dynamic changes of the viscoelastic properties during clotting under low shear stress. The procoagulant activities of microvesicles, oncosomes, or cancer cells were tested by this technique using whole blood as a medium. The test was performed in a specially designed TEG pin and cup apparatus. Briefly, 250 µl of whole blood containing 60 µl of a solution of 30 mM $CaCl_2$ and 30 µl of the sample with for example 10,000 tumor cells were added to each cup. The measurements were performed using the rotation thromboelastometry device from ROTEG.

3.2.22 Immunohistochemistry: Immunostaining of cryosections

Immunohistostaining is used to detect the localisation of specific antigens in tissue by the use of markers such as fluorescent dyes or enzymes based on antigen-antibody interactions [123].

Cryosections (10-15 µm) were fixed in 2%-4% of formalin for 15 min at room temperature, and subsequently washed three times with PBS. To reduce the non-specific immunostaining, a blocking step was performed with 2% BSA in PBS for 1 h at room temperature. After washing twice with PBS, the diluted primary antibody was added to the section and incubated in a humidified chamber overnight at 4˚C. The sections were rinsed twice with PBS, followed by an incubation with diluted secondary antibody for 1 h at RT. The excess of antibody was washed away with PBS. The sections were then mounted with glycerol and sealed with nail polish or mounting medium. The antibodies used here are listed in 3.1.3 and 3.1.4. The signals were

visualized with Confocal Laser Scanning Microscopy. Images were captured with a LSM700 microscope using the ZEN software (Zeiss).

3.2.23 Immunostaining of cells in suspension

Cells were harvested and centrifuged at 1,300 rpm for 5 min, and then re-suspended in PBS. The cell viability was counted using a Neubauer chamber with addition of trypan blue to identify dead cells. Cells with viability around 90%-95% were used for staining in sterile epicups. Then cells were fixed in 1% formaldehyde for 10 min at 37˚C, 200 µl PBS was added to the cells and a pellet was obtained by centrifugation at 1,300 rpm for 5 min. The pellets were re-suspended in PBS and centrifuged to remove the remaining formaldehyde. The primary antibody at an appropriate dilution, usually suspended in 200 µl PBS with 2% BSA, was added and the suspensions were incubated for 1-4 h at 37˚C with intermediate mixing. After incubation, the cells were washed three times with 200 µl PBS. The secondary antibody was diluted in PBS at a concentration of 2 µg/ml, and the cells were incubated with secondary antibody for 1 h at 4˚C in dark with intermediate vortexing. Then, the cells were washed three times with PBS and centrifuged at 1,300 rpm for 5 min, subsequently stored in 100 µl of PBS in the dark until microscopic analysis. In principle, the same procedure as described above for cells was used for staining of vesicles. The washing steps for the EVs were adjusted to the type of particles. Microvesicles were centrifuged at 12,600 rpm for 35 min whereas large oncosomes were centrifuged at 10,000 rpm for 35 min.

3.2.24 Immunostaining of adherent cells

Cells were seeded on glass cover-slides in a 6-well plate. After cell culture, the cells were fixed in 4% paraformaldehyde/PBS for 10 min, permeabilized in 0.2% Triton X-100 for 20 min and blocked in 100% FBS for 30 min. The primary antibody (in 200 µl PBS with 2% BSA) was added and incubated overnight with the samples. Then, the cells were washed three times with 200 µl of ice-cold PBS. The secondary antibody was diluted in PBS at a concentration of 2 µg/ml, and the cells were incubated with the antibody for 1 h at 4˚C in dark with intermediate vortexing. The cells were washed three times with PBS and centrifuged at 1,300 rpm for 5 min, and subsequently stored in 100 µl of PBS in the dark until microscopic analysis.

3.2.25 Staining with long-lived fluorophore

Cell-Tracker dyes (Invitrogen) were used for staining of tumor cells to monitor their movements and locations. The staining procedure was performed according the instructions. Briefly, 200 µl of PBS was used to suspend the tumor cells. A 40 µM working solution of the cell tracker dye pre-diluted from the stock was prepared in PBS and pre-warmed for 10 min at 37˚C. 200 µl of the dye solution was added to each cell sample to achieve a final concentration of 20 µM. The samples were mixed gently by pipetting and incubated at 37˚C for 30 min. After the incubation, the extra dyes were removed by centrifugation and washing of the cells with PBS. To be sure that the staining was successful, an aliquot of the stained samples was checked by fluorescence microscopy before injection.

3.2.26 Imaging and Image analysis

Imaging of immuno-histochemistry samples was performed by confocal laser scanning microscopy. Fluorescence pictures were taken by using a Zeiss 510-CLSM system and with argon lasers to generate lower wavelength light beams and a combination of three helium-neon lasers for wavelengths above 500 nm. Several versions of the ZEN software (Blue 2009/ 2011; Black 2012) were used to analyse the pictures.

3.2.27 Labelling of primary antibody

Alexafluor-mAb labelling kit was used to label primary antibodies that had been raised in mouse. In co-staining procedures, one pre-labelled primary antibody was used to facilitate the use of two antibodies raised in the same animal. The labelling was performed according to the instructions. 50-100 µg of antibody was incubated with the labelling reagent for 3 h at room temperature. In order to remove the extra dyes in the solution, the labelled antibody was recovered using Zeba spin columns equilibrated with the respective buffers according to the instructions of the manufacturer.

3.2.28 Total RNA extraction

Total RNA was extracted from the cells using the NucleoZOL reagent (MACHEREY-NAGEL, REF 740404.200) according to the manufacturer's instructions. Briefly, the cell culture medium was removed, followed by adding 500 µl

of NucleoZOL and 200 µl of RNase-free water, respectively. The samples were shaken vigorously for 15 s and incubated at room temperature for 5 min. In order to obtain the supernatant containing RNA, the samples were centrifuged at 12,000 g for 15 min. To precipitate RNA, 500 µl of supernatant was transferred to a fresh tube, and mixed well with 500 µl of isopropanol. After centrifugation at 12,000 g for 10 min, the supernatant was discarded. The white pellet at the bottom of the tube was washed three times with 70% ethanol (34852-M, Sigma) and the remaining ethanol was removed by pipetting. RNase-free water (AM9935, Invitrogen) was used to reconstitute RNA to obtain an RNA concentration of 1 µg/µl.

3.2.29 RNA reverse transcription

High-Capacity RNA-to-cDNA™ Kit (4387406, Thermo Fisher Scientific) was used for cDNA synthesis according the instructions of the manufacturer. 1 µg of total RNA isolated as described above was used for the reverse transcript reaction. The thermos cycle included 60 min incubation at 37°C, followed by a 65°C incubation for 10 min.

3.2.30 Quantitative real-time PCR (qPCR)

qPCR was performed with the PowerUp™ SYBR™ Green Master kit (A25741, Thermo Fisher Scientific) that is a pre-formulated, optimized, universal 2X master mix for real-time PCR workflows. 2 µl of cDNA per sample was used for the reactions. Expression of mRNA of the gene of choice was normalized to β-actin- or GAPDH-mRNA. The qPCR results were calculated using the ΔΔCt method[124].

Results are represented as fold induction of the treated/transfected condition compared with the control condition. All experiments were performed in triplicates. All qPCR primers are listed in 3.1.9.

3.2.31 Hematoxylin-eosin staining

Hematoxylin and eosin stain is the most widely used stain in medical diagnosis. The staining method involves application of hemalum, a complex formed from aluminium ions and oxidized hematoxylin [125]. Thereby nuclei are colored in blue. Subsequent counterstaining with an aqueous or alcoholic solution of eosin Y results in various shades of red, pink and orange. The tissues were hydrated in a series of decreasing concentration of ethanol, followed by incubation with Mayer's hemalum solution (Merck)/Hematoxylin for 5 min. In order to blue the stain, the slides were washed under running tap water for three times. Next, the tissues sections were stained with eosin solution and subsequently subjected to dehydration again to fix them. After that, the slides were mounted in glycerol.

3.2.32 Statistical analysis

Statistical analysis was performed using ANOVA with a post hoc Bonferroni correction for comparisons between multiple groups. Two-tailed unpaired T-test was performed for the comparisons between two groups. P-values < 0.05 were considered as significant. Asterisks generally indicate: *P < 0.05, **P < 0.01, ***P < 0.001 and ****P<0.0005. Mean values ± SEM (usually at least 3 biological replicates) are

provided.

4. Results

4.1 Whole transcriptome analysis of tumor cell lines

The RNA sequences of the 11 different pancreatic cell lines used in our study were compared. Analysis of the entire transcriptome of the cell lines was found to be overall identical as shown in the heatmap of Figure 9.

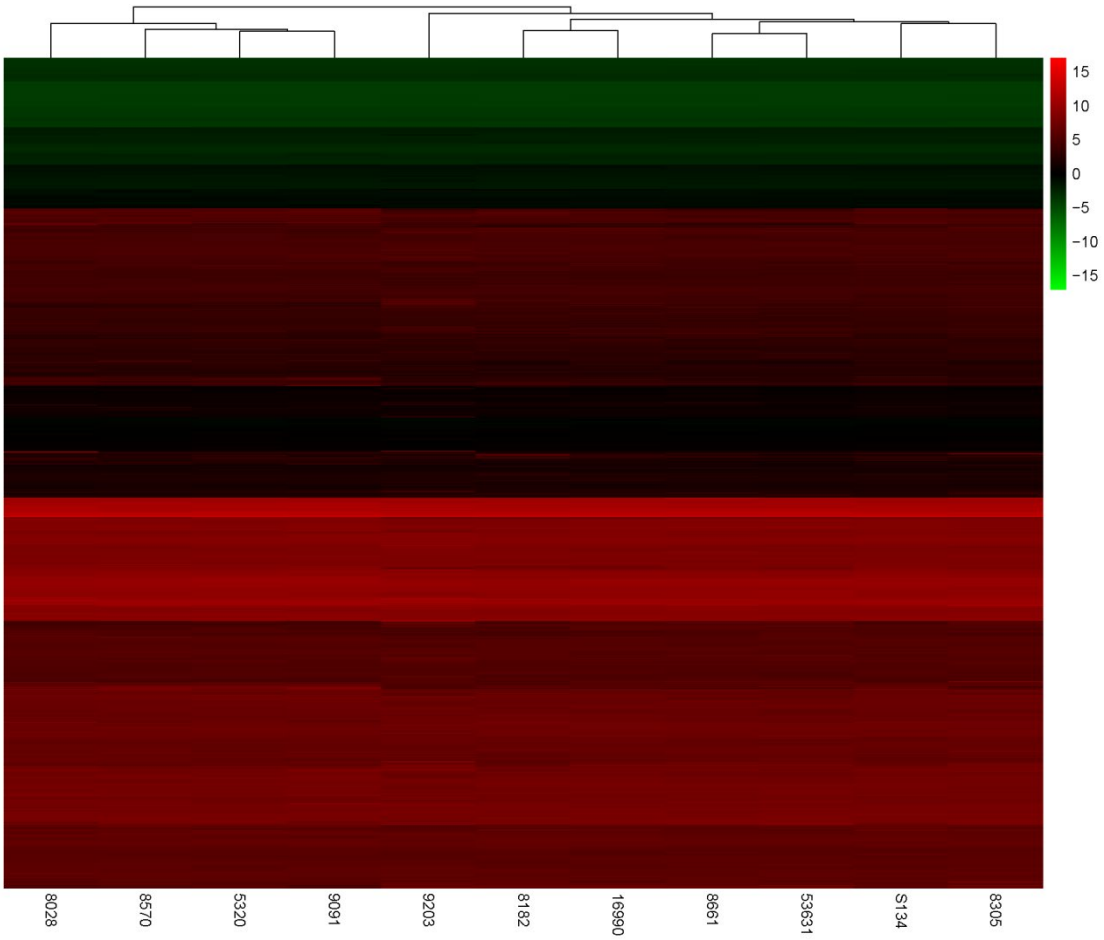

Figure 9 Heat map of the RNA sequence analyses of 11 pancreatic cancer cell lines

4.2 KRAS pathway analysis and correlation comparison

Since the KRAS pathway is a crucial pathway for tumor invasion and metastasis, the expressions of gene implicated in this pathway were analyzed in particular. Genes

participating in the KRAS pathway were largely comparable across the 11 pancreatic cell lines (Figure 10). Correlation comparison indicated that the correlation between each of two cell lines were > 0.98, which suggested strong similarities between the cell lines (Figure 11).

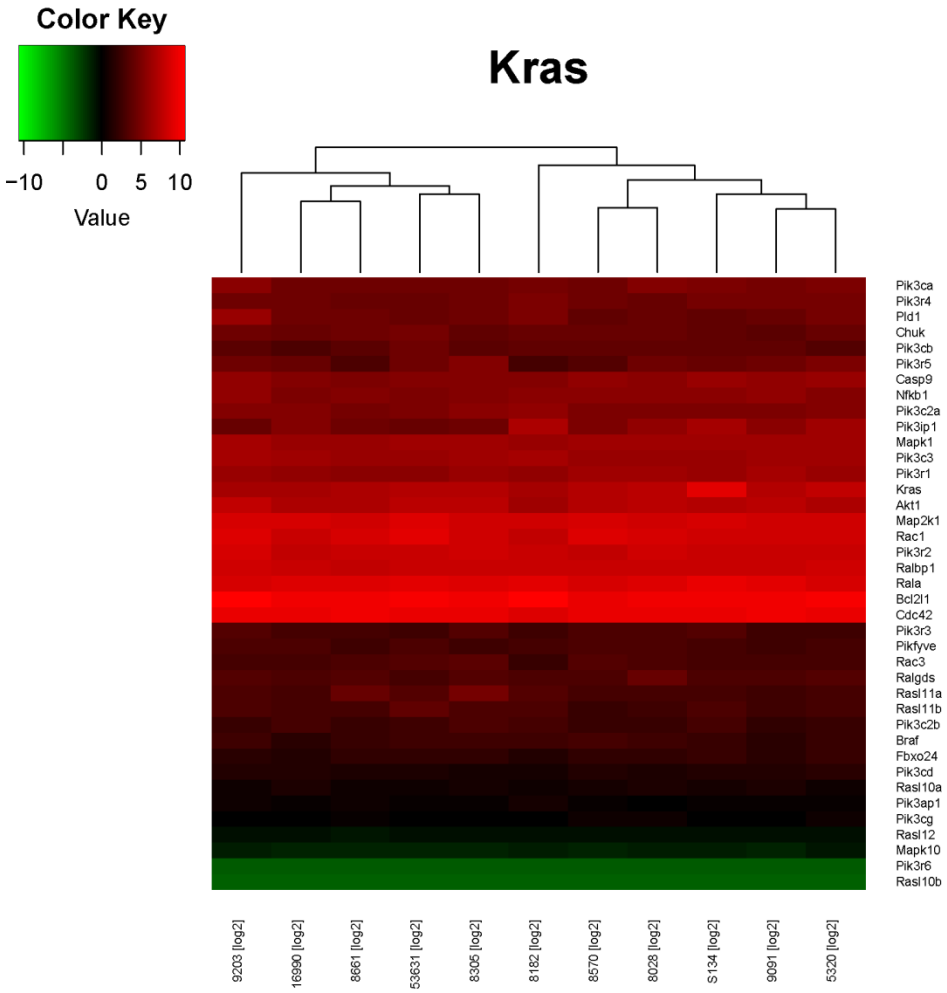

Figure 10 A Heat map for KRAS pathway gene expressions of 11 pancreatic cancer cell lines as determined by RNA-sequence analyses

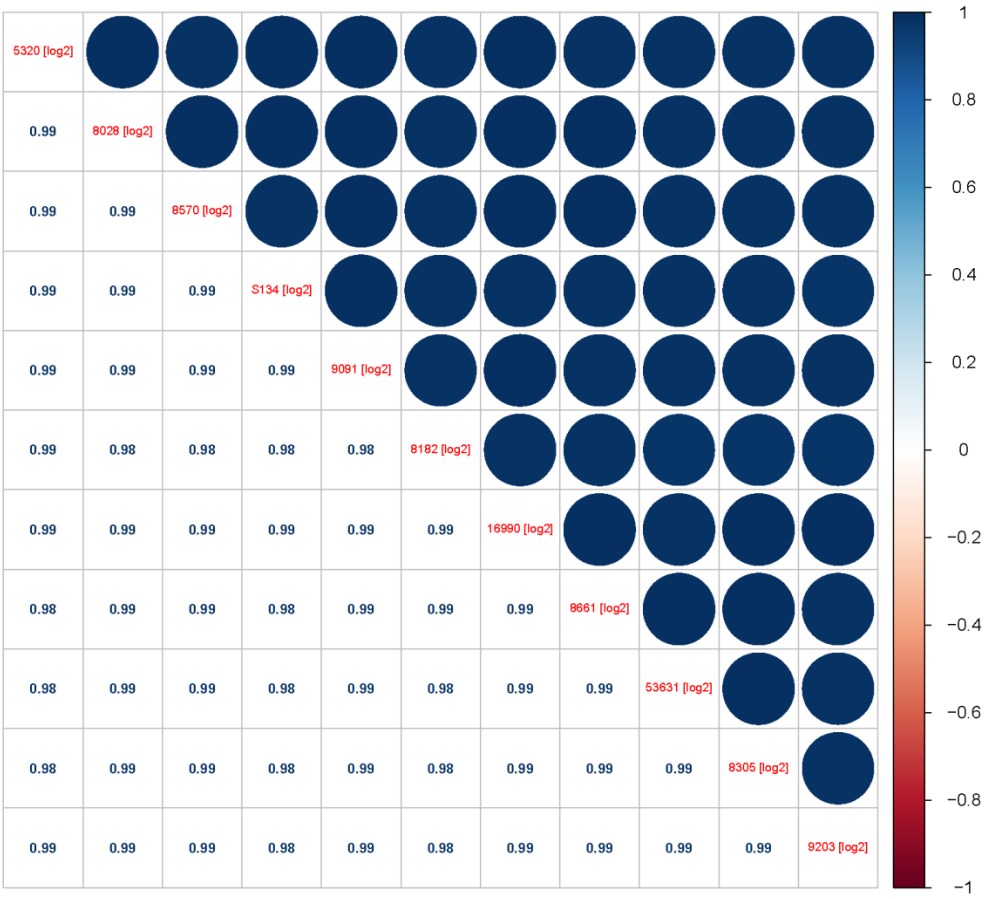

Figure 11 Correlation comparison analyses for the expression of genes implicated in the KRAS pathway for 11 pancreatic cancer cell lines

4.3 Procoagulant activities of pancreatic cancer cell lines

The clotting time (CT) parameter in whole blood coagulation analyses by TEG was used to evaluate the procoagulant activities of the pancreatic cancer cell lines, using blood of different healthy donors. To evaluate the procoagulant activity, the ratios of CT values with tumor cells to CT values without tumor cells (PBS) were calculated (Figure 12a). A lower ratio indicates a higher procoagulant activity of the cancer cells. The cell line 8182 showed the highest procoagulant activity and cell line 9091 the lowest ability to activate coagulation (Figure 12b, c). Therefore, cell line 8182 was

chosen to study the relationship between tumor-induced blood coagulation and extravasation.

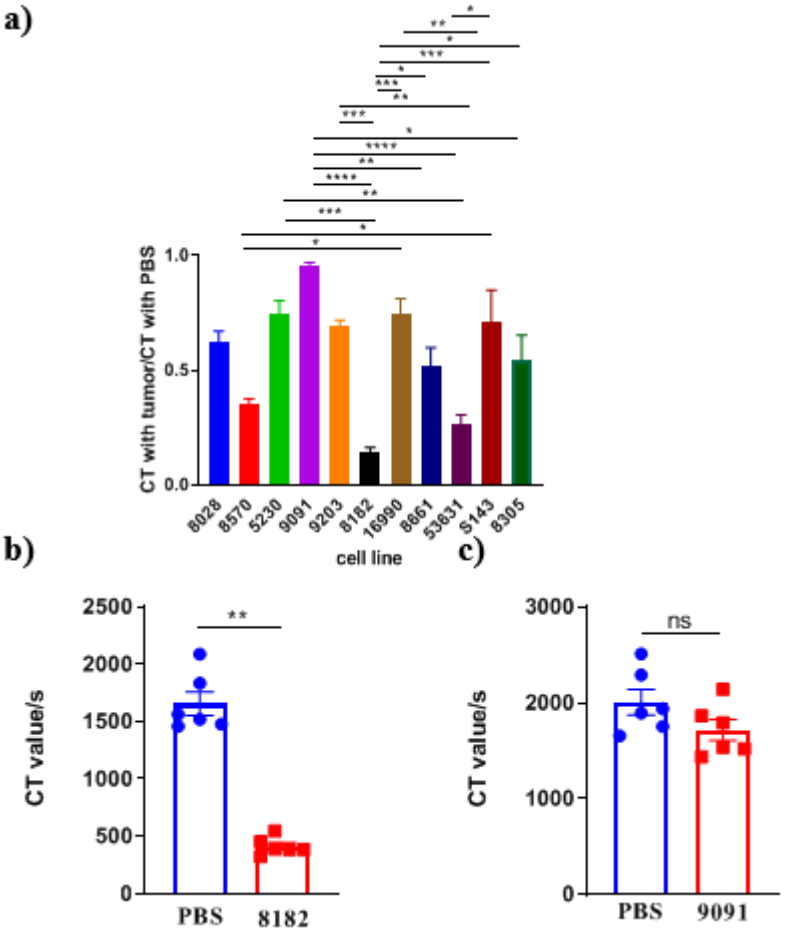

Figure 12 CT values of different pancreatic cancer cell lines. a) The ratios of CT values with tumor cells to CT values without tumor cells in 11 different pancreatic cancer cells. N=3. (different blood donors; for each cell line) b) CT values of cell line 8182 and control (PBS). c) CT values of cell line 9091 and control (PBS). The cell lines were added to whole blood from healthy donors. Dots indicate different healthy donors. *P < 0.05, **P < 0.01, *** P < 0.001, **** P<0.0005. Cell lines S143, 5230 and 16990 were checked by doctoral candidates Magda-Lena Berchtold and

Maximilian Wieser. Cell lines 8028, 8661, 9203 were checked by doctoral candidate Raphael Denz. Cell lines 8570 and 5230 were checked by doctoral candidate Raphael Denz and by the author.

4.4 Tumor-induced blood coagulation of cell line 8182

4.4.1 Role of FXII

FXIIa, which plays an important role in the contact pathway of blood coagulation,[29] was detected by a chromogenic assay. FXIIa formation was not affected by cell line 8182 (Figure 13a). Moreover, when cell line 8182 was added to normal plasma as well as to FXII deficient plasma (Figure 13b), the CT values were similarly shortened in normal plasma and FXII deficient plasma. Together, this indicated that the procoagulant activity of 8182 was not dependent on FXII.

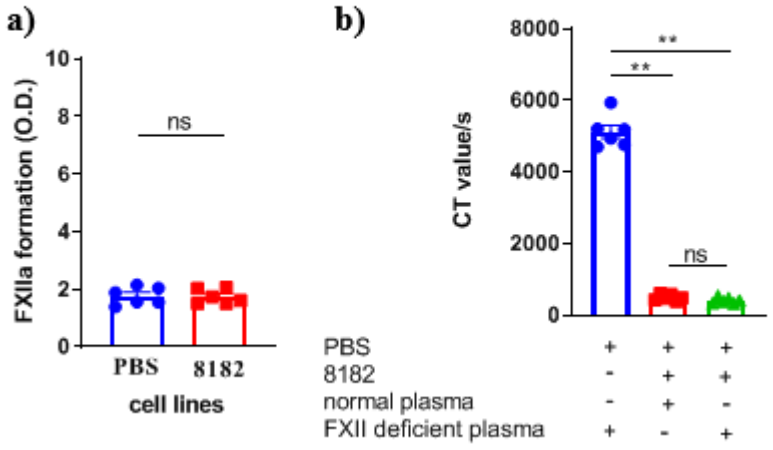

Figure 13 a) FXIIa formation chromogenic assay in presence of cell line 8182. b) CT values obtained using TEG with cell line 8182 in normal plasma and FXII deficient plasma. Dots indicated different healthy donors. **P < 0.01, ns, not significant.

4.4.2 Role of platelets

Since platelets are important promoters of clot formation, fibrin formation induced by cell line 8182 was measured in normal plasma and platelet-poor plasma (PPP). There was no significant difference in procoagulant activity of 8182 between the normal plasma and PPP, suggesting that the tumor-induced blood coagulation induced by cell line 8182 was independent of the presence of platelets (Figure 14).

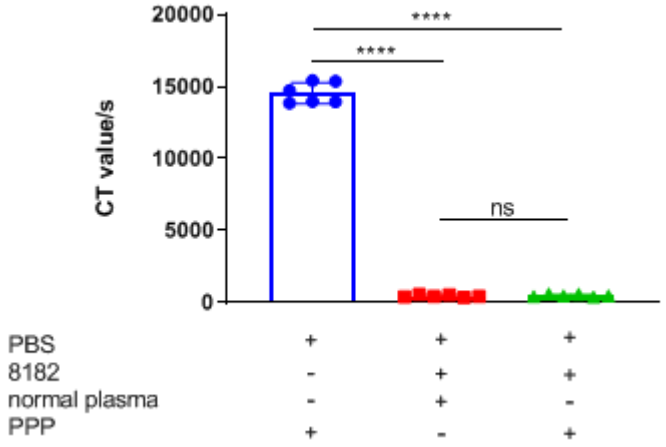

Figure 14 CT values in response to cell line 8182 in normal plasma and PPP. Dots indicate different healthy donors. **** P<0.0005, ns, not significant.

4.4.3 Role of Phosphatidylethanolamine (PE)

Since PE exposure could promote tumor-induced blood coagulation,[126] we next measured the procoagulant activity of cell line 8182 without or with Duramycin, a PE inhibitor. Duramycin did not affect fibrin formation in whole blood as induced by 8182 at a concentration of 10 μM (Figure 15).

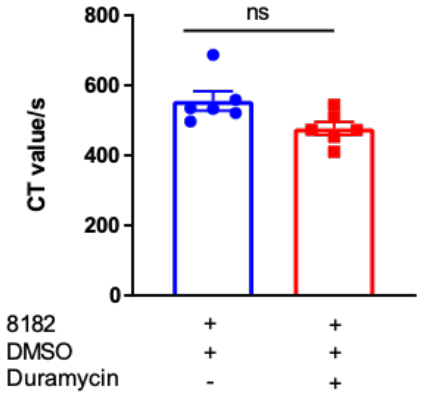

Figure 15 Cell line 8182 was pre-incubated with Duramycin (10 µM) or vehicle (DMSO), added to whole blood and the CT values were measured. Dots indicate different donors. ns, not significant.

4.4.4 Role of GAS6 in tumor-induced blood coagulation

The results of RNA sequencing analyses of cell lines 8182 and 9091 were compared using bioinformatics tools to search for potential genes responsible for tumor-induced blood coagulation, given that the procoagulant activities of these two cell lines differ dramatically. In M-A plots, any mRNA expression being increased more than 16-fold in 8182 vs. 9091 was highlighted in red. The Gas6 gene stood out since it was among the strongly increased genes in 8182 (Figure 16a) and since it is known to trigger blood coagulation.[127] Hence we evaluated the role of GAS6 for the coagulation competence of cell line 8182. Cell line 8182 was pre-incubated with neutralizing anti-GAS6 antibody or isotype control antibody. Inhibition of GAS6 did not alter the procoagulant activity of cell line 8182 (Figure 16b).

Figure 16 a) The expression matrix of the RNA sequence analyses of cell lines 8182 and 9091 were transformed into log2 format and a M-A plot obtained by subtracting the log2 value of 8182 from that of 9091. The expressions of genes with values above 4 or below -4 with more than 16-fold changes are highlighted in red. b) Cell line 8182 was pre-incubated with anti-mouse GAS6 neutralizing antibody (40 µg/ml) or isotype control antibody and CT values in whole blood were measured. Dots refer to different donors. ns, not significant.

4.4.5 Role of TF

To examine whether TF was involved in the procoagulant activity of 8182, first the cell line was analyzed for an eventual TF expression by immunofluorescence (IF). The cell membrane of 8182 expressed substantial TF (Figure 17a). Then FXa formation was measured by a chromogenic assay, which reflects the ability of the cells to trigger the TF pathway. Cell line 8182 strongly stimulated factor Xa formation (Figure 17c). Moreover, after pre-incubation of the cells with anti-TF neutralizing antibody, the CT value of whole blood was increased compared to that obtained with

the isotype control antibody, indicating that coagulation activity was reduced after TF blockage (Figure 17d). Together, these results showed that 8182 stimulated coagulation mostly via TF.

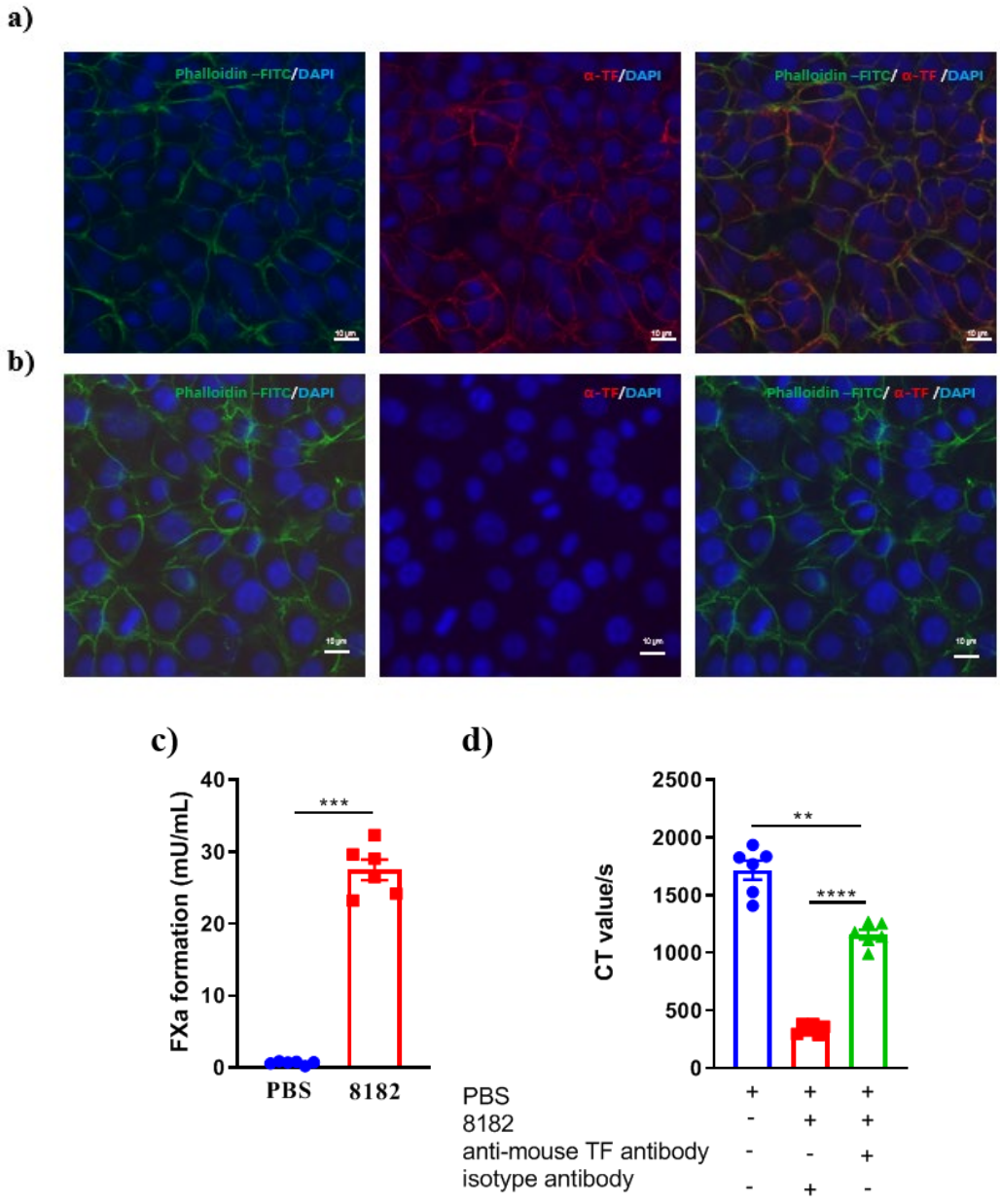

Figure 17 a) Representative IF images of 8182 cells stained with Phalloidin-FITC (green), anti-mouse TF antibody (1H1 red), DAPI (blue). Magnification fold x630. Scale bar, 10 µm. b) Representative IF images of 8182 cells stained with Phalloidin-FITC (green), anti-mouse IgG isotype antibody (red), DAPI (blue). Magnification fold x630. Scale bar, 10 µm. c) FXa formation assay with cell line 8182. d) Cell line 8182 was pre-incubated with anti-mouse TF antibody (1H1 1:100)

or isotype control antibody and CT values were measured (TEG). Dots indicate different donors. **P < 0.01, *** P < 0.001, **** P<0.0005.

4.4.6 Fibrin formation by cell line 8182 in vivo

As indicated by the in vitro results, stimulation of blood coagulation by cell line 8182 was dependent on TF and independent of FXII. To analyze the coagulation competence of 8182 in vivo, the cell line 8182 was injected into wild-type (WT) and *f12-/-* mice. At 2 h and 6 h, the mice were sacrificed to perform fibrin analysis in the liver microcirculation. Following injection of the cancer cells, fibrin depositions were visible in WT animals (Figure 18a). In *f12-/-* mice, fibrin production were unchanged. This suggested that the tumor-induced coagulation was strong enough to override host-induced blood coagulation (Figure 18a, b). Based on this conclusion, cell line 8182 was employed further to study tumor-induced blood coagulation in vivo.

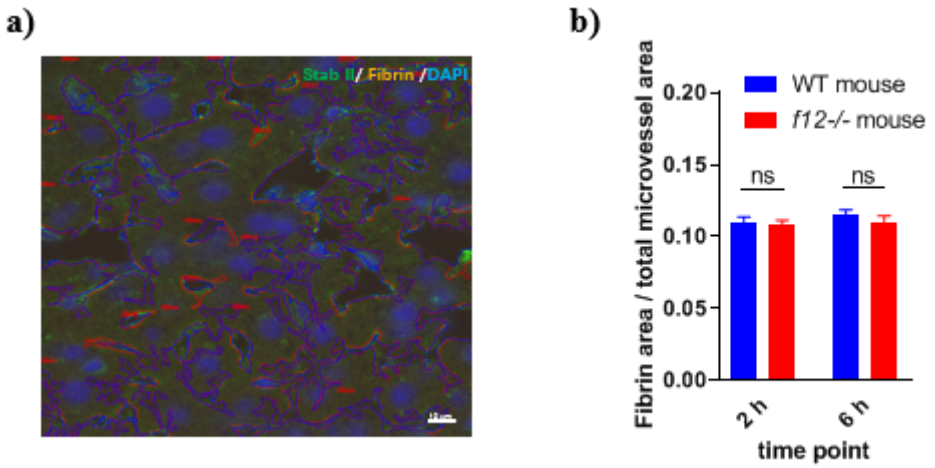

Figure 18 Fibrin formation analysis in the liver microcirculation after injection of 8182 cells. a) Representative picture showing liver micro-vessels (blue line), identified by Stab II, and intravascular fibrin (red line). Scale bar, 10 µm. b) Quantitative measurement of fibrin formation in micro-vessels of the liver. The fibrin-covered area in the micro-vessel was calculated as part of the total micro-vessel area. n=3 (different mice), ns, not significant.

4.4.7 Effect of 8182-triggered tumor-induced blood coagulation on tumor cell extravasation

4 h after administration of factor Xa inhibitor by Rivaroxaban or vehicle (DMSO), cell line 8182 was injected into WT mice. 6 h later, microvascular fibrin formation was noticeable in vehicle-treated group, consistent with the results in Figure 4.10b. Fibrin formation was decreased in the Rivaroxaban-treated group. Approximately 80% of tumor-induced blood coagulation could be inhibited by Rivaroxaban (Figure 19).

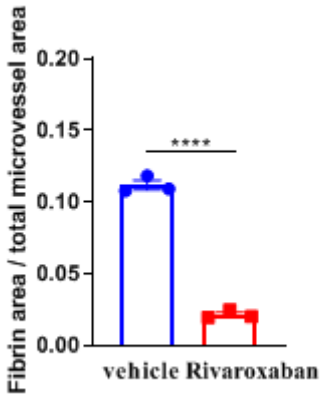

Figure 19 Effect of Rivaroxaban on microvascular fibrin formation. 4 h after vehicle (DMSO) or Rivaroxaban treatment of WT mice, cell line 8182 was injected. 6 h later fibrin analysis on liver tissue was performed. Dots indicate different animals. **** $P<0.0005$.

Next we analyzed the extravasation of the cancer cells at the same time point. 3D reconstruction made by Imaris (Figure 20a) showed that tumor cell extravasation had occurred after 6 h. With this approach, extravasation could be measured under different conditions (8182 injection alone, 8182 + vehicle (DMSO), 8182 + Rivaroxaban). In the Rivaroxaban treatment group, tumor cell extravasation was massively increased compared to the control (Figure 20b), potentially suggesting that tumor-induced blood coagulation might reduce tumor cell extravasation.

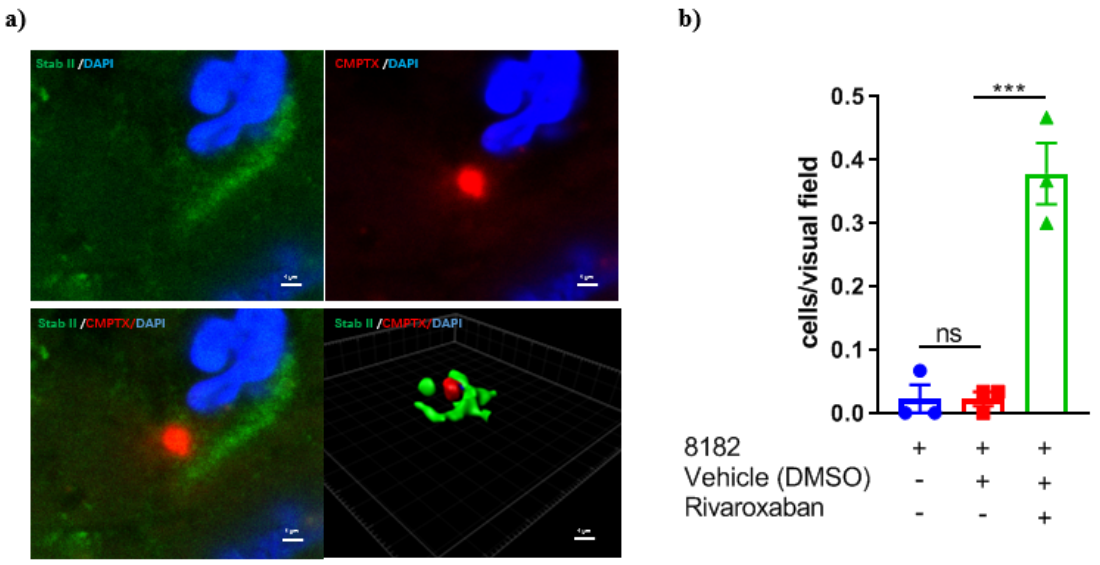

Figure 20 Effect of tumor-induced fibrin formation on tumor cell extravasation. a) Representative picture and 3D reconstruction of tumor cell extravasation. Micro-vessel (green), tumor cells (red), DAPI (blue). Scale bar 1 µm. b) Quantitative measurement of tumor cell extravasation. Dots refer to different animals. *** $P < 0.001$, ns, not significant.

4.4.8 Effect of 8182-induced blood coagulation on non-classical monocyte recruitment

After 4 h of administration of Rivaroxaban or vehicle (DMSO), cell line 8182 was injected into WT mice. 6 h later, the recruitment of different immune cells was examined. Recruitment of non-classical monocytes (visualized as shown in Figure 21a) was markedly reduced after Rivaroxaban treatment (Figure 21b), probably due to a suppressed tumor-induced blood coagulation. Indeed, fibrin production was diminished by approximately 80% due to Rivaroxaban (4.4.7 Figure 19).

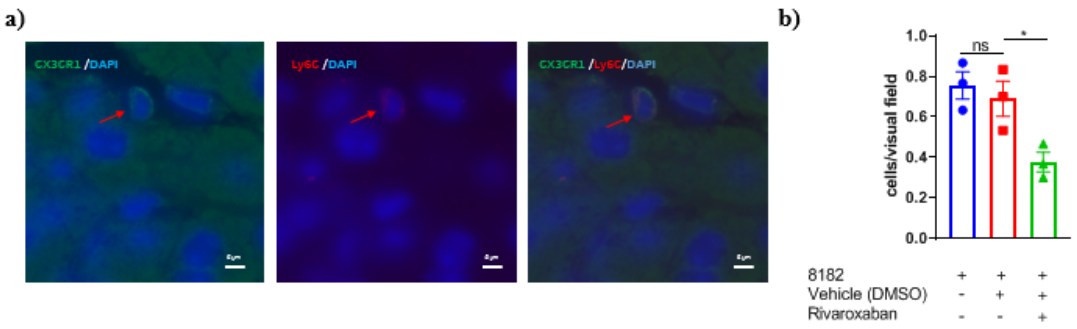

Figure 21 a) Representative picture of a non-classical monocyte (CX3CR1^{high} Ly6C^{low}) in the liver microcirculation. CX3CR1 (green), Ly6C (red), DAPI (blue). Scale bar 5 µm. b) 4 h after vehicle (DMSO) or Rivaroxaban treatment in WT mice, cell line 8182 was injected. Non-classical monocytes in the liver micro-vessels were counted 6 h later by IHC. Dots refer to different animals. * $P < 0.05$, ns, not significant.

4.4.9 Effect of non-classical monocytes on tumor cell extravasation

Nur77-/- mice lack non-classical monocytes.[128] To understand whether non-classical monocytes affect tumor cell extravasation, we injected cell line 8182 into Nur77-/- mice and respective WT mice. Tumor cell extravasation increased 6 h after injection of 8182 into Nur77-/- mice as compared to WT mice, suggesting that non-classical monocytes can reduce tumor extravasation (Figure 22).

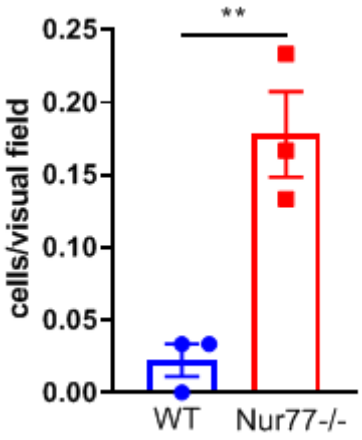

Figure 22 Tumor cell extravasation in WT and Nur77-/- mice 6 h after injection of cell line 8182. Dots refer to different animals. ** $P < 0.01$.

Ang-1 is an important regulator of tumor cell extravasation. Since Ang-1 can activate Tie-2 receptors which in turn promote the survival of endothelial cells, the maintenance of an endothelial barrier and a quiescent vasculature. We observed that Ang-1 was expressed in non-classic monocytes, as arrested in the liver microcirculation in response to the appearance of 8182 (Figure 23).

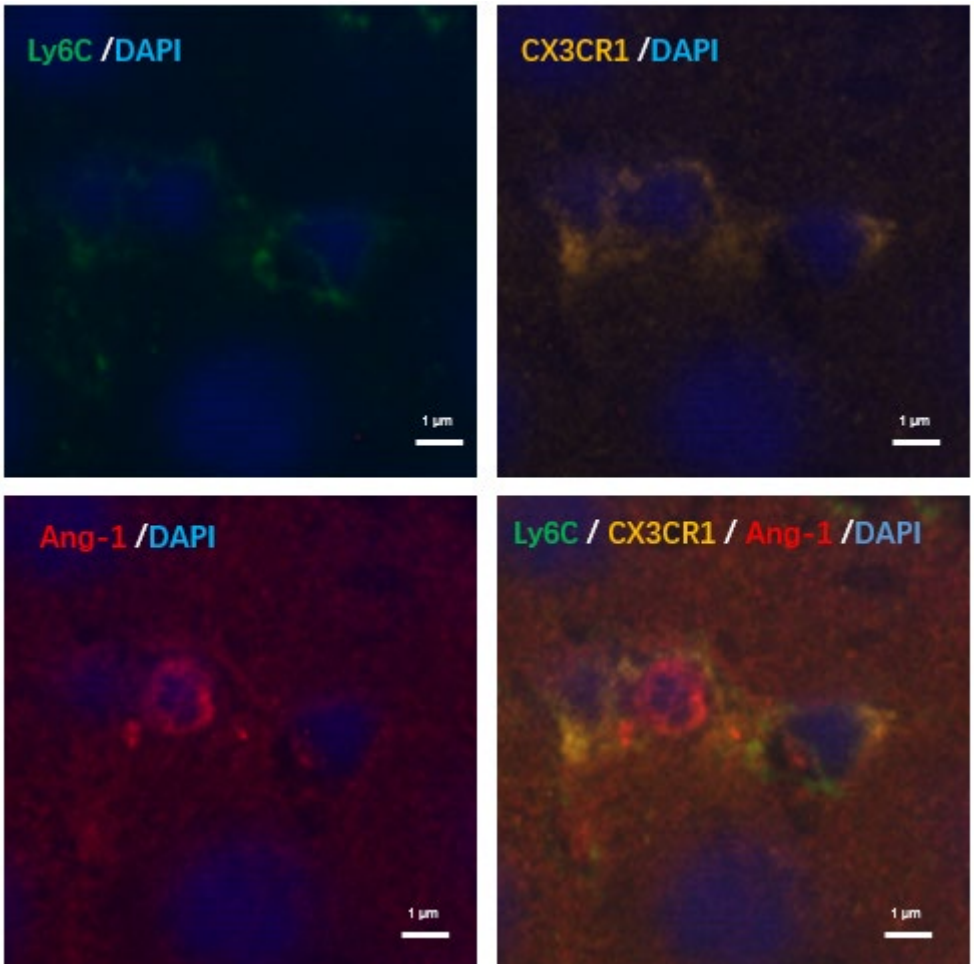

Figure 23 Representative picture of a non-classic monocyte expressing of Ang-1. Ly6C (green), CX3CR1 (orange), Ang-1 (red), DAPI (blue). Scale bar, 1 μm.

4.4.10 Effect of tumor-induced blood coagulation on CD4+ T cell recruitment

Fibrin deposition can be reduced by about 80% by Rivaroxaban, as shown in Figure 19. CD4+ T cells have been reported in the literature to reduce the permeability of blood vessels during malignancy[129]. We found that reduction of tumor-induced blood coagulation by Rivaroxaban decreased recruitment of CD4+ T cells (Figure 24a, b).

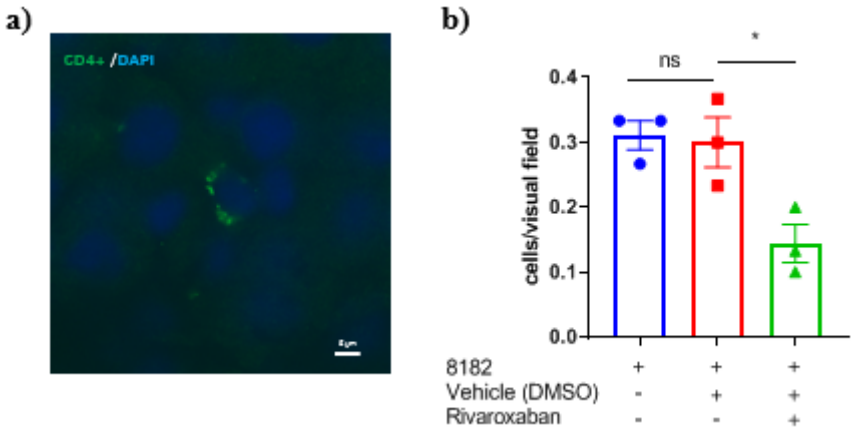

Figure 24 a) Representative picture of a CD4+ T cell as arrested in the liver microcirculation. CD4+ (green), DAPI (blue). Scale bar, 5 µm. b) In WT mice treated with Rivaroxaban, cell line 8182 was injected and CD4+ T cells in liver tissue were counted 6 h after tumor cell injection. Dots refer to different animals. * $P < 0.05$, ns, not significant.

4.4.11 Effect of 8182 on macroscopic liver metastasis

3 weeks after injection of the cancer cell line 8182 into the spleen capsule, livers were harvested. No metastasis could be detected by inspection (Figure 25a) and under the microscope (Figure 25b). Microscopic thrombi were detected, however, in each visual field, indicating that prothrombolic mechanisms had been provoked by the tumor cells.

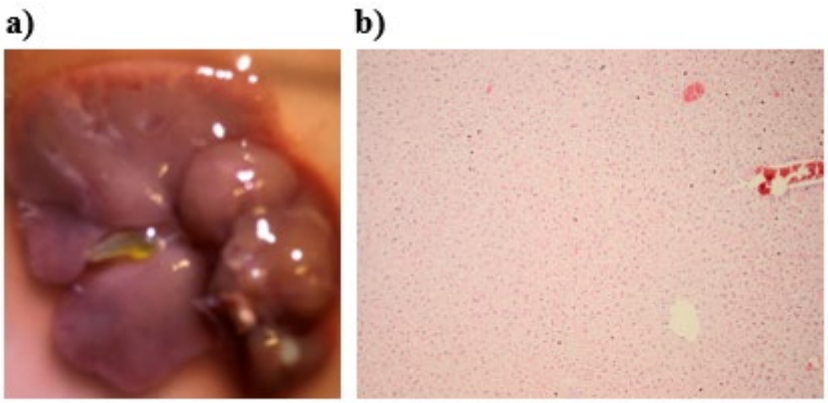

Figure 25 a) Macroscopic visualization of the liver 3 weeks after injection of cell line 8182 into the spleen capsule. b) HE staining of the liver showing thrombi without metastasis. Magnification, x100

4.5 Host-induced blood coagulation activation and tumor cell extravasation

4.5.1 Host-induced blood coagulation as triggered by cell line 9091

Cell line 9091 completely lacks prothrombotic activity (Figure 12). In order to examine whether the host triggers blood coagulation in response to 9091, cell line 9091 was injected into wild type (WT) mice and *f12-/-* mice. After 2 h and 6 h, the mice were sacrificed to perform fibrin analysis in the liver microcirculation. As shown in Figure 26, fibrin production was substantially higher in WT mice compared to *f12-/-* mice. This suggested the existence of host-induced blood coagulation, which can be triggered by FXII. Moreover, fibrin formation in WT after vehicle injection was similar to fibrin formation in FXII deficient mice after tumor injection (Figure 26), suggesting that the host-induced blood coagulation was completely FXII-dependent. From this experiment, we assumed that there was a host-induced blood coagulation, which was completely FXII-dependent.

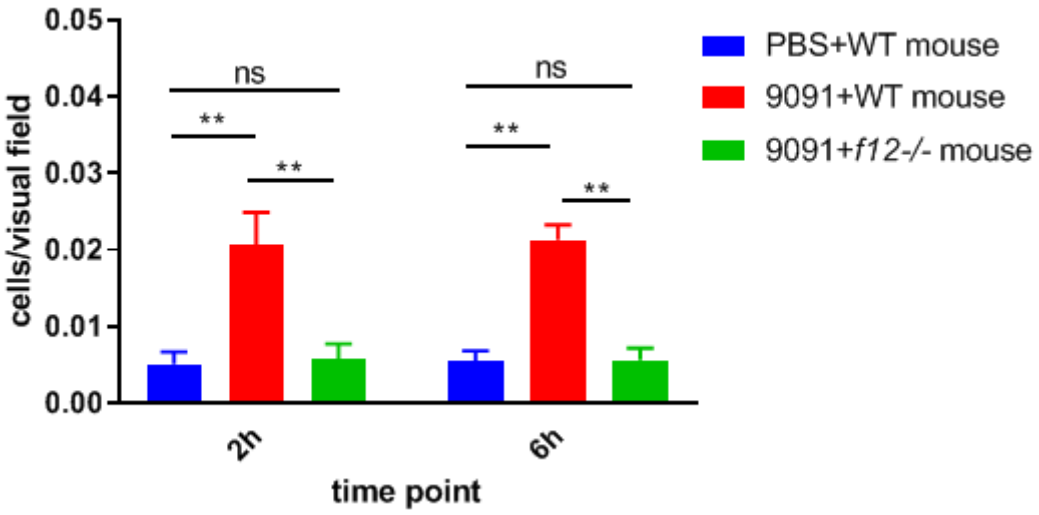

Figure 26 Quantitative determinations of fibrin in micro-vessels of the liver in WT and *f12*-/- mice injected with 9091. The fibrin-covered area in the micro-vessel was calculated as part of the total micro-vessel. n=3, ** $P < 0.01$, ns, not significant.

4.5.2 Effect of 9091 on tumor cell extravasation

After 4 h Rivaroxaban treatment, cell line 9091 was injected into WT mice. 6 h later, fibrin deposition in liver was clearly noted in the vehicle-treated group, consistent with the results in Figure 26, while it was significantly decreased in the Rivaroxaban-treated group (Figure 27a). As indicated in 4.5.1, the blood coagulation after injection of 9091 is exclusively host-induced. Thus, Rivaroxaban can inhibit the majority of host-induced blood coagulation (Figure 27a). Next tumor cell extravasation was measured in absence and presence of the FXa inhibitor. 6 h after Rivaroxaban treatment, extravasation of 9091 was increased, suggesting that host-induced blood coagulation might reduce tumor cell extravasation (Figure 27b).

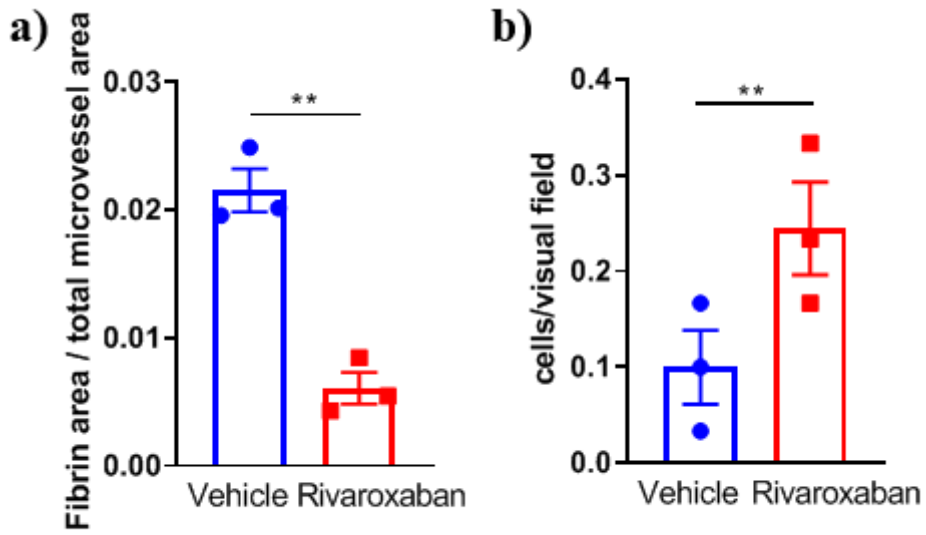

Figure 27 a) 4 h after treatment with Rivaroxaban treatment, cell line 9091 was injected into WT mice and fibrin analysis on liver tissue was performed 6 h later. b) Quantitative determinations of extravasation of 9091. Dots refer to different animals. ** $P < 0.01$.

4.5.3 Recruitment of non-classical monocytes and CD4+ T cells in Rivaroxaban treated mice supplemented with 9091

Arrest of non-classical monocytes and of CD4+ T cells was measured in both vehicle (DMSO) and Rivaroxaban-treated animals receiving 9091. No difference was detected (Figure 28a, b).

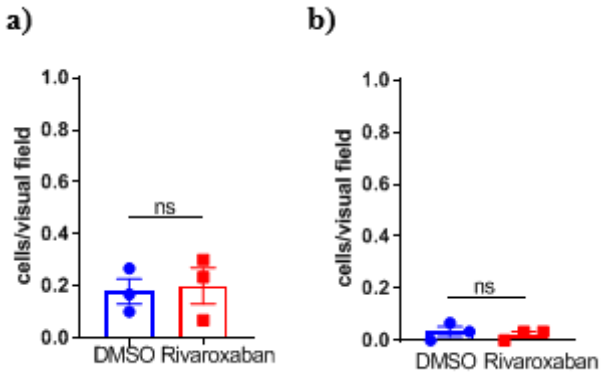

Figure 28 4 h after vehicle (DMSO) or Rivaroxaban treatment of WT mice, cell line 9091 was injected and the arrest of non-classical monocytes (a) and of CD4+ T cells in the liver microcirculation was determined. Dots refer to different animals. ns, not significant.

4.5.4 The effect of FXII on extravasation of 9091

After injection of cell line 9091 into WT and *f12-/-* mice, tumor cell extravasation was measured at 6 h. Tumor cells invasion into the perivascular tissue was higher in *f12-/-* mice compared to WT mice, indicating a suppressive role of FXII on tumor cell extravasation (Figure 29a). 9 h after tumor cell injection, extravasation of 9091 was still higher in *f12-/-* mice than in WT mice (Figure 29b).

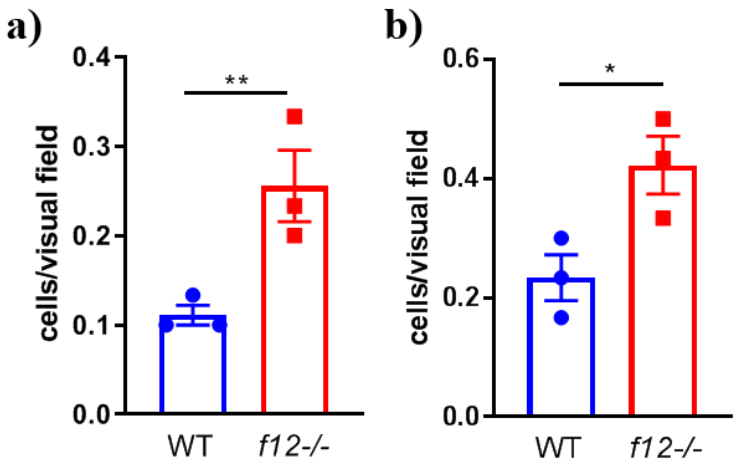

Figure 29 Tumor cell extravasation 6 h (a) and 9 h (b) after injection of 9091 in WT mice and *f12-/-* mice. Dots refers to different animals. * $P < 0.05$, ** $P < 0.01$.

4.5.5 Effect of FXII-deficiency and Rivaroxaban on neutrophil recruitment

The number of neutrophils arrested in the liver microcirculation in response to injection of 9091 was increased by Rivaroxaban (Figure 30a). Since Rivaroxaban inhibits coagulation and only host-induced blood coagulation was present in mice injected with cell line 9091, host-induced blood coagulation might prevent neutrophil recruitment. In order to corroborate this conclusion, the number of neutrophils in liver was compared in WT mice and *f12-/-* mice. The arrested neutrophils in the liver microcirculation were increased in *f12-/-* mice (Figure 30b). Taking together, it is plausible to assume that host-induced blood coagulation might decrease the recruitment of neutrophils

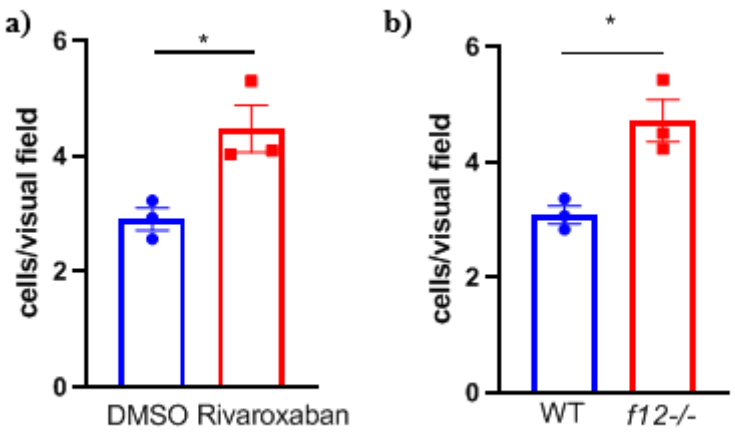

Figure 30 a) Effect of Rivaroxaban treatment in WT mice supplemented with cancer cell line 9091 on arrest of neutrophils in the liver microcirculation (6 h). b) Neutrophil recruitment in WT and *f12-/-* mice 6 h after injection of cell line 9091. Dots refer to different animals. * $P < 0.05$.

4.5.6 NETs formation and tumor extravasation

The emergence of NETs was examined 6 h and 9 h after injection of tumor cell line 9091 into WT mice. At 6 hours, no NETs were observed. Nonetheless, at 9 h NETs formation was clearly visible (Figure 31a-c). NETs could be seen in the vicinity of single neutrophils or around clusters of neutrophils (Figure 31b). Next, extravasation of 9091 was determined at 6 h and 9 h. At 9 h, extravasation of 9091 was elevated compared to 6 h (Figure 31d). In subsequent experiment, before injection of 9091, DNaseI was administered to degrade NETs. DNaseI treatment strongly reduced NET formation in response to cell line 9091 (Figure 31e). Concomitantly, tumor cell extravasation was markedly diminished by DNaseI (Figure 31f). This suggested that formation of NETs may support tumor cell extravasation.

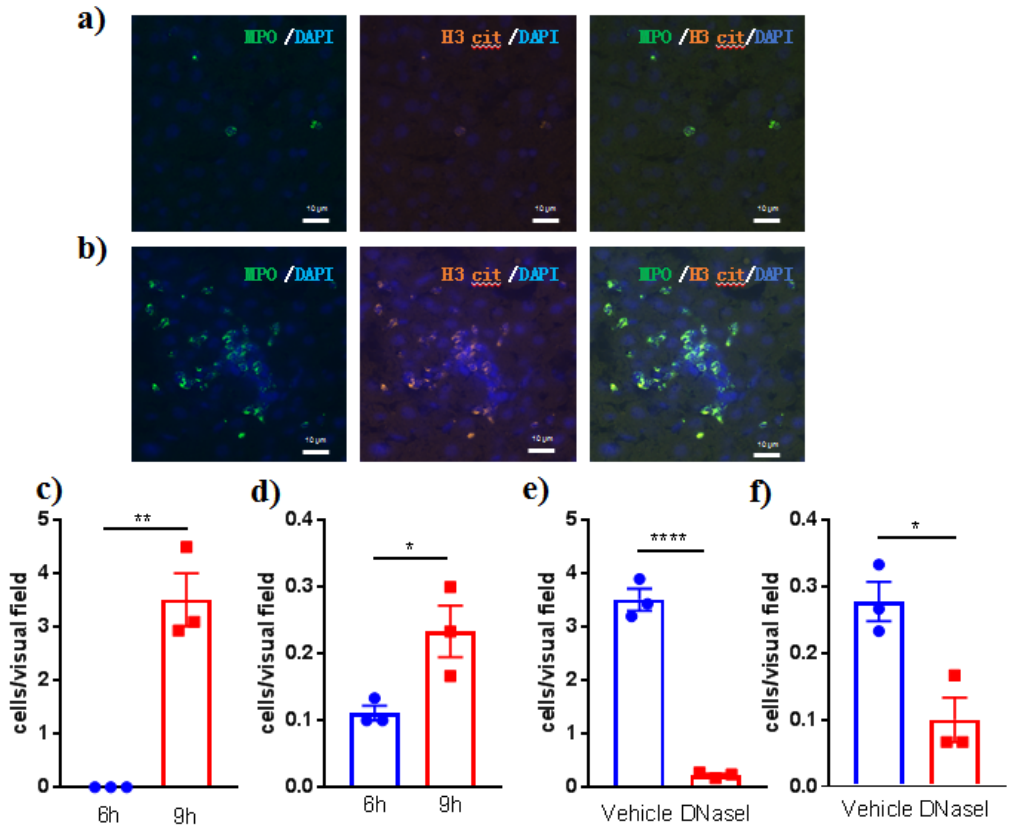

Figure 31 a) Representative picture of a single neutrophil with NETs in WT mice injected with 9091. MPO (green), H3 cit (orange), DAPI (blue). Scale bar 10 µm b) Representative picture of neutrophil aggregates with NETs. MPO (green), H3 cit (orange), DAPI (blue). Scale bar 10 µm c) NET formation at 6 h and 9 h in 9091-supplemented WT mice. d) Extravasation of 9091 at 6 h and 9 h in WT mice. e) Formation of NETs after DNase I treatment at 9 h in 9091-supplemented WT mice. f) Extravasation of 9091 after DNaseI treatment (9 h, WT mice). Dots refer to different animals. *P < 0.05, **P < 0.01, **** P<0.0005.

4.5.7 Potential underlying mechanism of the influence of NETs on tumor cell extravasation

Since NETs can induce vessel occlusion and blood flow stop,[130] we were interested in whether NETs formation in response to tumor cells was associated with signs of hypoxia. HIF1α is a marker of hypoxic areas. Thus fluorescence intensities originating from HIF1α were measured 9 h after injection of 9091. As a result, clear HIF1α staining was observed which was mainly restricted to the endothelium. After treatment with DNaseI, HIF1α labeling was reduced (Figure 32b), potentially suggesting that NETs might increase hypoxic area. Next, the expression of Ang-1 and -2 were measured in the microvascular compartment. Indeed, both Ang-1 and Ang-2 could be detected (Figure 32c, d). Following treatment of mice with DNaseI, the expression of Ang-1 was elevated while that of Ang-2 was decreased (Figure 32e). Thus, NET formation may up-regulate expression of Ang-2 and down-regulate Ang-1 expression.

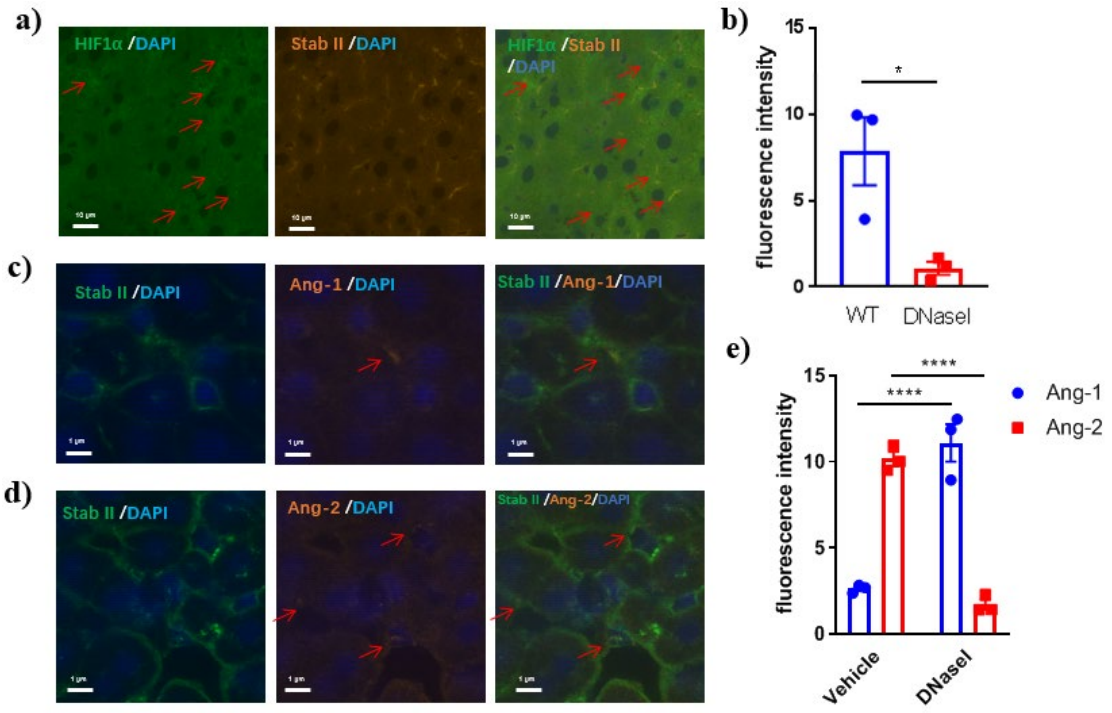

Figure 32 a) Representative picture of HIF1α staining in liver microvessels following injection of 9091. HIF1α, green, Stab II, orange, DAPI, blue. Scale bar, 10μm. Red arrow, expression of HIF1α. b) Fluorescence intensities of HIF1α staining in the liver microcirculation after DNaseI treatment. c) Representative picture of Ang-1 staining in endothelial cells. Stab II, green, Ang-1, orange, DAPI, blue. Scale bar, 1 μm. Red arrow, expression of Ang-1. d) Representative picture of Ang-2 staining in endothelial cells. Stab II, green, Ang-2, orange, DAPI, blue. Scale bar 1 μm. Red arrow, expression of Ang-2. e) Fluorescence intensities of Ang-1 and Ang-2 staining in liver micro-vessels after DNaseI treatment. Dots refer to different animals. *P < 0.05, **** P<0.0005

4.5.8 Effect of 9091 on macroscopic liver metastasis

3 weeks after injection of cancer cell line 9091 into the spleen capsule, livers were harvested. Pronounced metastasis was observed in the liver by inspection (Figure 33 a) and by HE staining (Figure 33 b).

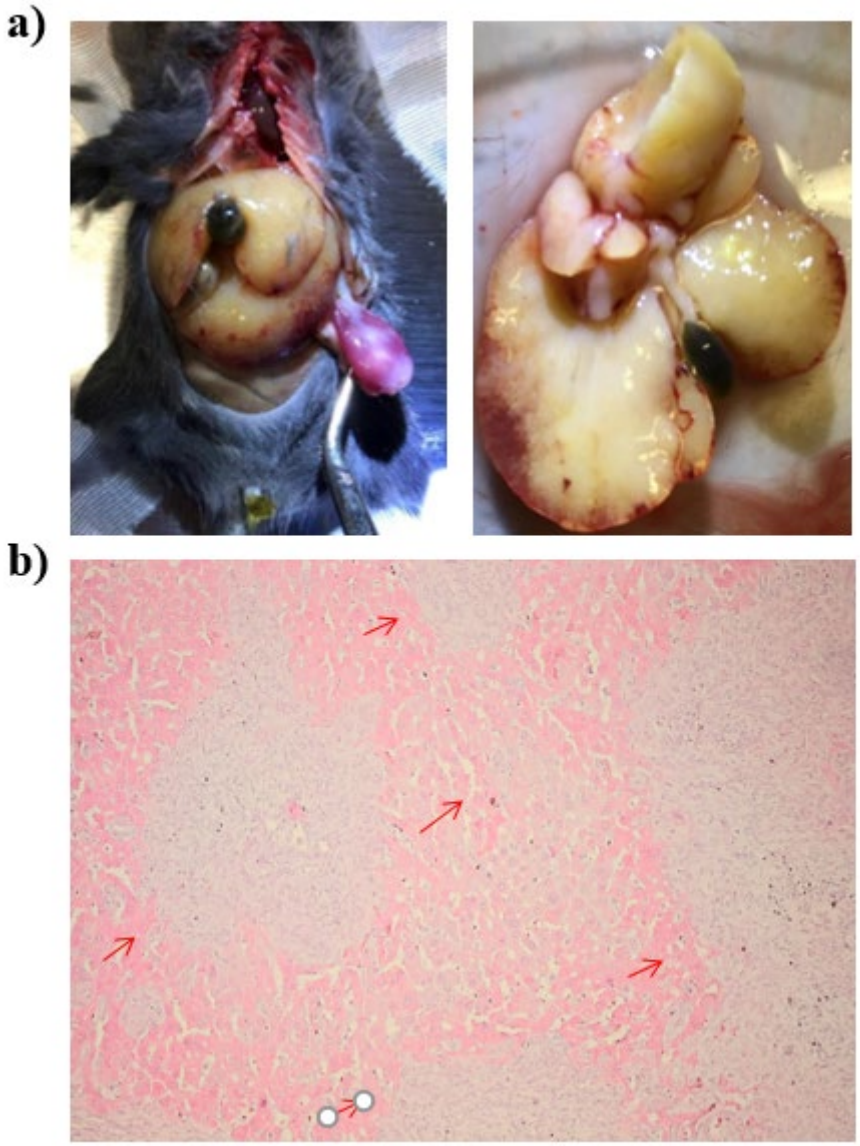

Figure 33 a) Inspection of the liver 3 weeks after injection of cell line 9091. Presence of a large metastasis. b) HE staining of the liver showing metastatic niches (red arrows). Magnification: x100.

4.6 Role of cancer cell extracellular vesicles (EVs) for tumor cell extravasation

4.6.1 Release of EVs by pancreatic cancer cell lines

Apart from exosomes, there are two important subgroups of EVs that could be crucial to tumor invasion and metastasis, namely MVs and LOs. The release of LOs by 11 different pancreatic tumor cell lines was evaluated by counting them in the tumor cell supernatant. Cell line 53631 had the strongest ability to produce LOs, while cell line 8182 had the weakest (Figure 34a). Since nanoparticle tracking analyses can detect EVs < 1 µm, they were used to measure EV release by cell lines 53631 and 8182. As shown in Figure 34b, there were also clear differences in the amount of EVs released between 53631 and 8182. Thus, these two cell lines were used in the following experiment.

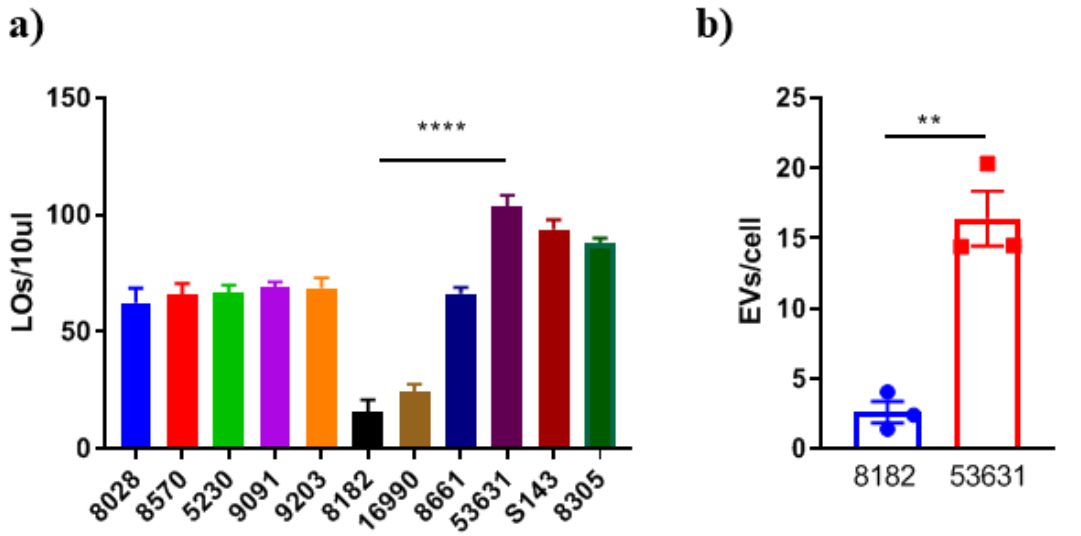

Figure 34 a) Release of LOs in 11 different pancreatic cell lines measured as determined by light microscopy in the tumor cell supernatant. N=3, **** P < 0.0005. b) Release of EVs by cell lines 53631 and 8182 as detected by nanoparticle tracking. N=3. Dots refer to different biological repeat of nanoparticle tracking. ** P < 0.01.

4.6.2 Bioinformatic analyses to search for genes responsible for EV release

In order to search for genes potentially responsible for EV release, bioinformatic analyses of the transcriptomes of cell lines 53631 and 8182 were performed. Any difference between 53613 and 8182 in gene expression that was greater than 16-fold was highlighted in red in the M-A plot showing in Figure 35a. Among such genes was Padi4 which was previously reported to promote release of LOs.[131] Additionally, the mRNA expressions of all 11 pancreatic cell lines were analyzed and over 20,000 genes were classified into 20 different subgroups (Figure 35b). Padi4, the gene of interest, was in profile 10 with another 5 genes. The correlation coefficients between these 5 genes were calculated and shown through a heatmap (Figure 35c). The expression of Slc9a2 stood out with a coefficient correlation of 0.94 to Padi4 expression. Moreover, the fold change of Slc9a2 was over 4 according to the M-A plot in Figure 35d.

a)

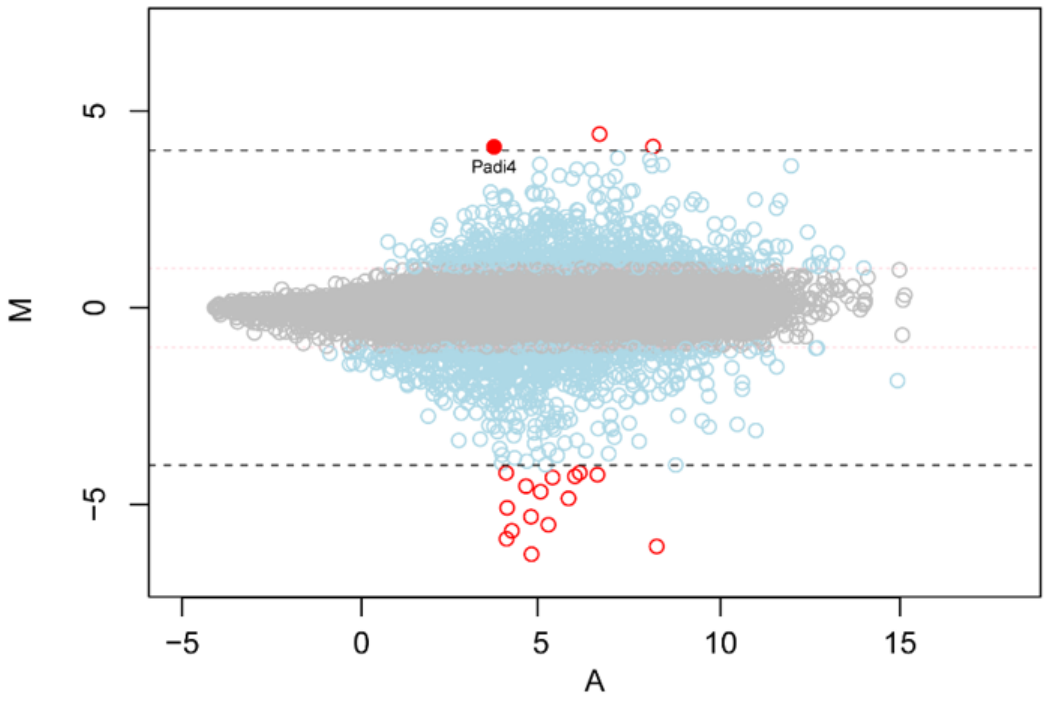
Padi4
M
A
5
0
−5
−5
0
5
10
15

b)

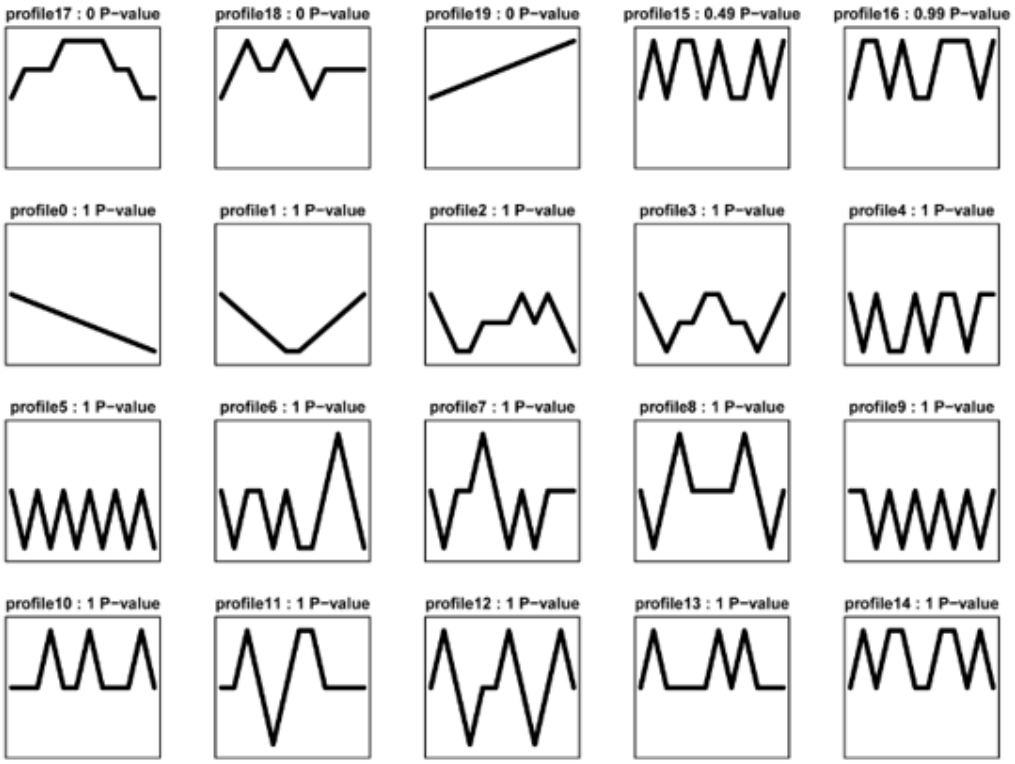
profile17 : 0 P−value
profile18 : 0 P−value
profile19 : 0 P−value
profile15 : 0.49 P−value
profile16 : 0.99 P−value
profile0 : 1 P−value
profile1 : 1 P−value
profile2 : 1 P−value
profile3 : 1 P−value
profile4 : 1 P−value
profile5 : 1 P−value
profile6 : 1 P−value
profile7 : 1 P−value
profile8 : 1 P−value
profile9 : 1 P−value
profile10 : 1 P−value
profile11 : 1 P−value
profile12 : 1 P−value
profile13 : 1 P−value
profile14 : 1 P−value

c)

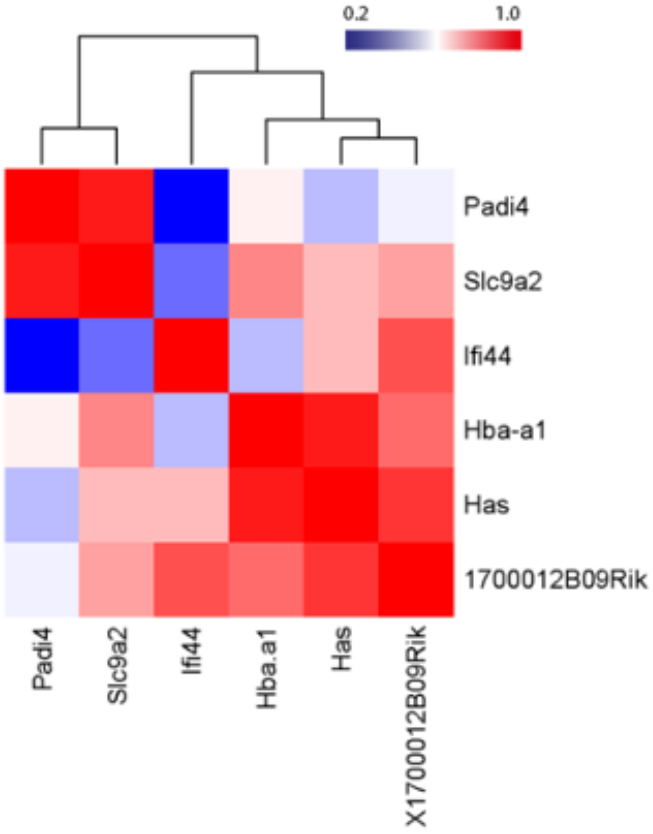
0.2
1.0
Padi4
Slc9a2
Ifi44
Hba-a1
Has
1700012B09Rik
Padi4
Slc9a2
Ifi44
Hba.a1
Has
X1700012B09Rik

d)

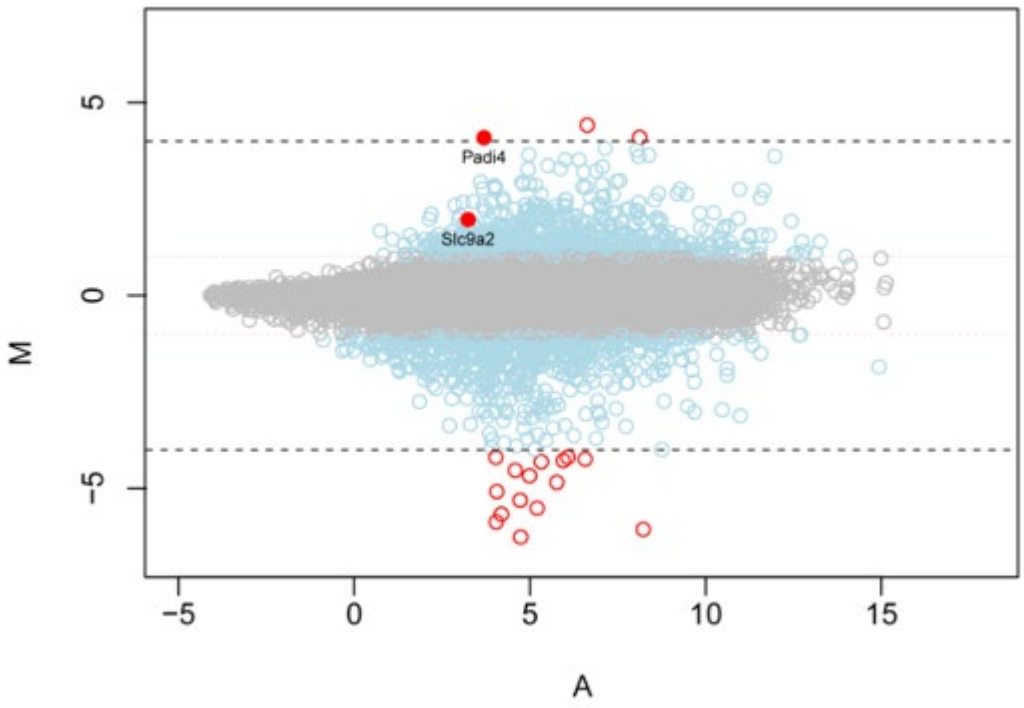
Padi4
Slc9a2
M
A
5
0
−5
−5
0
5
10
15

Figure 35 a) Comparison of the RNA expression matrix between cell lines 53631 and 8182. The gene names, with values above 4 or below -4 (log_2 format) are highlighted in red, indicating more than a 16-fold difference. b) Gene expression trends of 11 pancreatic cell lines. The profiles are reordered based on actual size based p-value enrichment for genes. c) Correlation coefficients between the 5 genes in profile 10 in gene expression trends analyses. d) M-A plot of cell line s53631 and 8182. Padi 4 and Slc9a2 are highlighted in red.

4.6.3 Validation of Padi4 - Slc9a2 association by qPCR and WB

qPCR of Padi4 and Slc9a2 were performed for cell lines 53631 and 8182. The fold-increase of Padi4 mRNA expression was around 1,500 and of Slc9a2 mRNA expression was about 6000 for cell line 53631 compared to cell line 8182 (Figure 36a, b). On the protein level, PADI 4 expression was about 25 times higher in cell line 53631 than in 8182, while the expressions of SLC9A2 were comparable between the two cell lines (Figure 36c, d).

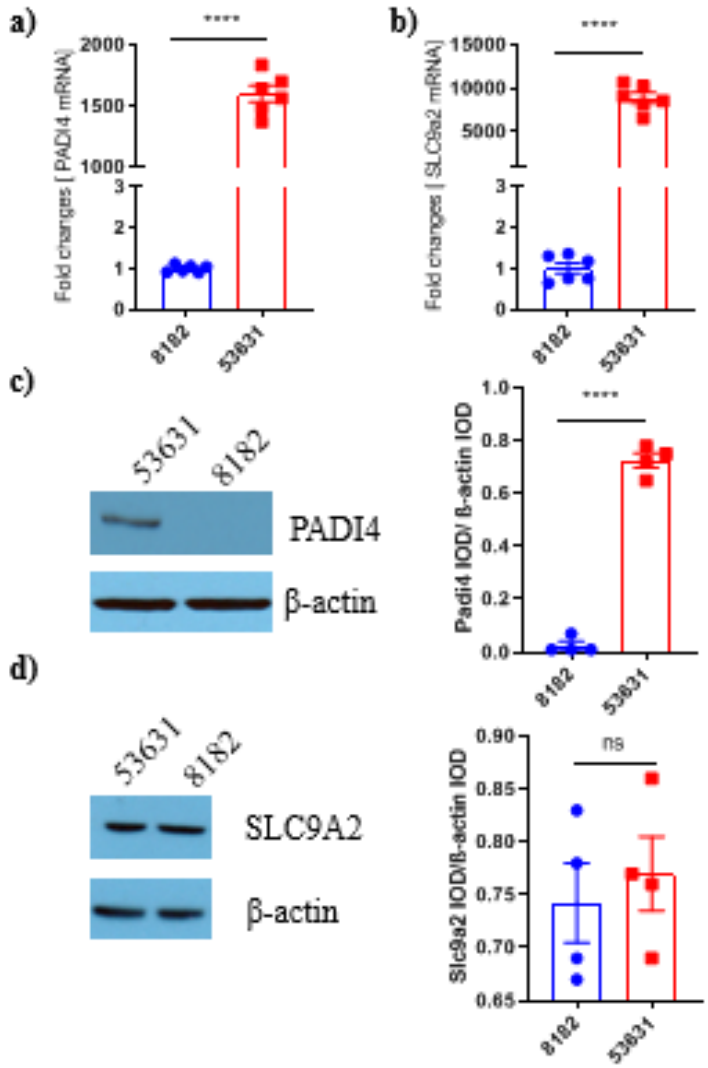

Figure 36 a) Padi4 mRNA expressions of cell lines 8182 and 53631 (qPCR). N=6, ****P<0.0005. b) Slc9a2 mRNA expressions of cell lines 8182 and 53631 (qPCR). N=6, ****P<0.0005. c) Representative WB images of PADI4 in cell lines 8182 and 53631. Densitometric quantification of WB analyses (right). N=4, ****P<0.0005. d) Representative WB images of SLC9A2 in cell line 8182 and 53631. Densitometric quantification of WB analyses (right). N=4, ns: not significant.

4.6.4 Padi4 knockdown in cell line 53631 by shRNA

After transfection of the 53631 cell line with Padi4 shRNA and antibiotic selection, a stable transfected cell line was established. On the mRNA level, Padi4 expression was markedly decreased compared to non-target shRNA transfected cells (Figure 37a). On the protein level, the expression of PADI4 was clearly reduced as well. However, this lowering of PADI4 had no effect on the SLC9A2 expression (Figure 37b, c).

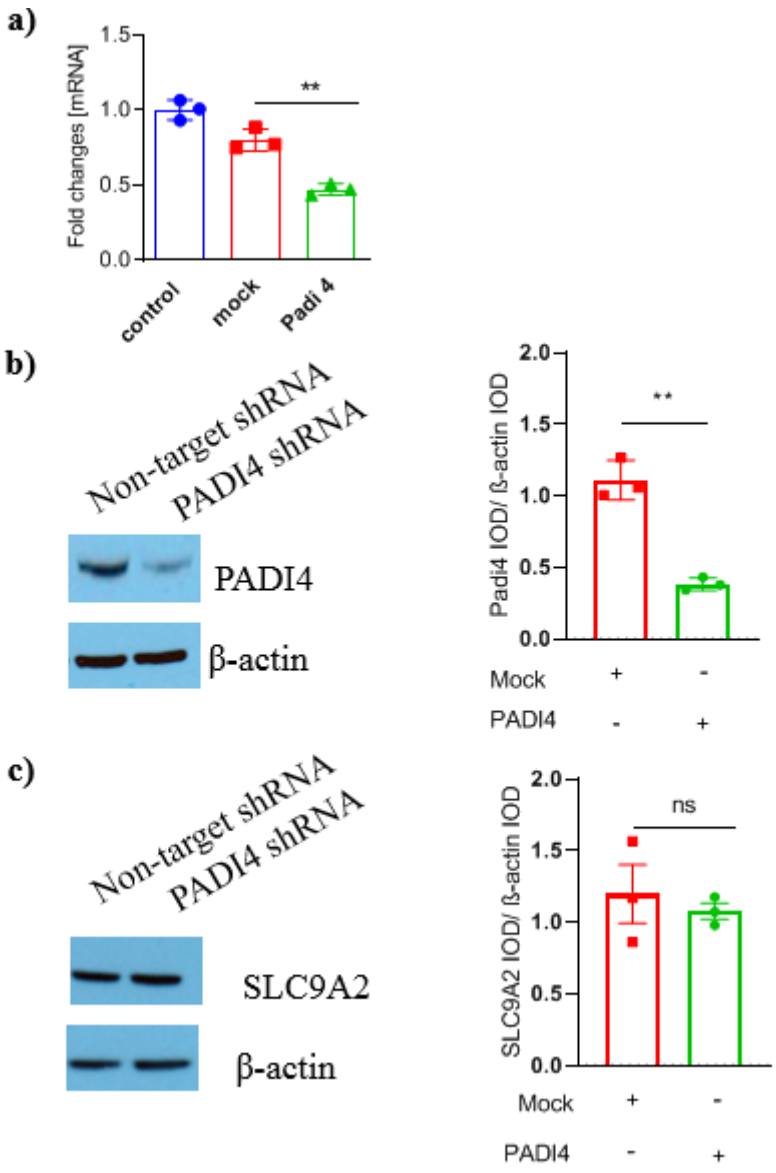

Figure 37 a) Padi4 mRNA expression in Padi4 shRNA stable transfected 53631 cells, and mock shRNA transfected 53631 cells. N=3, ** P < 0.01. b) Representative WB images for PADI4 expression in Padi4 shRNA stable transfected 53631 cells and mock shRNA transfected 53631 cells (left). Densitometric analyses of PADI4 in Padi4 shRNA stable transfected 53631 cells (right). N=3, ** P < 0.01. c) Representative WB images for SLC9A2 in Padi4 shRNA stable transfected 53631

cells (left). Densitometric analyses for SLC9A2 expression in Padi4 shRNA stable transfected 53631 cells. N=3, ns, not significant.

4.6.5 Release of EVs from Padi4-shRNA-transfected 53631 cells

In Padi4-shRNA-transfected 53631 cells, release of LOs and EVs were strongly reduced as measured by light microscopy and with nanoparticle tracking analysis, respectively compared to that of mock shRNA transfected 53631 cells (Figure 38a, b).

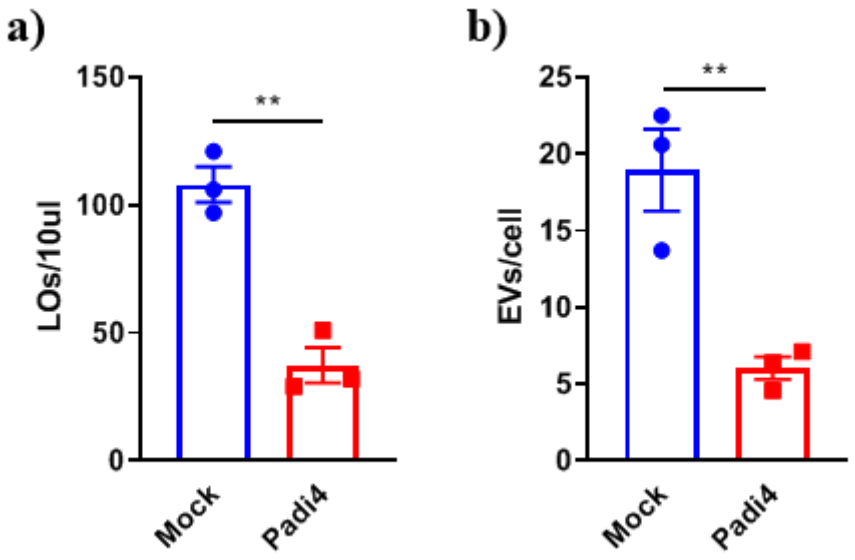

Figure 38 a) Release of LOs from Padi4-shRNA-transfected 53631 cells. b) Release of EVs from Padi4-shRNA-transfected 53631 cells. N=3, ** $P < 0.01$.

4.6.6 Procoagulant activities of Padi4-shRNA-transfected 53631 cells

The procoagulant activities in mock shRNA-transfected 53631 cells and Padi4-shRNA-transfected 53631 cells were compared. As shown in Figure 39, there was no significant difference between these two cell lines. Thus, changes in

procoagulant activities can be excluded if the mock- and Padi4-shRNA-transfected 53631 differ in their extravasation behavior.

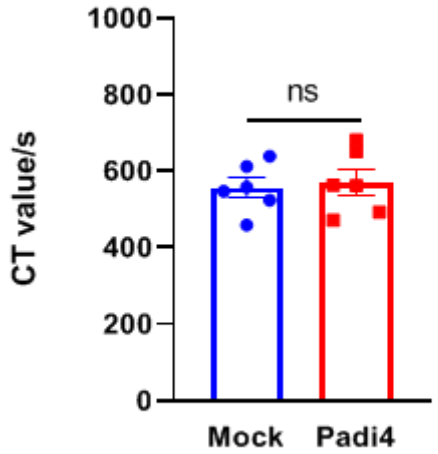

Figure 39 CT values (TEG) of mock- and Padi4-shRNA-transfected 53631cells. Dots refer to different donors. ns, not significant.

4.6.7 Role of EV release on tumor extravasation

As shown in 4.6.5, the release of EVs strongly decreases after Padi4 down-regulation in cell line 53631. To examine the role of EV release for tumor cell extravasation, both mock- and Padi4-shRNA-transfected 53631 cells were injected into WT mice and after 6 h tumor cell extravasation was analyzed in the liver microcirculation (Figure 40). Extravasation of Padi4-shRNA-transfected 53631 cells was higher than the mock-shRNA-transfected 53631 cells, suggesting that the ability to release EVs increases tumor cell extravasation.

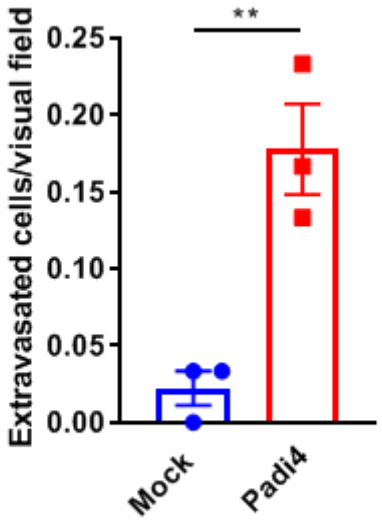

Figure 40 Numbers of Padi4-shRNA-transfected 53631 cells extravasated in the liver microcirculation after 6 h of cancer cell injection. Dots refer to different animals. ** $P < 0.01$.

4.6.7 Role of tumor-induced blood coagulation and of EV release for tumor cell extravasation

The amounts of non-classical monocytes and CD4+ T cells were counted in the liver microcirculation. There were no apparent differences between mock- and Padi4-shRNA-transfected 53631 cells for both immune cell species (Figure 41a,b). Some of the non-classical monocytes were found to contain cancer cell-derived EVs (Figure 41c). Moreover, part of the non-classical monocytes expressed Ang-2 instead of Ang-1 (Figure 41d).

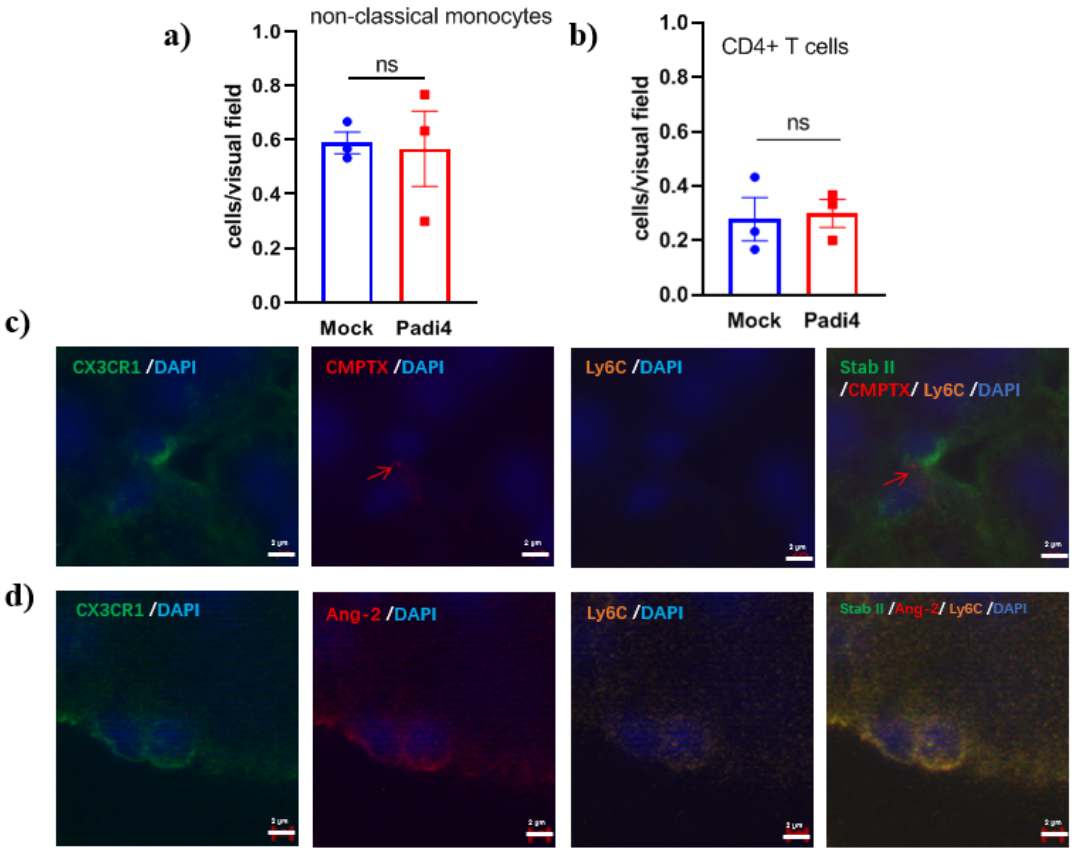

Figure 41 Recruitment of non-classical monocytes (a) and CD4+ T cells (b) after injection of mock- and Padi4-shRNA-transfected 53631 cells (6 h after injection). Dots refer to different animals. ns, not significant. c) Non-classical monocytes with engulfed tumor-derived EVs. CX3CR1, green, EVs, red, Ly6C, orange. Scale bar, 2 μm; EVs are highlighted with red arrow. d) Non-classical monocytes with Ang-2 staining. CX3CR1, green, Ang-2, red, Ly6C, orange. Scale bar, 2 μm.

5. Discussion

Extravasation is a key step in the process of tumor metastasis. After intravasation, circulating tumor cells can seed the tissue at distant sites and subsequently form a metastatic niche.[22, 23] Generally, a high primary tumor burden and the presence of circulating tumor cells are associated with an elevated risk for venous thromboembolism and activation of blood coagulation.[31] However, the role of blood coagulation in tumor extravasation or metastasis has not been clearly elucidated so far. Hence it is the focus of this study.

In my experiments, I have used several pancreatic cancer cell lines with KRAS mutations to check the role tumor-induced blood coagulation plays in tumor cell extravasation. With the help of RNA sequencing of these cell lines, the analyses of entire transcriptomes were accomplished. The transcriptomes of the all cell lines tended to be almost identical. Moreover, CT values were obtained by TEG measurement to evaluate the procoagulant activities of each cell line. The highest tumor-induced blood coagulation activity was present in cell line 8182, while the lowest was present in cell line 9091. Tumor-induced blood coagulation by cell line 8182 was found to be completely dependent on the TF pathway *in vitro and in vivo*. Such strong tumor-induced blood coagulation could override even FXII-host-induced fibrin generation. Surprisingly, after inhibition of factor Xa by Rivaroxaban, the extravasation of 8182 was increased, suggesting an inhibiting role of tumor-induced blood coagulation on extravasation. The underlying mechanism is not fully clear at present.

It was observed that tumor-induced blood coagulation is associated with a recruitment of non-classical monocytes. The most important function of non-classical monocytes is to patrol the endothelium as part of a local innate surveillance under physiological conditions.[56-58] In the present work, non-classical monocytes were found to express Ang-1. Ang-1 is known to activate the Tie-2 receptor, which can promote the survival of endothelial cells, the maintenance of the endothelial barrier, and a quiescent vasculature.[109, 110] Thus, non-classical monocytes expressing Ang-1 could potentially regulate the permeability of the endothelium, thereby reducing tumor extravasation.

When tumor-induced blood coagulation was weak or even absent such as in cell line 9091, host-induced blood coagulation was well evident. It was found to be crucially dependent on coagulation FXII. Activation of FXII is dispensable in the process of hemostasis. Yet, FXII plays a more important role in both physiological and pathological thrombosis.[29] Thus, cell line 9091 was selected to study FXII-host-induced blood coagulation, since this cell line lacked coagulation activity *in vitro*. Activation of coagulation observed in the presence of 9091 *in vivo* could be explained by an immune response of the host. Rivaroxaban was demonstrated to be able to inhibit FXII-host-induced coagulation in this model as well. Extravasation of 9091 was compared in WT and *f12-/-* mice. Tumor invasion of 9091 was substantially higher in *f12-/-* mice than in control mice. Rivaroxaban treatment eliminated the difference in extravasation between the two different mouse species, indicating that activation of FXII prevented extravasation by a

coagulation-dependent mechanism. Taken together, FXII-dependent blood coagulation, as triggered by the host (potentially by endothelial cells), reduces tumor extravasation.

FXII-host-induced blood coagulation might impede tumor extravasation through additional mechanisms, as for example by reduction of neutrophil recruitment. Indeed, following Rivaroxaban treatment of mice injected with 9091, the amount of neutrophils in the liver microcirculation was elevated, suggesting a suppressive role of host-induced coagulation on neutrophil recruitment. Moreover, neutrophil levels in the liver microcirculation were significantly higher in *f12-/-* mice compared to WT mice. This also suggested that host-induced blood coagulation had suppressed neutrophil recruitment.

The emergence of NETs was not observed until 9 h after injection of tumor cells, indicating a slow formation. These NETs were arranged as part of a NET-covered area in which several neutrophils were clustered. It is plausible that the formation of these areas can induce the obstruction of blood flow in microvessels.[130] Such occlusion could potentially cause the formation of hypoxia areas. When HIF1α expression was employed to detect hypoxic areas, it was found to accumulate in association with endothelial cells. In hypoxia areas, the expression of Ang-2 can be increased,[111, 112] which could promote vessel permeability (Figure 41). To sum up, upstream formation of NETs increases formation of hypoxic areas and results in Ang-2 expression by local endothelial cells, which could further support tumor extravasation. Of relevance for this process is the recruitment of neutrophils and

the subsequent formation of NETs. Indeed, DNaseI treatment which can dissolve NETs, reduced the hypoxic areas and simultaneously increased expression of Ang-1 and decreased Ang-2 expression. As a conclusion, host-induced blood coagulation might hinder tumor extravasation by reducing the arrest of neutrophils and the formation of NETs.

The release of EV is a typical feature of most cancer cells and has been suggested to support metastasis. In my study, cell line 53631 had the strongest EV release activity among 11 different pancreatic cancer cell lines with KRAS mutations. Hence it was chosen to study the relationship between EV release and tumor extravasation. Transcriptomic analyses showed that the Padi4 gene was associated with the high EV release in 53631 cells. Suppression of Padi4 expression by shRNA showed that Padi4 was responsible for EV release. The Padi4 shRNA stable-transfected 53631 cells were used to perform animal experiments. It was clearly shown that the release of EV by cancer cells can increase tumor cell extravasation.

Surprisingly, cell line 53631 had the second strongest abilities to enhance blood coagulation among all 11 cancer cell lines, consistent with a marked tumor-induced blood coagulation activity. The procoagulant activities of cell line 53631 and 8182 were comparable. Yet, our hypothesis was challenged when cell line 53631 showed much higher tumor extravasation compared to that of 8182, although both had similar procoagulant activities. Why tumor-induced blood coagulation acted so differently in these two cell lines is still unresolved.

Thus it appears that EV-release and tumor-induced blood coagulation somehow cooperate to assist in tumor cell extravasation. It was reported that tumor cell-derived EVs can educate monocytes and, as a result, these cells can differentiate into tumor-associated macrophages, which in turn can increase tumor cell extravasation.[132] We observed here that non-classical monocytes can be recruited by fibrin and we found that these monocytes were stimulated in response to tumor-induced coagulation. Also non-classical monocytes took up tumor cell derived EVs. Moreover, while some non-classical monocytes express Ang-2 in mice injected with mock-shRNA-transfected 53631 cells, this expression was absent in mice injected with cell lines 8182 and Padi4-downregulated cell line 53631. Both cell line 8182 and Padi4-downregulated cell line 53631 have a weak capacity to release EVs. On the other hand, the uptake of tumor cell-derived EVs by non-classical monocytes in the case of mice injected with cell line 53631 may cause the non-classical monocytes to express Ang-2 (Figure 42).

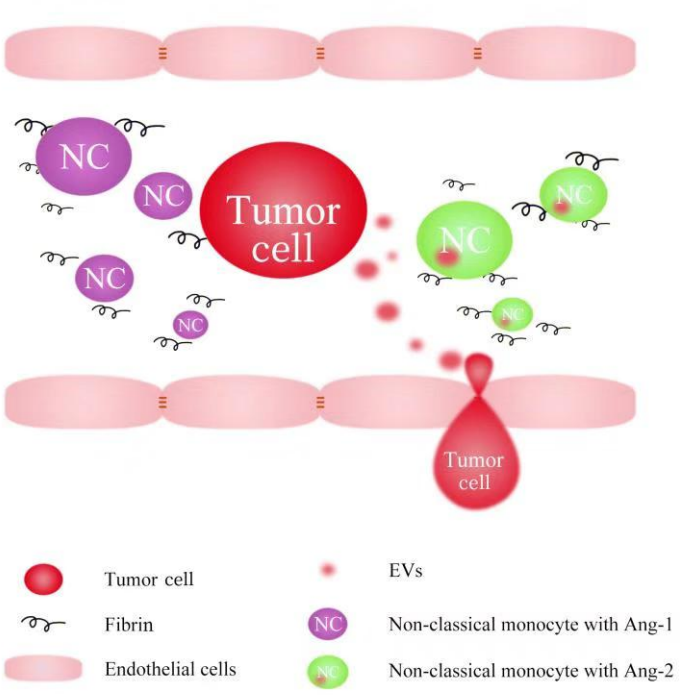

Figure 42 Scheme of the effect of tumor-induced blood coagulation on tumor cell extravasation.

Prometastatic tumor cells are in general master survivor cells. Tumor-induced blood coagulation, by this logic, shouldn't possibly prevent tumor cell extravasation. Yet, our results suggest that under some conditions tumor-induced blood coagulation can recruit non-classical monocytes, which appears beneficial for the host to reduce tumor cell extravasation through expression of Ang-1. The EVs originating from the tumor cells, on the other hand, may educate non-classical monocytes to act as prometastatic agents. As a result, non-classic monocytes lose their expression of Ang-1, and some of them express Ang-2, which might result in an increased vessel permeability and facilitation of tumor cell extravasation.

6. Summary

Thrombotic diseases are often observed in tumor patients and a high tumor burden is a crucial independent risk factor for the development of venous thromboembolism which is in part due to the ability of tumor cells directly to trigger blood coagulation. In the present study it was shown that two different types of microvascular blood coagulation can be distinguished in mice exposed to circulating pancreatic tumor cells, namely tumor-induced blood coagulation and host-induced blood coagulation. Tumor-induced blood coagulation in the microcirculation of the liver was found to increase the recruitment of non-classical monocytes. These immune cells expressed Ang-1, which is able to impede tumor cell extravasation. Moreover, non-classical monocytes engulfed tumor-cell derived EVs. It appeared that, following ingestion of tumor-cell derived EVs, non-classical monocytes lost their expression of Ang-1. Some of them, on the contrary, now expressed Ang-2, which is known to facilitate tumor cell extravasation. The effect of FXII-mediated-host-induced blood coagulation on tumor cell extravasation varied according to the type of mice studied. FXII suppressed the recruitment of neutrophils, whereby formation of NETs was decreased and the tumor cell extravasation was diminished. On the other hand, formation of NETs increased local HIF1α expression and Ang-2 expression by endothelial cells, which favored tumor cell extravasation. Phenotypic screens based on several pancreatic cancer cell lines revealed Padi4 as candidate gene promoting EV release and Gas6 as candidate gene for tumor-induced blood coagulation.

In conclusion, both tumor-induced blood coagulation and FXII-host-induced blood

coagulation can in principle inhibit extravasation of pancreatic tumor cells during early tumor metastasis. However, release of EVs by tumor cells and tumor-cell-induced NETs formation could overcome the suppressive influence of coagulation.

7. Zusammenfassung

Bei Patienten mit Tumorerkrankungen werden oftmals thrombotische Erkrankungen diagnostiziert. Zusätzlich stellt eine hohe Tumorlast einen wichtigen unabhängigen Risikofaktor für die Entwicklung von venösen Thromboembolien dar, die teilweise auf die Fähigkeit des Tumors, die Blutkoagulation zu induzieren, zurückzuführen ist. In der vorliegenden Arbeit konnte gezeigt werden, dass in der Maus zwischen zwei verschiedene Arten der Blutkoagulation unterschieden werden können, die die Tumor-induzierte Blutkoagulation und Wirts-induzierte Blutkoagulation bezeichnen. Die Tumor-induzierte Koagulation verstärkte die Rekrutierung nicht-klassischer Monozyten. Diese Immunzellen exprimierten Ang-1, wodurch die Extravasation der Tumorzellen behindert wurde. Zudem inkorporierten nicht-klassische Monozyten EV, welche von der Tumorzelle abgegeben wurden. Jedoch verloren die nicht-klassischen Monozyten nach erfolgreicher Aufnahme der EV die Expression des Wachstumsfaktors Ang-1. Stattdessen zeigte sich anschließend bei einigen Zellen eine vermehrte Expression von Ang-2. Die mittels FXII verstärkte wirts-induzierte Koagulation bewirkte unterschiedliche Effekte in der Extravasation der Tumorzellen. FXII induzierte eine Unterdrückung der Rekrutierung von Neutrophilen, wodurch die Bildung von NETs abnahm und die Extravasation der Tumorzellen vermindert wurde. Die Bildung der NETs bewirkte einen Anstieg der Expression von lokalem HIF1α und der Expression von Ang-2 auf Endothelzellen, wodurch die Extravasation von Tumorzellen begünstigt werden könnte. Phänotypische Screens mit Pankreas Karzinom-Zelllinien ergaben Kandidaten Gene für Freisetzung von EV aus

Tumorzellen (Padi4) und für die Tumor-induzierte Koagulation (Gas6).

Zusammenfassend kann gesagt werden, dass sowohl die Tumor-induzierte Blutkoagulation als auch die Wirts-induzierte Blutkoagulation die Extravasation von Tumorzellen in der frühen Phase der Metastasierung hemmen kann. Jedoch kann durch die Freisetzung von EV und durch die Tumorzell-induzierte Bildung der NETs die unterdrückende Wirkung der Blutkoagulation antagonisiert werden.

8. Publications related to this thesis

Coagulation-mediated immune cells functions in early metastasis. (In preparation) Xiaopeng Zhang, Hellen Ischikava-Ankerhold, Manoviriti Thakur, Maximilian Wieser, Magda-Lena Berchtold, Esra Büyüközkan, Rapheal Denz, Kathrin Gärtner, Christian Schulz, Roland Rad, Steffen Massberg, Bernd Engelmann.

9. Acknowledgement

At the end of this thesis, I would like kindly to thank my supervisor Prof. Dr. med Bernd Engelmann. Because of his endorsement, I have had such a wonderful chance to work and learn in this cutting-edge laboratory of the world. His profound knowledge and unparalleled understanding of science and research always show me the direction of my study. He is not only my supervisor in science but also help me a lot to overcome difficulties in my life. Please allow me to express my warm and sincerely appreciation to Prof. Engelmann.

As a doctoral candidate, life is always full of challenges and works. I appreciate my parents' understanding. Even though I do not have so much time to accompany with them, I always get the encouragements from them. What they taught me are the eternal treasure of my life.

Many thanks should be given to Prof. Steffen Massberg, Prof. Christian Schulz, Prof. Roland Rad, Dr. Hellen Ischikava-Ankerhold and Dr. Kathrin Gärtner. With the collaboration with them, the process of this study accelerated. They were always there to offer me useful advices and assistance.

Because of the support of Dr. Jingang Huang, Dr. Huiling Weng, Dr. Yingying Yang, Dr. Zheming Liu, Dr. Manoviriti Thakur and doctoral candidate Mr. Xiaolong Shi, Mr. Zhe Zhang, Mr. Mingsong Wang, Mr. Flavio Karaj, Mr. Maximilian Wieser, Mr. Marian Radev, Ms. Fangfang Chen, Ms. Magda-Lena Berchtold, Ms. Esra Büyüközkan, Ms. Tonina Müller, Ms. Mona Wohlrab, I can overcome all the troubles and finish this complicated but promising project.

Last but not least, I will never forget some days before, I knew Ms Zijun Cindy Zheng in our student dormitory. We have different nationalities, but your love encourages me to go further forever.

REFERENCE

1. Tempero MA, Malafa MP, Al-Hawary M, et al. Pancreatic Adenocarcinoma, Version 2.2017, NCCN Clinical Practice Guidelines in Oncology. J Natl Compr Canc Netw 2017;15:1028-1061.
2. Xu YP, Yang M. Advancement in treatment and diagnosis of pancreatic cancer with radiopharmaceuticals. World J Gastrointest Oncol 2016;8:165-72.
3. Smith RA, Andrews KS, Brooks D, et al. Cancer screening in the United States, 2018: A review of current American Cancer Society guidelines and current issues in cancer screening. CA Cancer J Clin 2018;68:297-316.
4. Miller KD, Nogueira L, Mariotto AB, et al. Cancer treatment and survivorship statistics, 2019. CA Cancer J Clin 2019. DOI: 10.3322/caac.21565.
5. Kranenburg O. The KRAS oncogene: past, present, and future. Biochim Biophys Acta 2005;1756:81-2.
6. Scolnick EM, Papageorge AG, Shih TY. Guanine nucleotide-binding activity as an assay for src protein of rat-derived murine sarcoma viruses. Proc Natl Acad Sci U S A 1979;76:5355-9.
7. Welman A, Burger MM, Hagmann J. Structure and function of the C-terminal hypervariable region of K-Ras4B in plasma membrane targetting and transformation. Oncogene 2000;19:4582-91.
8. Pylayeva-Gupta Y, Grabocka E, Bar-Sagi D. RAS oncogenes: weaving a tumorigenic web. Nat Rev Cancer 2011;11:761-74.
9. Collisson EA, Trejo CL, Silva JM, et al. A central role for RAF-->MEK-->ERK signaling in the genesis of pancreatic ductal adenocarcinoma. Cancer Discov 2012;2:685-93.
10. Eser S, Reiff N, Messer M, et al. Selective requirement of PI3K/PDK1 signaling for Kras oncogene-driven pancreatic cell plasticity and cancer. Cancer Cell 2013;23:406-20.
11. Feldmann G, Mishra A, Hong SM, et al. Inhibiting the cyclin-dependent kinase CDK5 blocks pancreatic cancer formation and progression through the suppression of Ras-Ral signaling. Cancer Res 2010;70:4460-9.
12. Lim KH, Baines AT, Fiordalisi JJ, et al. Activation of RalA is critical for Ras-induced tumorigenesis of human cells. Cancer Cell 2005;7:533-45.
13. Ardito CM, Gruner BM, Takeuchi KK, et al. EGF receptor is required for KRAS-induced pancreatic tumorigenesis. Cancer Cell 2012;22:304-17.
14. Molina-Arcas M, Hancock DC, Sheridan C, et al. Coordinate direct input of both KRAS and IGF1 receptor to activation of PI3 kinase in KRAS-mutant lung cancer. Cancer Discov 2013;3:548-63.
15. Navas C, Hernandez-Porras I, Schuhmacher AJ, et al. EGF receptor signaling is essential for k-ras oncogene-driven pancreatic ductal adenocarcinoma. Cancer Cell 2012;22:318-30.
16. Moore MJ, Goldstein D, Hamm J, et al. Erlotinib plus gemcitabine compared with gemcitabine alone in patients with advanced pancreatic cancer: a phase III trial of the National Cancer Institute of Canada Clinical Trials Group. J Clin Oncol 2007;25:1960-6.
17. Butler TP, Gullino PM. Quantitation of cell shedding into efferent blood of mammary adenocarcinoma. Cancer Res 1975;35:512-6.
18. Chang YS, di Tomaso E, McDonald DM, et al. Mosaic blood vessels in tumors: frequency of cancer cells in contact with flowing blood. Proc Natl Acad Sci U S A 2000;97:14608-13.
19. Wong CW, Lee A, Shientag L, et al. Apoptosis: an early event in metastatic inefficiency. Cancer

Res 2001;61:333-8.
20. Chen DS, Mellman I. Elements of cancer immunity and the cancer-immune set point. Nature 2017;541:321-330.
21. Reymond N, d'Agua BB, Ridley AJ. Crossing the endothelial barrier during metastasis. Nat Rev Cancer 2013;13:858-70.
22. Liu Y, Cao X. Characteristics and Significance of the Pre-metastatic Niche. Cancer Cell 2016;30:668-681.
23. Peinado H, Zhang H, Matei IR, et al. Pre-metastatic niches: organ-specific homes for metastases. Nat Rev Cancer 2017;17:302-317.
24. Palta S, Saroa R, Palta A. Overview of the coagulation system. Indian J Anaesth 2014;58:515-23.
25. Roderique EM, Wynands JE. Blood coagulation and haemostasis: a review. Can Anaesth Soc J 1967;14:129-51.
26. Renne T, Pozgajova M, Gruner S, et al. Defective thrombus formation in mice lacking coagulation factor XII. J Exp Med 2005;202:271-81.
27. Kleinschnitz C, Stoll G, Bendszus M, et al. Targeting coagulation factor XII provides protection from pathological thrombosis in cerebral ischemia without interfering with hemostasis. J Exp Med 2006;203:513-8.
28. Kannemeier C, Shibamiya A, Nakazawa F, et al. Extracellular RNA constitutes a natural procoagulant cofactor in blood coagulation. Proc Natl Acad Sci U S A 2007;104:6388-93.
29. van der Meijden PE, Munnix IC, Auger JM, et al. Dual role of collagen in factor XII-dependent thrombus formation. Blood 2009;114:881-90.
30. Khan MM, Shibuya Y, Kambara T, et al. Role of alpha-2-macroglobulin and bacterial elastase in guinea-pig pseudomonal septic shock. Int J Exp Pathol 1995;76:21-8.
31. Blom JW, Vanderschoot JP, Oostindier MJ, et al. Incidence of venous thrombosis in a large cohort of 66,329 cancer patients: results of a record linkage study. J Thromb Haemost 2006;4:529-35.
32. Di Nisio M, Ferrante N, Feragalli B, et al. Arterial thrombosis in ambulatory cancer patients treated with chemotherapy. Thromb Res 2011;127:382-3.
33. Timp JF, Braekkan SK, Versteeg HH, et al. Epidemiology of cancer-associated venous thrombosis. Blood 2013;122:1712-23.
34. Khorana AA, Connolly GC. Assessing risk of venous thromboembolism in the patient with cancer. J Clin Oncol 2009;27:4839-47.
35. Levin J, Conley CL. Thrombocytosis Associated with Malignant Disease. Arch Intern Med 1964;114:497-500.
36. Kakkar AK, Lemoine NR, Scully MF, et al. Tissue factor expression correlates with histological grade in human pancreatic cancer. Br J Surg 1995;82:1101-4.
37. Khorana AA, Ahrendt SA, Ryan CK, et al. Tissue factor expression, angiogenesis, and thrombosis in pancreatic cancer. Clin Cancer Res 2007;13:2870-5.
38. Wang JG, Geddings JE, Aleman MM, et al. Tumor-derived tissue factor activates coagulation and enhances thrombosis in a mouse xenograft model of human pancreatic cancer. Blood 2012;119:5543-52.
39. Gyorgy B, Szabo TG, Pasztoi M, et al. Membrane vesicles, current state-of-the-art: emerging role of extracellular vesicles. Cell Mol Life Sci 2011;68:2667-88.

40. Gardiner C, Harrison P, Belting M, et al. Extracellular vesicles, tissue factor, cancer and thrombosis - discussion themes of the ISEV 2014 Educational Day. J Extracell Vesicles 2015;4:26901.
41. Dvorak HF, Van DeWater L, Bitzer AM, et al. Procoagulant activity associated with plasma membrane vesicles shed by cultured tumor cells. Cancer Res 1983;43:4434-42.
42. Hisada Y, Ay C, Auriemma AC, et al. Human pancreatic tumors grown in mice release tissue factor-positive microvesicles that increase venous clot size. J Thromb Haemost 2017;15:2208-2217.
43. Geddings JE, Hisada Y, Boulaftali Y, et al. Tissue factor-positive tumor microvesicles activate platelets and enhance thrombosis in mice. J Thromb Haemost 2016;14:153-66.
44. Khorana AA, Kuderer NM, Culakova E, et al. Development and validation of a predictive model for chemotherapy-associated thrombosis. Blood 2008;111:4902-7.
45. Blix K, Jensvoll H, Braekkan SK, et al. White blood cell count measured prior to cancer development is associated with future risk of venous thromboembolism--the Tromso study. PLoS One 2013;8:e73447.
46. Brinkmann V, Reichard U, Goosmann C, et al. Neutrophil extracellular traps kill bacteria. Science 2004;303:1532-5.
47. Gregory SA, Morrissey JH, Edgington TS. Regulation of tissue factor gene expression in the monocyte procoagulant response to endotoxin. Mol Cell Biol 1989;9:2752-5.
48. Jensvoll H, Blix K, Braekkan SK, et al. Platelet count measured prior to cancer development is a risk factor for future symptomatic venous thromboembolism: the Tromso Study. PLoS One 2014;9:e92011.
49. Khorana AA, Francis CW, Culakova E, et al. Risk factors for chemotherapy-associated venous thromboembolism in a prospective observational study. Cancer 2005;104:2822-9.
50. Simanek R, Vormittag R, Ay C, et al. High platelet count associated with venous thromboembolism in cancer patients: results from the Vienna Cancer and Thrombosis Study (CATS). J Thromb Haemost 2010;8:114-20.
51. Guilliams M, Ginhoux F, Jakubzick C, et al. Dendritic cells, monocytes and macrophages: a unified nomenclature based on ontogeny. Nat Rev Immunol 2014;14:571-8.
52. Ginhoux F, Jung S. Monocytes and macrophages: developmental pathways and tissue homeostasis. Nat Rev Immunol 2014;14:392-404.
53. Ziegler-Heitbrock L, Ancuta P, Crowe S, et al. Nomenclature of monocytes and dendritic cells in blood. Blood 2010;116:e74-80.
54. Epelman S, Lavine KJ, Randolph GJ. Origin and functions of tissue macrophages. Immunity 2014;41:21-35.
55. Ginhoux F, Guilliams M. Tissue-Resident Macrophage Ontogeny and Homeostasis. Immunity 2016;44:439-449.
56. Wong KL, Yeap WH, Tai JJ, et al. The three human monocyte subsets: implications for health and disease. Immunol Res 2012;53:41-57.
57. Clements M, Gershenovich M, Chaber C, et al. Differential Ly6C Expression after Renal Ischemia-Reperfusion Identifies Unique Macrophage Populations. J Am Soc Nephrol 2016;27:159-70.
58. Yona S, Kim KW, Wolf Y, et al. Fate mapping reveals origins and dynamics of monocytes and tissue macrophages under homeostasis. Immunity 2013;38:79-91.

59. Franklin RA, Liao W, Sarkar A, et al. The cellular and molecular origin of tumor-associated macrophages. Science 2014;344:921-5.
60. Movahedi K, Laoui D, Gysemans C, et al. Different tumor microenvironments contain functionally distinct subsets of macrophages derived from Ly6C(high) monocytes. Cancer Res 2010;70:5728-39.
61. Qian BZ, Pollard JW. Macrophage diversity enhances tumor progression and metastasis. Cell 2010;141:39-51.
62. Oosterling SJ, van der Bij GJ, Meijer GA, et al. Macrophages direct tumour histology and clinical outcome in a colon cancer model. J Pathol 2005;207:147-55.
63. Gallina G, Dolcetti L, Serafini P, et al. Tumors induce a subset of inflammatory monocytes with immunosuppressive activity on CD8+ T cells. J Clin Invest 2006;116:2777-90.
64. Hanna RN, Cekic C, Sag D, et al. Patrolling monocytes control tumor metastasis to the lung. Science 2015;350:985-90.
65. Takei H, Araki A, Watanabe H, et al. Rapid killing of human neutrophils by the potent activator phorbol 12-myristate 13-acetate (PMA) accompanied by changes different from typical apoptosis or necrosis. J Leukoc Biol 1996;59:229-40.
66. Wang S, Wang Y. Peptidylarginine deiminases in citrullination, gene regulation, health and pathogenesis. Biochim Biophys Acta 2013;1829:1126-35.
67. Papayannopoulos V, Metzler KD, Hakkim A, et al. Neutrophil elastase and myeloperoxidase regulate the formation of neutrophil extracellular traps. J Cell Biol 2010;191:677-91.
68. Sorensen OE, Borregaard N. Neutrophil extracellular traps - the dark side of neutrophils. J Clin Invest 2016;126:1612-20.
69. Cools-Lartigue J, Spicer J, McDonald B, et al. Neutrophil extracellular traps sequester circulating tumor cells and promote metastasis. J Clin Invest 2013.
70. Tohme S, Yazdani HO, Al-Khafaji AB, et al. Neutrophil Extracellular Traps Promote the Development and Progression of Liver Metastases after Surgical Stress. Cancer Res 2016;76:1367-80.
71. Pieterse E, Rother N, Garsen M, et al. Neutrophil Extracellular Traps Drive Endothelial-to-Mesenchymal Transition. Arterioscler Thromb Vasc Biol 2017;37:1371-1379.
72. Millrud CR, Kagedal A, Kumlien Georen S, et al. NET-producing CD16(high) CD62L(dim) neutrophils migrate to tumor sites and predict improved survival in patients with HNSCC. Int J Cancer 2017;140:2557-2567.
73. Turturici G, Tinnirello R, Sconzo G, et al. Extracellular membrane vesicles as a mechanism of cell-to-cell communication: advantages and disadvantages. Am J Physiol Cell Physiol 2014;306:C621-33.
74. Kanada M, Bachmann MH, Hardy JW, et al. Differential fates of biomolecules delivered to target cells via extracellular vesicles. Proc Natl Acad Sci U S A 2015;112:E1433-42.
75. Anderson HC. Vesicles associated with calcification in the matrix of epiphyseal cartilage. J Cell Biol 1969;41:59-72.
76. Wolf P. The nature and significance of platelet products in human plasma. Br J Haematol 1967;13:269-88.
77. Crawford N. The presence of contractile proteins in platelet microparticles isolated from human and animal platelet-free plasma. Br J Haematol 1971;21:53-69.
78. Dalton AJ. Microvesicles and vesicles of multivesicular bodies versus "virus-like" particles. J

Natl Cancer Inst 1975;54:1137-48.
79. Trams EG, Lauter CJ, Salem N, Jr., et al. Exfoliation of membrane ecto-enzymes in the form of micro-vesicles. Biochim Biophys Acta 1981;645:63-70.
80. Taylor DD, Homesley HD, Doellgast GJ. Binding of specific peroxidase-labeled antibody to placental-type phosphatase on tumor-derived membrane fragments. Cancer Res 1980;40:4064-9.
81. Pan BT, Teng K, Wu C, et al. Electron microscopic evidence for externalization of the transferrin receptor in vesicular form in sheep reticulocytes. J Cell Biol 1985;101:942-8.
82. Poutsiaka DD, Schroder EW, Taylor DD, et al. Membrane vesicles shed by murine melanoma cells selectively inhibit the expression of Ia antigen by macrophages. J Immunol 1985;134:138-44.
83. Harding C, Heuser J, Stahl P. Receptor-mediated endocytosis of transferrin and recycling of the transferrin receptor in rat reticulocytes. J Cell Biol 1983;97:329-39.
84. Raposo G, Tenza D, Mecheri S, et al. Accumulation of major histocompatibility complex class II molecules in mast cell secretory granules and their release upon degranulation. Mol Biol Cell 1997;8:2631-45.
85. Zitvogel L, Regnault A, Lozier A, et al. Eradication of established murine tumors using a novel cell-free vaccine: dendritic cell-derived exosomes. Nat Med 1998;4:594-600.
86. Stein JM, Luzio JP. Ectocytosis caused by sublytic autologous complement attack on human neutrophils. The sorting of endogenous plasma-membrane proteins and lipids into shed vesicles. Biochem J 1991;274 (Pt 2):381-6.
87. Elmore S. Apoptosis: a review of programmed cell death. Toxicol Pathol 2007;35:495-516.
88. Di Vizio D, Kim J, Hager MH, et al. Oncosome formation in prostate cancer: association with a region of frequent chromosomal deletion in metastatic disease. Cancer Res 2009;69:5601-9.
89. Di Vizio D, Morello M, Dudley AC, et al. Large oncosomes in human prostate cancer tissues and in the circulation of mice with metastatic disease. Am J Pathol 2012;181:1573-84.
90. Fackler OT, Grosse R. Cell motility through plasma membrane blebbing. J Cell Biol 2008;181:879-84.
91. Minciacchi VR, You S, Spinelli C, et al. Large oncosomes contain distinct protein cargo and represent a separate functional class of tumor-derived extracellular vesicles. Oncotarget 2015;6:11327-41.
92. Otranto M, Sarrazy V, Bonte F, et al. The role of the myofibroblast in tumor stroma remodeling. Cell Adh Migr 2012;6:203-19.
93. Giannoni E, Bianchini F, Masieri L, et al. Reciprocal activation of prostate cancer cells and cancer-associated fibroblasts stimulates epithelial-mesenchymal transition and cancer stemness. Cancer Res 2010;70:6945-56.
94. Webber JP, Spary LK, Sanders AJ, et al. Differentiation of tumour-promoting stromal myofibroblasts by cancer exosomes. Oncogene 2015;34:290-302.
95. Inal JM, Ansa-Addo EA, Stratton D, et al. Microvesicles in health and disease. Arch Immunol Ther Exp (Warsz) 2012;60:107-21.
96. Antonyak MA, Li B, Boroughs LK, et al. Cancer cell-derived microvesicles induce transformation by transferring tissue transglutaminase and fibronectin to recipient cells. Proc Natl Acad Sci U S A 2011;108:4852-7.
97. Baj-Krzyworzeka M, Szatanek R, Weglarczyk K, et al. Tumour-derived microvesicles carry

several surface determinants and mRNA of tumour cells and transfer some of these determinants to monocytes. Cancer Immunol Immunother 2006;55:808-18.

98. Richards DM, Hettinger J, Feuerer M. Monocytes and macrophages in cancer: development and functions. Cancer Microenviron 2013;6:179-91.

99. Pfeiler S, Thakur M, Grunauer P, et al. CD36-triggered cell invasion and persistent tissue colonization by tumor microvesicles during metastasis. FASEB J 2019;33:1860-1872.

100. Ekstrom EJ, Bergenfelz C, von Bulow V, et al. WNT5A induces release of exosomes containing pro-angiogenic and immunosuppressive factors from malignant melanoma cells. Mol Cancer 2014;13:88.

101. Figliolini F, Cantaluppi V, De Lena M, et al. Isolation, characterization and potential role in beta cell-endothelium cross-talk of extracellular vesicles released from human pancreatic islets. PLoS One 2014;9:e102521.

102. Eklund L, Olsen BR. Tie receptors and their angiopoietin ligands are context-dependent regulators of vascular remodeling. Exp Cell Res 2006;312:630-41.

103. Davis S, Papadopoulos N, Aldrich TH, et al. Angiopoietins have distinct modular domains essential for receptor binding, dimerization and superclustering. Nat Struct Biol 2003;10:38-44.

104. Kim KT, Choi HH, Steinmetz MO, et al. Oligomerization and multimerization are critical for angiopoietin-1 to bind and phosphorylate Tie2. J Biol Chem 2005;280:20126-31.

105. Fagiani E, Christofori G. Angiopoietins in angiogenesis. Cancer Lett 2013;328:18-26.

106. Thurston G. Role of Angiopoietins and Tie receptor tyrosine kinases in angiogenesis and lymphangiogenesis. Cell Tissue Res 2003;314:61-8.

107. Kim I, Kim HG, So JN, et al. Angiopoietin-1 regulates endothelial cell survival through the phosphatidylinositol 3'-Kinase/Akt signal transduction pathway. Circ Res 2000;86:24-9.

108. Xu Y, Yu Q. Angiopoietin-1, unlike angiopoietin-2, is incorporated into the extracellular matrix via its linker peptide region. J Biol Chem 2001;276:34990-8.

109. Jones N, Chen SH, Sturk C, et al. A unique autophosphorylation site on Tie2/Tek mediates Dok-R phosphotyrosine binding domain binding and function. Mol Cell Biol 2003;23:2658-68.

110. Jones N, Master Z, Jones J, et al. Identification of Tek/Tie2 binding partners. Binding to a multifunctional docking site mediates cell survival and migration. J Biol Chem 1999;274:30896-905.

111. Mandriota SJ, Pepper MS. Regulation of angiopoietin-2 mRNA levels in bovine microvascular endothelial cells by cytokines and hypoxia. Circ Res 1998;83:852-9.

112. Oh H, Takagi H, Suzuma K, et al. Hypoxia and vascular endothelial growth factor selectively up-regulate angiopoietin-2 in bovine microvascular endothelial cells. J Biol Chem 1999;274:15732-9.

113. Yuan HT, Khankin EV, Karumanchi SA, et al. Angiopoietin 2 is a partial agonist/antagonist of Tie2 signaling in the endothelium. Mol Cell Biol 2009;29:2011-22.

114. Kim I, Kim JH, Moon SO, et al. Angiopoietin-2 at high concentration can enhance endothelial cell survival through the phosphatidylinositol 3'-kinase/Akt signal transduction pathway. Oncogene 2000;19:4549-52.

115. Saharinen P, Eklund L, Pulkki K, et al. VEGF and angiopoietin signaling in tumor angiogenesis and metastasis. Trends Mol Med 2011;17:347-62.

116. Falcon BL, Hashizume H, Koumoutsakos P, et al. Contrasting actions of selective inhibitors of

angiopoietin-1 and angiopoietin-2 on the normalization of tumor blood vessels. Am J Pathol 2009;175:2159-70.
117. Holopainen T, Saharinen P, D'Amico G, et al. Effects of angiopoietin-2-blocking antibody on endothelial cell-cell junctions and lung metastasis. J Natl Cancer Inst 2012;104:461-75.
118. Renne SL, Redaelli S, Paolini B. Cryoembedder, automatic processor/stainer, liquid nitrogen freezing, and manual staining for frozen section examination: A comparative study. Acta Histochem 2019.
119. He J, Hajj KA, Knapp CM, et al. Development of a clinically relevant chemoresistant mantle cell lymphoma cell culture model. Exp Biol Med (Maywood) 2019:1535370219857594.
120. Gavini K, Parameshwaran K. Western Blot (Protein Immunoblot). StatPearls. Treasure Island (FL), 2019.
121. Kruger NJ. The Bradford method for protein quantitation. Methods Mol Biol 1994;32:9-15.
122. Thalji NK, Ivanciu L, Davidson R, et al. A rapid pro-hemostatic approach to overcome direct oral anticoagulants. Nat Med 2016;22:924-32.
123. Gomes IC, Acquarone M, Maciel Rde M, et al. Analysis of pluripotent stem cells by using cryosections of embryoid bodies. J Vis Exp 2010.
124. Livak KJ, Schmittgen TD. Analysis of relative gene expression data using real-time quantitative PCR and the 2(-Delta Delta C(T)) Method. Methods 2001;25:402-8.
125. Lyle HM. An improved tissue technique with hematoxylin-eosin stain. Am J Med Technol 1947;13:178-81.
126. Neuenschwander PF, Bianco-Fisher E, Rezaie AR, et al. Phosphatidylethanolamine augments factor VIIa-tissue factor activity: enhancement of sensitivity to phosphatidylserine. Biochemistry 1995;34:13988-93.
127. Foley JH, Conway EM. Gas6 gains entry into the coagulation cascade. Blood 2013;121:570-1.
128. Hanna RN, Carlin LM, Hubbeling HG, et al. The transcription factor NR4A1 (Nur77) controls bone marrow differentiation and the survival of Ly6C- monocytes. Nat Immunol 2011;12:778-85.
129. Tian L, Goldstein A, Wang H, et al. Mutual regulation of tumour vessel normalization and immunostimulatory reprogramming. Nature 2017;544:250-254.
130. Noubouossie DF, Reeves BN, Strahl BD, et al. Neutrophils: back in the thrombosis spotlight. Blood 2019;133:2186-2197.
131. Kholia S, Jorfi S, Thompson PR, et al. A novel role for peptidylarginine deiminases in microvesicle release reveals therapeutic potential of PAD inhibition in sensitizing prostate cancer cells to chemotherapy. J Extracell Vesicles 2015;4:26192.
132. de Vrij J, Maas SL, Kwappenberg KM, et al. Glioblastoma-derived extracellular vesicles modify the phenotype of monocytic cells. Int J Cancer 2015;137:1630-42.

Affidavit

Zhang, Xiaopeng

Surname, first name

I hereby declare, that the submitted thesis entitled

Role of Blood Coagulation and Extracellular Vesicles in Pancreatic Cancer Cell Extravasation

is my own work. I have only used the sources indicated and have not made unauthorised use of services of a third party. Where the work of others has been quoted or reproduced, the source is always given.

I further declare that the submitted thesis or parts thereof have not been presented as part of an examination degree to any other university.

Munich, 28.04.2020

Place, Date

Xiaopeng Zhang

Signature doctoral candidate